Bioremediation of an Arsenic-Contaminated Site, Using Sulfate-Reducing Bacteria, Bay County, Florida

by

Shahrzad Saffari Ghandehari

A thesis submitted to the Graduate Faculty of
Auburn University
in partial fulfillment of the
requirements for the Degree of
Master of Science

Auburn, Alabama
December 10, 2016

Keywords: arsenic, bioremediation, pyrite, adsorption

Approved by

James A. Saunders, Chair, Professor
Ming-Kuo Lee, Professor
Ashraf Uddin, Professor

Abstract

In this study an in-situ bioremediation field demonstration project using sulfate-reducing bacteria was conducted at an As-contaminated site, in Bay County, Florida. The background levels of As ranged from 0.13 to 0.34 $\frac{mg}{L}$ which is above the USEPA drinking water standard of 0.01 $\frac{mg}{L}$. Prior to the bioremediation experiment, groundwater was mildly reducing and slightly acidic. A mixture of water, molasses, ferrous sulfate and agricultural grade-fertilizer was gravity fed to the groundwater through two injection wells. Solid samples of aquifer material were collected from four drilled holes and pre- and post-injection groundwater geochemistry were measured. Field measurements showed that oxidation-reduction potential (ORP) decreased to around -200 mV and pH increased to around 8 in the four injection and monitoring wells the first week after the injections that led to establishment of sulfate-reduction conditions. ORP and pH values are returning back to background levels three month after the injections. One week after the injections, As concentration increased in the injection wells and monitoring wells, due to the effects of oxidation and resuspension. However since the second week after the injections, As concentrations have decreased as a result of sulfate-reducing conditions that were established at the site. Three month after the injections, the As concentration in the filtered water samples of two of the monitoring wells have decreased to below the EPA drinking water standard of 0.01 $\frac{mg}{L}$. The XRD and XRF analyses of solid samples, which precipitated from groundwater and were collected at the bottom of the wells, confirm the presence of As in iron sulfides that appears to be arsenian-pyrite. Decreased concentration of dissolved As in the groundwater and presence of As in the form of arsenian-pyrite in the sediments suggest that the As is being adsorbed on to iron sulfide minerals that are being formed. The reduction of sulfate to sulfide, which reacts with ferrous iron in the groundwater appears to have caused the observed As decrease. This As

decrease occurred at the same time as the formation of iron sulfide that precipitated at the bottom of the wells.

Groundwater flow and solute transport modeling shows that the iron concentration that had been increased up to 483 $\frac{mg}{L}$ in the groundwater after the injections, will decrease to 2.6 $\frac{mg}{L}$ after one year, due to mixing with the groundwater, advective transport and hydrodynamic dispersion, and it will move in a north-west direction. Combination of data from groundwater geochemistry and solid samples analyses are encouraging and indicate that the sorption and co-precipitation of As on biogenic pyrite is happening in the groundwater. Monitoring and sampling of the amended groundwater, at the site, is going to continue for one year to evaluate the efficiency of this bioremediation method over a longer time period.

Acknowledgments

Grants from National Science Foundation (#142004), the Geological Society of America, and Advisory Board of Department of Geosciences, Auburn University made this study possible. I would like to thank Dr. James Saunders, Dr. Ming-Kuo Lee, and Dr. Ashraf Uddin for their time, supports, and advices. I would also like to thank Dr. Mehmet Billor for his assistance in ICP-MS analyses and Dr. Jim Redwine who made the field works possible. Gratitude also go out to the graduate students who assisted me during the sampling events and analyzing the samples; Brian Miller, Eric Levitt and Nur Ahmed. Finally, many thanks to my best friend Mohammadnaser Ansari who morally supported me through out these two years and my parents who their patience and love, from thousands of miles away, motivated me in pursuing my dreams.

Table of Contents

List of Figures

List of Tables

List of Abbreviations

As	Arsenic
Ba	Barium
bgs	Below Ground Surface
Ce	Cerium
Co	Cobalt
DOC	Dissolved Organic Carbon
FDEP	Florida Department of Environmental Protection
Fe	Iron
gpm	Gallon Per Minute
ICP-MS	Inductively Coupled Plasma Mass Spectroscopy
K	Potassium
Mg	Magnesium
Ni	Nickel
ORP	Oxidation Reduction Potential
P	Phosphorus
SRB	Sulfate-Reducing Bacteria
TDS	Total Dissolved Solids

USEPA	United States Environmental Protection Agency
XRD	X-Ray Diffraction
XRF	X-Ray Fluorescence
Zn	Zinc

Chapter 1

Introduction

Millions of people around the world are dealing with poisoning by arsenic (As), which results from drinking As-contaminated water. Arsenic is one of the most hazardous chemicals; it is a carcinogen and can cause other types of human ailments, including respiratory diseases, gastro-intestinal, liver and cardiovascular problems (Mondal et al., 2013; Kruger et al., 2013). Although As is not an abundant element in Earth's crust, it can be found around the world because it is concentrated in many types of ore deposits as well as some rocks (Kruger et al., 2013). Arsenic contamination in groundwater is caused by both natural and anthropogenic sources. The most important anthropogenic sources of As in groundwater are mining, burning of fossil fuels, wood treatment, and the use of arsenical herbicides and pesticides (Bissen & Frimmel, 2003; Mondal et al., 2013; Rice et al., 2002). The maximum contamination level (MCL) for As can be different in each country (Mondal et al., 2013). Figure 1.1 shows the countries with major As contamination problems, and their established MCLs.

Arsenic mobility is affected by its oxidation state; Arsenite [As (III)] and arsenate [As (V)] are the two of main oxidation states of As in aquatic systems (Egal et al., 2010). Major forms of As (V) in aquatic environments are H_3AsO_4, $H_2AsO_4^-$, and AsO_4^{3-} and As(III) is most common in form of H_3AsO_3 and $H_2AsO_3^-$. As (III) is more dominant in anoxic environments and As (V) is more dominant in oxic environments. Under anoxic, sulfidic conditions, up to 83% of total As may consists of thioarsenites and thioarsenates (Kruger et al., 2013). Another important factor in behavior of As is the oxidation-reduction potential (ORP). As (V) is more dominant under all conditions in redox sequences above the ORP

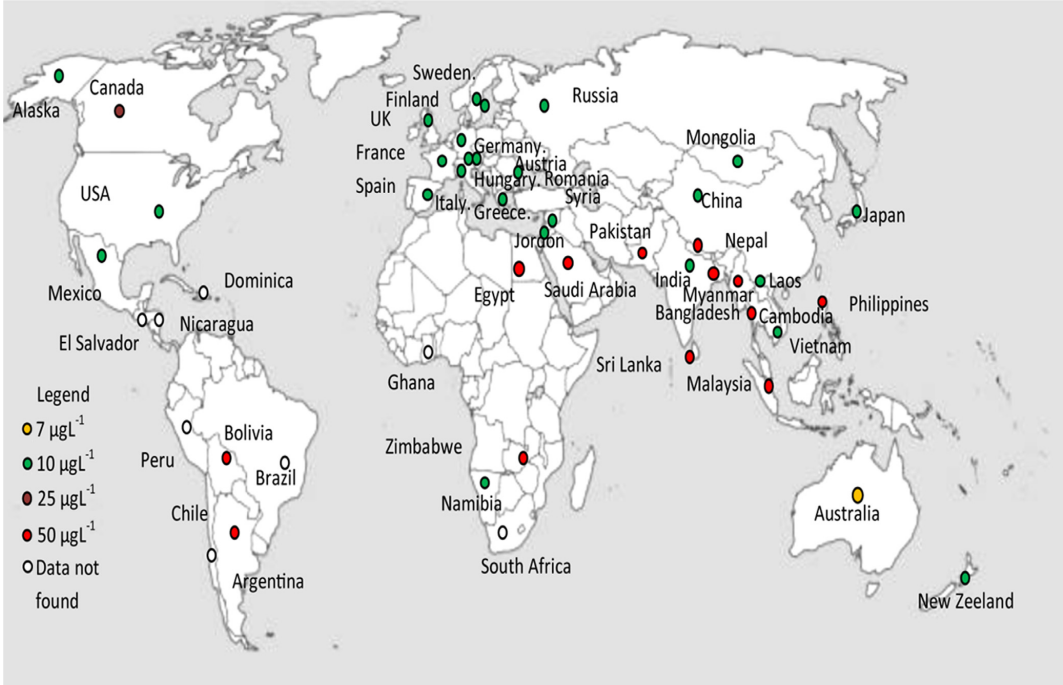

Figure 1.1: Map showing As contamination in different countries and their respective maximum contamination level (MCL) (Mondal et al., 2013).

of sulfate-reduction (Wolthers, 2003). Although arsenopyrite (FeAsS) is the most abundant mineral of As, realgar (AsS) and orpiment (As_2S_3) are the two reduced forms of As.

Ferric iron oxyhydroxide and amorphous and crystalline Fe- sulfide minerals are strong adsorbers of As and can control As mobility (Egal et al., 2010; Kocar et al., 2010). Arsenate sorption on Fe and Al-hydroxides and clay minerals is maximum in the pH range 3 to 7 and drops at high pH. Similarly arsenite adsorption increases up to pH 9. However, arsenite adsorption is often greater than arsenate on amorphous Fe-oxides, at pH above 7 and thus is more strongly bound to soil components(Goldberg, 2002; Manning & Goldberg, 1997). Experiments by Farquhar et al. (2002) indicated that mackinawite (FeS) is more effective in removing As from a prepared solution, than iron oxides, and there was no significant difference in uptake between arsenate and arsenite (Farquhar et al., 2002).In typical ground-water evolution, after reduction of manganese minerals and hydrous ferric oxides, sulfate reduction occurs. During this process, the resulting sulfide reacts with any available Fe (II)

to form iron sulfides. Arsenic (V) reduction would normally be expected to occur after Fe (III) reduction and before sulfate reduction (Wolthers, 2003).

Mackinawite (FeS) is the first iron sulfide that is produced in most natural aqueous environments, and with time it reacts to form more stable sulfate phases, such as pyrite (FeS_2) (Wolthers, 2003). The unique crystal structure of mackinawite allows for the incorporation of considerable amounts of other transition metals and trace elements such as As. It has a tetragonal layer structure and the iron atoms are located in a tetrahedral coordination to four sulfur atoms (Figure 1.2). Reaction of aqueous sulfide (-II) solution with Fe (0), Fe (II) or via sulfate-reducing bacteria metabolism are different ways of forming mackinawite at low temperature (Wolthers, 2003). Arsenic also can be present in impurities that occur in natural pyrite (Wolthers, 2003). Pyrite is the most common form of sulfide minerals and can be found in many different geological settings. Understanding pyrite surface characteristics and reactivity has been the main goal of many researches (Scott et al., 2007). Figure 1.3 shows the minimum and maximum concentration of trace elements in pyrite. Arsenic, Co and Ni are most common trace elements in low temperature pyrites (Huerta-Diaz & Morse, 1992; Saunders et al., 1997). Studies show that adsorption of As on the surface of sulfide minerals, such as pyrite, is important for As removal from water (Saunders et al., 2008). In a research by Blanchard et al. (2007), incorporation of As into pyrite was studied and suggested that As substitution for S is more energetically favorable rather than for Fe.

1.1 Sulfate-reducing bacteria

Sulfate-reducing bacteria (SRB) are anaerobic microorganisms that use sulfate as a terminal electron acceptor and form aqueous sulfide by reducing sulfate (Muyzer & Stams, 2008). Many species of SRB, notably genus *Desulfovibrio*, are gram negative rods. They can use hydrogen and some simple organic compounds such as acetate as their energy source (Chapelle, 1993). These bacteria can use sugars, polysaccharides, organic acids such as

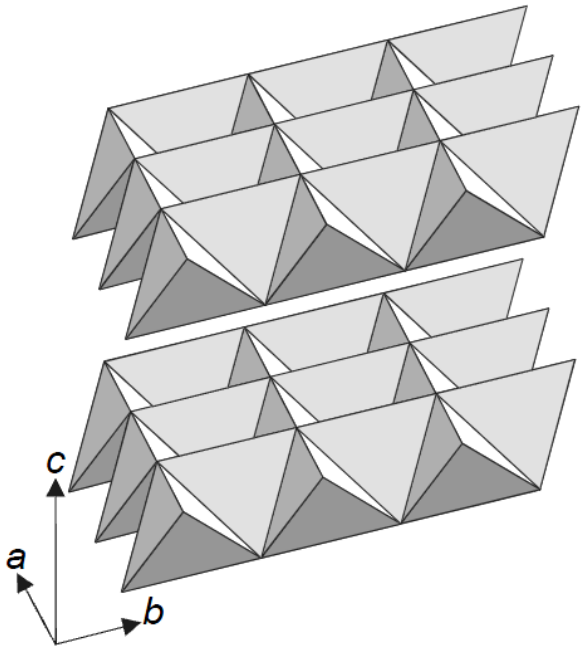

Figure 1.2: Structure of mackinawite, from Wolthers (2003).

acetate, lactate, formate, and proteins as their carbon source. Glucose is the most preferred carbon source by *Desulfovibrio* (Chapelle, 1993).

Anaerobic SRB are known for their ability to influence iron-sulfur systems in nature. SRB can make iron sulfide minerals precipitate in sediments (Saunders et al., 2005b). They require organic carbon for their metabolism, and they are capable of catalyzing reactions such as sulfate reduction. Sulfate reduction occurs in reducing conditions (redox potential approximately below -100 mV), in presence of sulfate, and it controls cycling of iron in these environments (Rittle et al., 1995). Geochemical evidence implies that As accumulation in many naturally As-contaminated aquifers only occurs if the activity of SRB is limited by low sulfate concentration (Kirk et al., 2010). If these bacteria have access to reactive organic carbon, can lead to precipitation of metal sulfides (Southam & Saunders, 2005).

In this project, a mixture of water, organic carbon, ferrous sulfate, and agricultural grade fertilizer were injected into an As-contaminated aquifer, through two injection wells, to stimulate SRB metabolism. Molasses which is made of thirty to fifty percent sucrose and is a

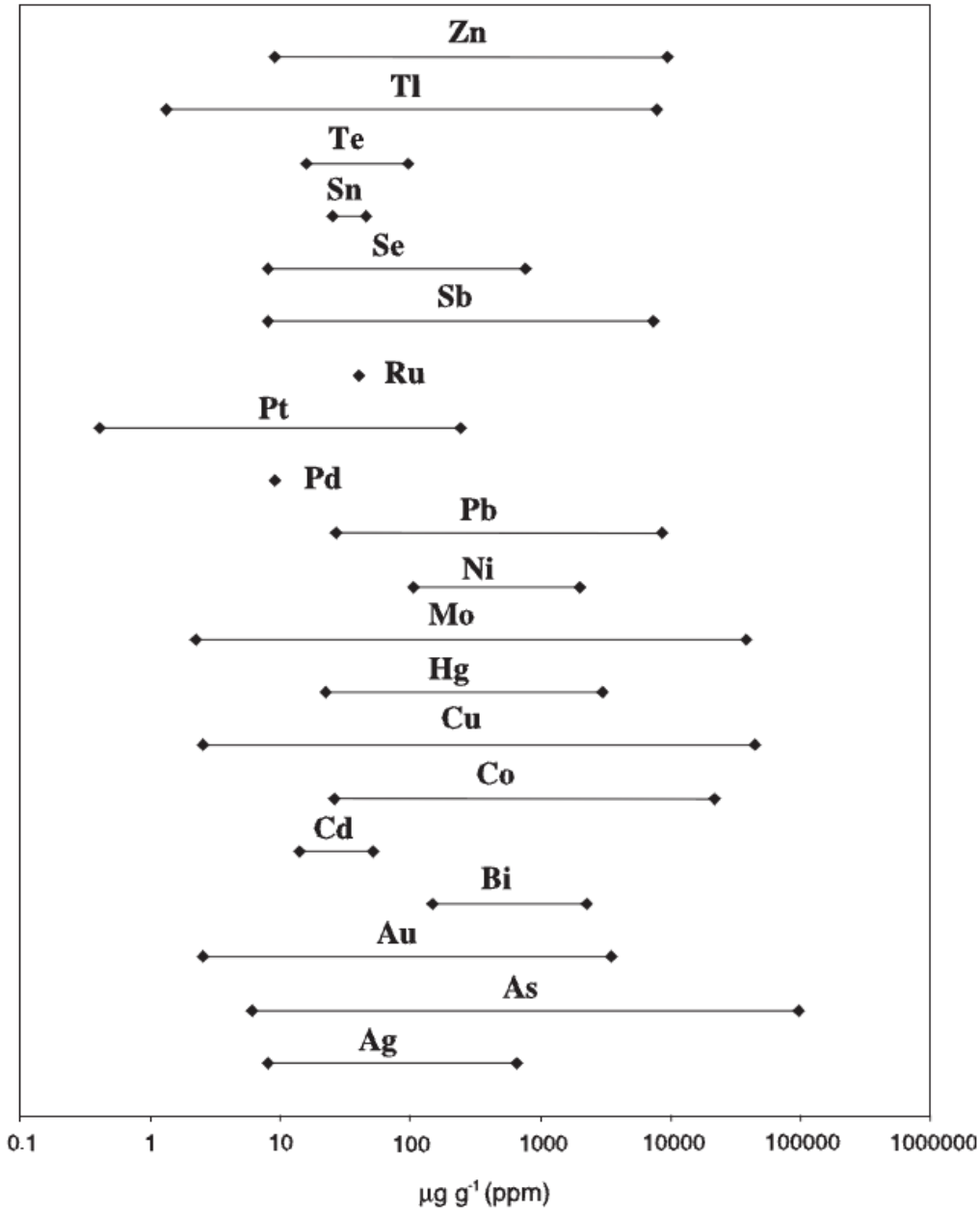

Figure 1.3: Plot of detectable range of concentration of different trace elements which can be found in pyrite, from Abraitis et al. (2004).

relatively inexpensive material serves as the organic carbon that was injected into the aquifer. Sucrose is relatively easily biodegraded (Annachhatre & Suktrakoolvait, 2001) and was used by Saunders et al. (2005a) in another bioremediation field experiment. Based on previous studies, if biogenic sulfate reduction can be engineered by treating the groundwater with

appropriate electron donors, such as organic carbon, and acceptors (e.g., sulfate), remediating As-contaminated groundwater by sorption on to sulfide minerals should be possible and relatively irreversible (Bostick & Fendorf, 2003; Saunders et al., 2008; Omoregie et al., 2013).

This thesis conducts geochemical studies in conjunction with a field bioremediation demonstration experiment at an industrially contaminated site, and evaluates the progress of the As removal along with data from our weekly and monthly monitoring of the site. This research also focuses on investigating the capability of iron sulfide bio-minerals formed in nature to mitigate As mobility and the long-term behavior of the groundwater system after injections. There are still uncertainties about the geochemistry of low-temperature sulfide minerals, and this study can help us better understand how microbial community and characteristics of the environment can affect iron sulfide mineralogy.

Chapter 2

Background

2.1 Site History

The study site is located in Bay County, Florida. Bay County is situated in the central Florida Panhandle. The annual average temperature is 68 °F. The highest amount of precipitation occurs in July, August, and September and the average annual rainfall is 58 inches (Schmidt & Clark, 1980). Arsenic-rich herbicides, containing As trioxide, were used extensively in this industrially contaminated area to control plant growth at the site. As a result, both soil and groundwater were contaminated with As. The site has been gone through extensive contamination assessment and analysis from 1989 to 1993, which showed the contamination extended out of the boundaries of the property to the north and west (Starnes, 2015). Analyses of initial water and solid samples have indicated the presence of SRB, suggesting that they are removing As to a limited extent. A semi-confining unit is located at 20 feet below the surface level, and it is situated below calcareous material of Jackson Bluff and intracoastal formations. In this site, silt increases with depth and therefore the hydraulic conductivity decreases with depth. Soil at the site, mostly consists of brown to black fine-quartz sand (organic-rich) with layers of white quartz sand and gravel. Slug tests have shown that the conductivity of the aquifer is between $2.5 \times 10^{-4} - 7.4 \times 10^{-6}$ $\frac{ft}{Sec}$ (Patel, 1989).

In 1989, samplings from the groundwater indicated that the highest As concentration occurred between LH-2 and LH-3 (2.06 and 3.89 $\frac{mg}{L}$ respectively), which are close to the area that was treated with herbicides. Alkalinity was low in the site (less than 1-51 $\frac{mg}{L}$ $CaCO_3$) and groundwater was slightly acidic (5.6-6.7). Fe and Al oxides in the soil were detected,

which cause the soil capacity for adsorbing As to be high. Kaolinite and illite are effective in adsorbing As to some extents (Patel, 1989).

770 cubic yards of soil was removed and was disposed in a nonhazardous waste landfill, in 1992, which decreased the As concentration from 30-70 percent. During 1994-1999 a pump and treat system was used with a combination of iron co-precipitating, ceramic membrane filtration, and soil flushing with selected reagents. These operations were not successful in lowering the As concentration below Florida Department of Environment Protection (FDEP) and EPA levels, and therefore they were stopped. In 2008, the last excavation was conducted along the 11th street and impacted soil was removed. A monitoring program began at the site afterward with FDEP approval (Starnes, 2015). Figure 2.1 shows the map of the study area in Bay County.

2.2 The Geologic Background

The Florida platform basement rocks consists of Precambrian- Cambrian igneous rocks, Ordovician- Devonian sedimentary rocks and Triassic- Jurassic volcanic rocks and they underlie a landscape that is mostly flat-lying (Scott, 2001). The few studies that have been conducted specifically on Bay County divide the area into four physiographic divisions, which have been formed on marine terraces and developed during the Pleistocene as a result of sea level fluctuations, including: The Sand Hills, Sinks and Lakes, Flat-Woods Forest, and Beach Dunes and Wave-cut Bluffs (Schmidt & Clark, 1980). Figure 2.2 shows the location of each of these physiographic divisions (Schmidt & Clark, 1980)

The Sand Hills are erosional remnants of the higher marine terraces and are located in the north of Bay County. Sinks and lakes consist of numerous sink holes and sink-hole lakes. Solution of underlying limestone and collapse of overlying material into the formed hole has created this physiographic division. Most of these lakes have drainage to the underlying aquifer. Near the Gulf coast the Beach Dunes and Wave-Cut Bluffs division is located, which has the youngest sediments in the basin and are changing rapidly (Schmidt & Clark, 1980).

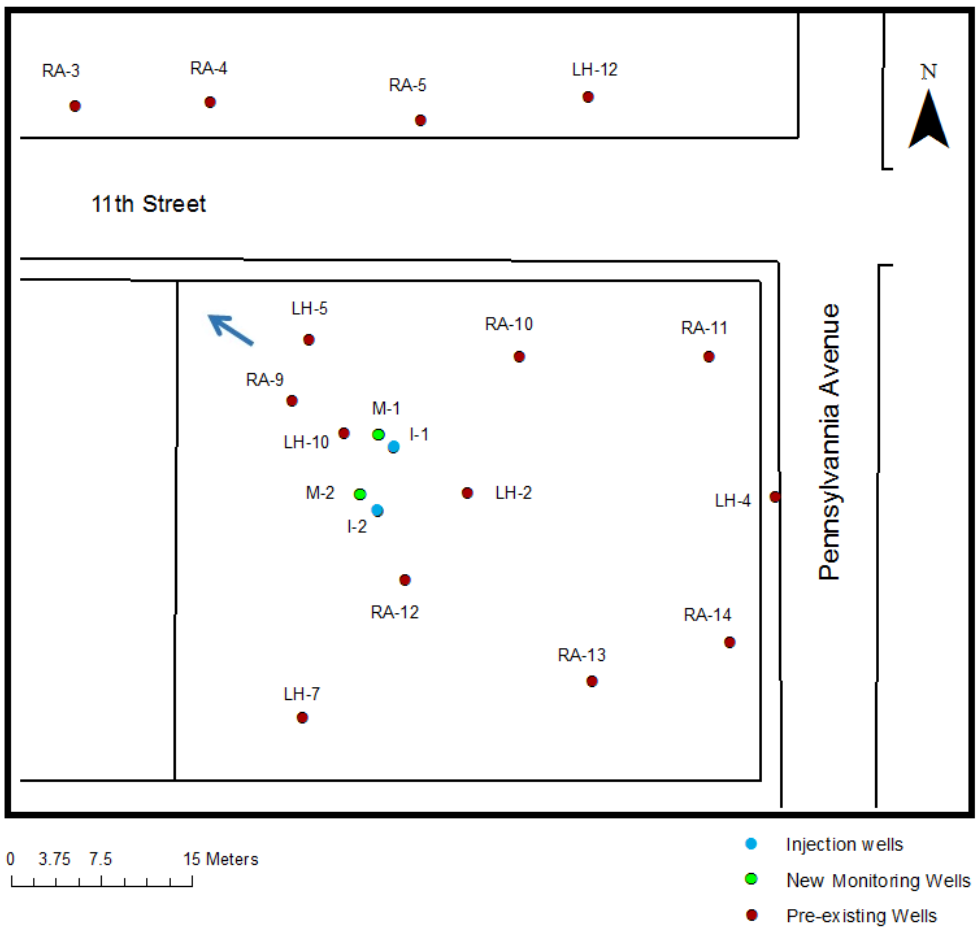

Figure 2.1: Map showing the locations of all the wells at the site (The blue arrow shows groundwater flow direction).

The present study area is located in the Flat-Woods Forest division, which occupies the largest portion of the county. The area is usually covered with pines and is well drained. There are a few small perennial swamps in the flat-woods forest. Terraces with elevation of less than 70 feet underlie these flat and slightly rolling lands. Heavy rainfalls can flood the low elevation areas in this physiographic division (Schmidt & Clark, 1980).

Bay County is located on the western part of the most important geologic structure affecting the county, which is the Apalachicola Embayment. Apalachicola Embayment is a shallow basin between the Ocala and Chattahoochee uplifts. In the northeast it is the

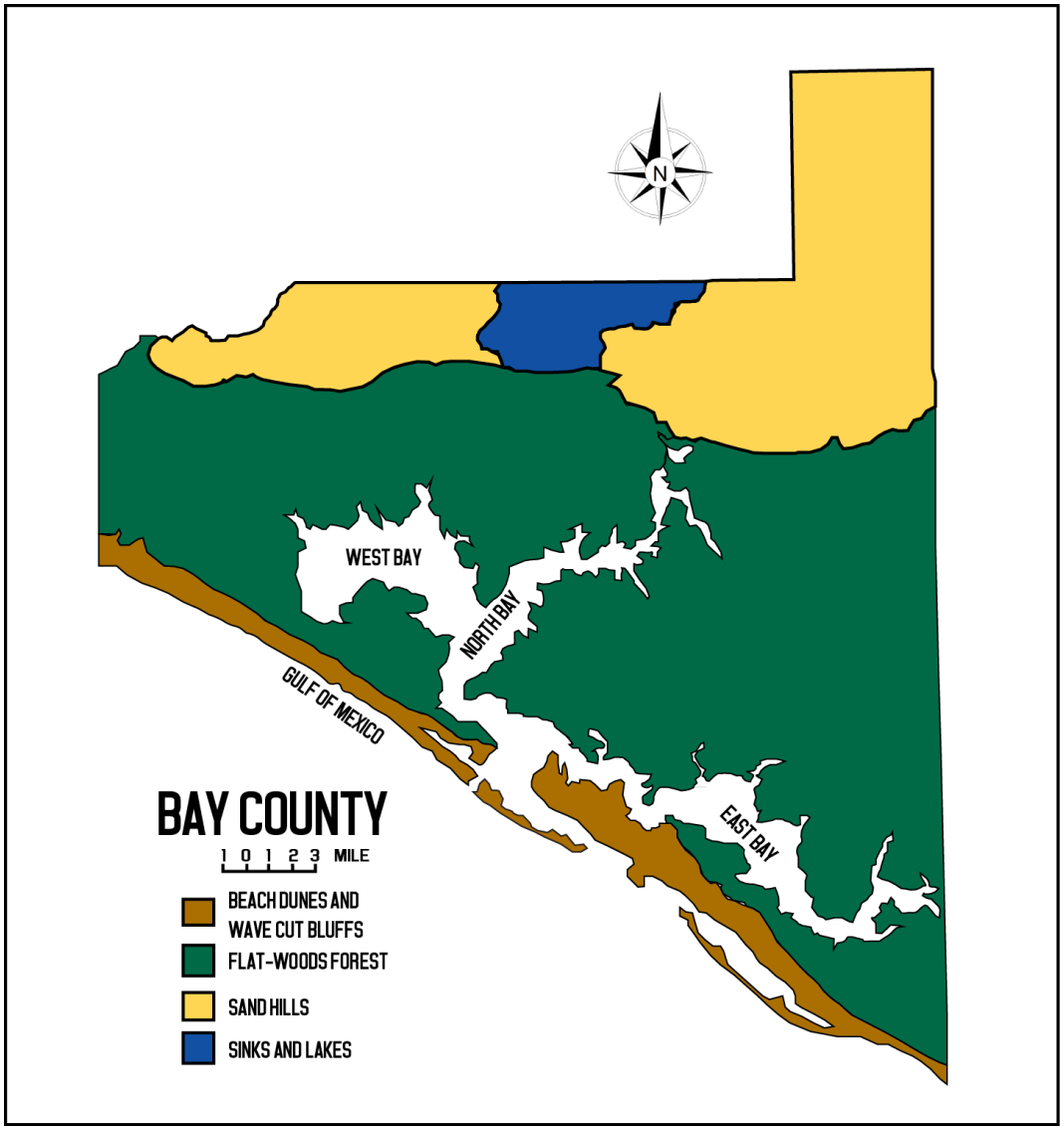

Figure 2.2: Map showing physiographic subdivisions in Bay county. Modified from Schmidt & Clark (1980).

narrowest and it gets wider to the southwest. The embayment has a northeast-southwest trend (Schmidt & Clark, 1980). Four faults have been reported in Bay County in the upper limestone of the Floridan Aquifer and overlying clays, shell beds and sands. Figure 2.3 shows the important geologic structures near Bay County.

The Chipola Formation is the oldest rock exposure in the Bay County, which consists of Early Miocene limestones. The age of the rocks that underlie the county is between late

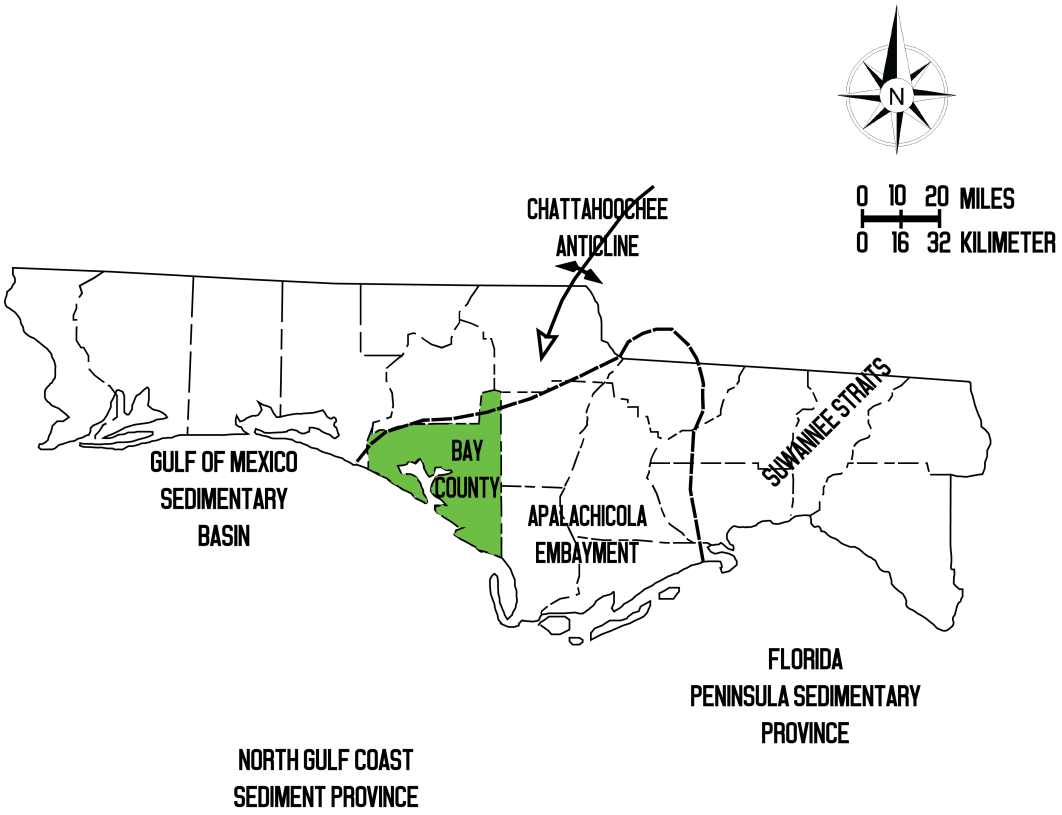

Figure 2.3: Map showing important geologic structures near Bay County. The arrows show the axis of Chattahoochee Anticline. Modified from Schmidt & Clark (1980).

Pre-Cambrian to Recent. The young sands cover the limestone units that are up to 3000 feet deep, and these limestones overlie sandstones and shales (Schmidt & Clark, 1980).

2.3 Hydrogeology

Bay County has both unconfined (the water-table) and confined (the Floridan) aquifers. Quartz sand and gravel, with clayey sand and sandy clay lenses are the main constituents in the unconfined aquifer, which can approach 150 feet in thickness along the coast. The water in this aquifer has high amounts of iron and is slightly acidic. The water table in this aquifer ranges from close to surface to a depth of 65 feet, and the sediments are from Pliocene to Recent sand units (Schmidt & Clark, 1980). Figure 2.4 shows the hydrogeologic units present in Bay County. The rainfall is adsorbed by the sandy surface and penetrates

to the unconfined aquifer. This water eventually discharges through streams and springs, and some of it percolates downward into the clay and sandy shale unit.

The Floridan Aquifer consists of limestone and dolomite and the water moves generally in a southwest direction toward Gulf of Mexico. Limestones near the surface in the north of Bay County are the source of recharge for this aquifer. The potable zone of this aquifer is between 250 to 1000 feet in depth. In 1967, most domestic supplies changed from Floridan aquifers to a surface water supply, due to declining water levels and salt-water intrusion potential (Schmidt & Clark, 1980).

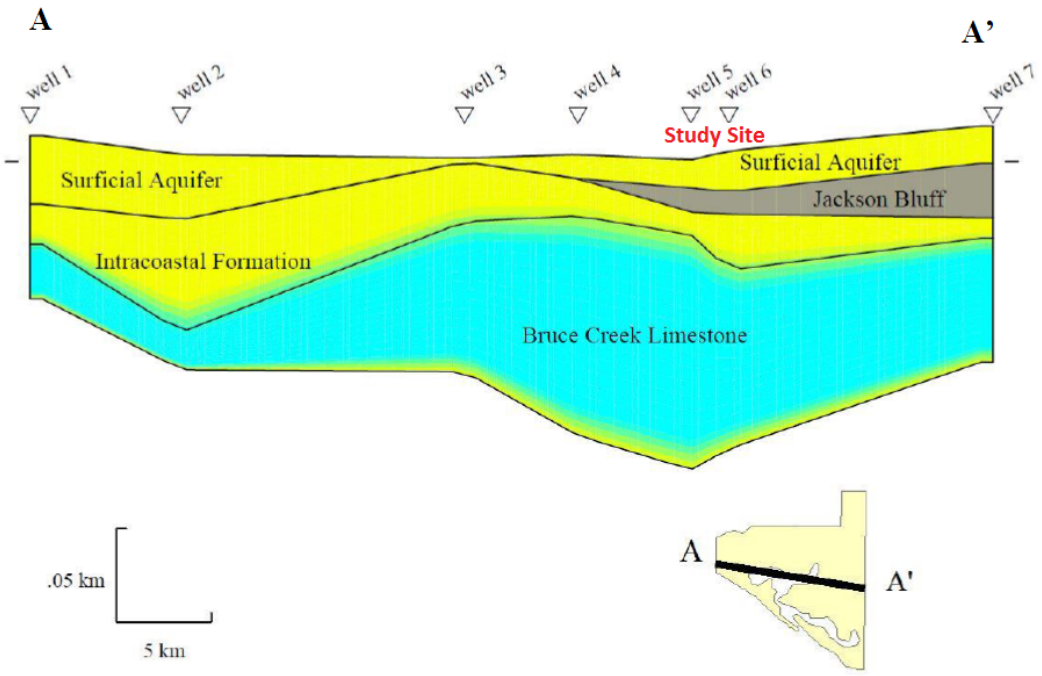

Figure 2.4: Hydrogeologic cross section, showing principal units in Bay county from west to east, from Starnes (2015).

Chapter 3

Previous Studies

Saunders et al. (1997) conducted an investigation on an alluvial aquifer in Alabama, which contained elevated levels of Co , Ni , As, Zn , Ce and Ba . They found a correspondence between trace elements in the groundwater and the black ferromanganese coating on alluvium in the study area. They also found autheigenc euhedral pyrite crystals that had replaced lignitic wood fragments in the aquifer. SRB involvement in pyrite formation was confirmed using sulfur isotope studies, in the precipitated pyrites in the study area. The pyrite contained high levels of As, Co, and Ni which demonstrated the co-precipitation of these trace elements in pyrite during bacterial sulfate reduction. Therefore, they concluded that SRB, using organic products from bacterial degradation of wood fragments, which reduced sulfate to hydrogen sulfide, caused the formation of pyrite around lignitic wood. Arsenic and other trace elements co-precipitate with the pyrite in this process. This study actually indicated that SRB could potentially be used to remove these trace elements from contaminated water. Therefore, in 1998, Saunders patented a bioremediation process that employed the geochemical effects of SRB metabolism to remove metals, radionuclides and metalloids from groundwater.

In another study, Kirk et al. (2004) proposed that SRB produce sulfide that reacts with iron and forms pyrite, and during the process, As co-precipitate with it. They also proposed that in the absence of SRB, the dominant metabolism in the groundwater is methanogenesis that cause the accumulation of As to high concentrations. Their results suggested that low sulfate content can cause elevated levels of As, also less iron is detectable when sulfate is present and methane generally follows the same pattern (Figure 3.1). Saunders et al. (2005b) proposed a Geo-Bio-Hydro (GBH) As model that explained how As can naturally

contaminate shallow groundwater in alluvial aquifers, and how SRB were significant in As geochemical cycling in Southeast Asia.

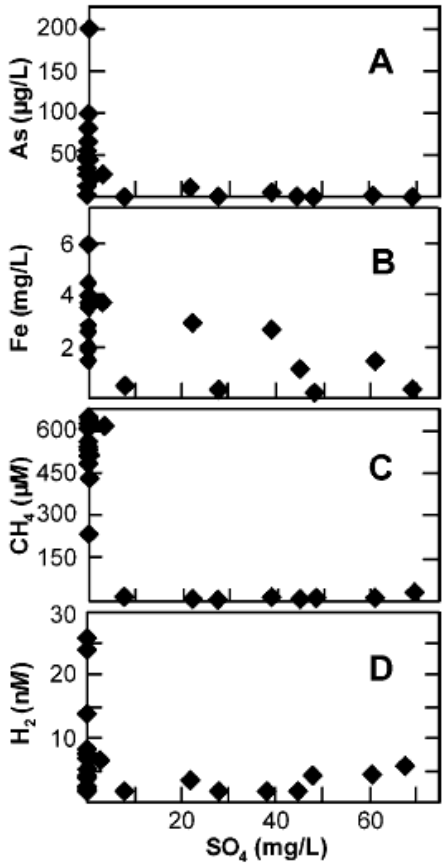

Figure 3.1: Plots showing changes in As (A), Fe (B), methane (C), and dihydrogen concentration in water samples with sulfate concentration from, Kirk et al. (2004).

Another study conducted by Lee et al. (2005) indicated that reductive dissolution of hydrous ferric oxides (HFOs) is the main reason that causes release of As under neutral pH conditions. They also showed that As(V) sorbs onto protonated sites of HFO in pH range of 3 to 6, and As(III) sorption increases with increase in pH. However, As (III) desorbs at very low oxidation state. Therefore, they proposed that As is immobile under sulfate-reducing conditions and mobile under Fe-reducing conditions. Later, Keimowitz et al. (2007) confirmed the results from the Lee et al. (2005) study.

Saunders et al. (2005a) conducted a field-scale bioremediation process using SRB in an area with high levels of Pb, Cd, Zn, Cu and sulfuric acid with a pH of 3.1, where the contaminants were derived from a car-battery recycling plant. Genetic assays demonstrated that the dominant SRB involved in the process of bioremediation was *Desulfosporosinus orientis*. The injection solution that they used contained sucrose, diammonium phosphate and water and they injected the solution into the groundwater system three times with different portions of ingredients. Their investigations indicated that the bacteria can be stimulated to remove metals by injection of electron donating substrates into a contaminated aquifer, by making sulfide minerals of Fe, Cd, Zn, Pb and Co.

In a study by Saunders et al. (2008), two bioremediation projects were conducted. The first project was conducted in Bangladesh, where complex water-sediments-bacteria interactions in alluvial aquifers were investigated. Their injection solution consisted of molasses and magnesium sulfate. They were successful in decreasing the As concentrations in the injection wells five months after injection was done. They also studied the behavior of As under artificially induced Fe-and sulfate-reducing conditions. As decreased drastically when sulfate-reduction began, however it increased to background levels when sulfate reduction stopped (Figure 3.2).

In their second project in the United States, they worked on bioremediation of an industrial site that was contaminated with Zn, Cd, and sulfate in Oklahoma which was under oxidizing conditions. To stimulate the sulfate-reducing bacteria metabolism they injected a mixture of sucrose and methanol into the groundwater. Dissolved Fe and As concentration increased at the site shortly after the injections due to establishment of Fe-reducing conditions. When the conditions got more reducing and sulfate-reduction increased, concentration of As, Cd, and Zn decreased, due to precipitation of metal sulfides. After six month dissolved As concentration increased to background levels. They proposed that adsorption of As on sulfide minerals can play an important role in As removal by biogenic

sulfate reduction. And they also proposed the possibility of bioremediation and removing As using SRB under field conditions.

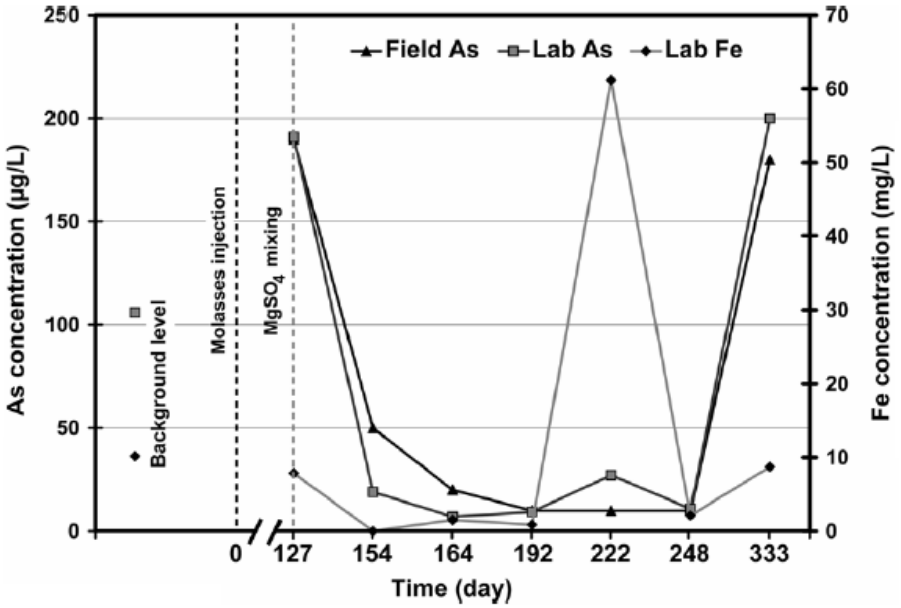

Figure 3.2: Plot showing As and Fe concentration at Bangeladesh site. Injection of molasses increased the dissolved As concentration at the begining of the process, but decreased drastically afterwards, from Saunders et al. (2008).

DeFlaun et al. (2009), investigated the stability of As precipitates formed by microbial sulfate reduction. They designed a lab experiment and then applied their experiences from the lab experiment to a field research. Sodium lactate, ethanol, ferrous iron and sulfate were injected to an anaerobic environment. As-bearing sulfides were present in the analyzed sediments and they were successful in decreasing As concentrations by almost ten times in the lab experiment. After changing the anaerobic conditions of the experiment to aerobic, they observed that only 2 percent of the sequestered As was redissolved.

The results from the lab experiment encouraged them to design a pilot field demonstration for this method. Adjustments were made on the injection solution to make the groundwater condition more reducing and their final injection solution was consist of sodium

lactate, sodium sulfate, and diammonium phosphate. In a period of six month a significant decrease in As, iron, and sulfide concentration was observed. Analysis of sediment samples also confirmed the As increase and being associated with iron and sulfide in solid phase. Based on the results in their lab experiment and in the field demonstration, they concluded that fine-grained assemblage of Fe and As-bearing sulfides minerals are resistant to dissolution under aerobic conditions (DeFlaun et al., 2009).

Another lab experiment was conducted by Onstott et al. (2011) to examine the mobility of adsorbed As after going through an in-situ bioremediation. They collected As-contaminated groundwater and sediments from a field site in Florida and circulated the groundwater through columns that were filled with the collected sediments. Mixture of groundwater with Na_2SO_4, ethanol, lactate, $(N_4)_3PO_4$, and NaBr was injected into columns to stimulate sulfate-reducing bacteria. Arsenic concentration decreased in the groundwater as a result of As-sulfide precipitations. They used K_2HPO_4 and H_2O_2 to create an iron phosphate coating that was previously suggested that can protect sulfides from oxidation. $MgSO_4$, NaOCl, Na-acetate/acetic acid, ammonium oxalate, hydroxylamine and HCl solution, and aqua regia was added into sediment samples from one column in order to observe As behavior after extraction of adsorbed species, organic species, carbonate species, amorphous Fe oxide phase, crystalized Fe oxide phase, and sulfide phase respectively. The phosphate coating was not useful in protecting the iron sulfides since the As release from the treated samples with K_2HPO_4 was 3-4 times higher than untreated samples.

The results from by Onstott et al. (2011) once again indicated the possibility of As removal under sulfate-reducing conditions and also suggested that the precipitated As-bearing sulfides are resistant to dissolution under aerobic conditions. The dominant As phase was arsenopyrite and minor realgar (based on the modeling results). Possible released As due to oxidation of sulfide minerals, under aerobic conditions, converted to AsO_3^{4-} that could be adsorbed to ferric iron oxyhydroxides that were formed by iron-sulfides oxidation.

In another study, Kirk et al. (2010), conducted a lab experiment using anaerobic flow bioreactors to investigate partitioning of As into As-and Fe-sulfide minerals. The medium was used, had a composition close to natural As-contaminated aquifers and contained acetate. They used a reactor with As(V), Fe-oxide and sulfate (As-Fe-S reactor), one with only As(V) and sulfate (As-S reactor), and another that was the sterile reactor with As(V), Fe(III) oxide and sulfate to show the abiologic condition. To stimulate pyrite formation, they also added a polysulfide solution to the reactors. Their results indicated that in Fe-limited conditions pure As-sulfide minerals did not form. Although orpiment was theoretically saturated during the experiment, slow kinetics perhaps prevented its precipitation while sulfide content was low. Fe-bearing reactor created an environment that caused the mackinawite to form rapidly and consumed the dissolve sulfide. Mackinawite formation in the reactors indicates that its precipitation kinetics are rapid, its stability field is broad, and it requires lower sulfide concentration than most As-sulfides.

In the Kirk et al. (2010) experiment not much As was adsorbed to mackinawite, and microbial reduction of Fe(III) led to release of As from goethite. Pyrite did not form before the injection of tetrasulfide in the reactors, which caused a small amount to precipitate. They concluded that the As-sequestration is most likely associated with pyrite formation, not formation of initial Fe-sulfides such as mackinawite, because pyrite was more successful at adsorbing As. Their study seems to contradict results from previous publications that showed mackinawite was an effective adsorber of As. They also suggested that the reason they could observe more As uptake by pyrite than mackinawite is probably because the only mechanism for As uptake in mackinawite is adsorption, whereas As can be both adsorbed and substitute in the crystal structure of pyrite. They concluded that rate of spyrite formation and solubility of As-sulfides can affect the bio-remediation of As-contaminated water using microbial sulfate reduction.

More recently Burton et al. (2014) conducted a lab experiment on As-contaminated soils from Australia and created three different sulfate treatment conditions for their samples. They also added Na_3N to inhibit microbial activity in additional samples and created abiotic and biotic set of samples. They conducted XANES, SEM and TEM analysis on their samples, and observed that in the most elevated and medium sulfate treatments, As concentrations decreased during the first week. Subsequently, As started to increase, but increased at a lower rate in high-sulfate treatment condition. The TEM results indicated the presence of As-rich mackinawite in the biotic high-sulfate treatment samples. The adsorbed As on mackinawite was distributed homogenously whereas the existing As sulfides were spread unevenly, indicating that As was adsorbed to newly formed mackinawite. Porewater sulfate concentration decreased in the biotic treatment, which was due to microbial sulfate reduction that led to the production of H_2S that reacted with Fe^{2+} and produced mackinawite. They observed greater microbial sulfate reduction in the medium and high-sulfate treatment samples, which they proposed could be the reason for lower levels of As mobilization in comparison to the low-sulfate treatment. Therefore, they believe that microbial sulfate reduction under Fe^{2+}-rich conditions can help to decrease As mobility in flooded soil. They suggested a range of different ways that microbial sulfate reduction may lower As mobility: 1) microbially-generated H_2S can react with soil organic matter and create organic thiol groups (C-SH) which can later form complexes with As; 2) formation of orpiment by direct reaction of As and the microbially produced H_2S ; 3) adsorption of As to mackinawite which forms by reaction of microbially- produced H_2S and Fe^{2+}.

Because the first two paths occur mostly in environments with low Fe^{2+} concentration, and the Fe^{2+} concentration in this study is high, the only major reason for lowered As mobility is through sorption to mackinawite. Although in many other studies, mackinawite was proposed as a major sorbent of As in sulfidic systems, there has been little microscopic evidence to substantiate that. Burton et al. (2014) provides microscopic evidence that confirms sorption of As to mackinawite in such systems (Figure 3.3). These results are in contrast to

some previous studies such as Kirk et al. (2010), which the Burton et al. (2014) believe can be due to the differences in complexation of As oxyanions at low loadings that were used in previous studies, to the stronger As-S bonds at higher loadings in their research. This study is the first to prove As sorption on mackinawite in natural soil.

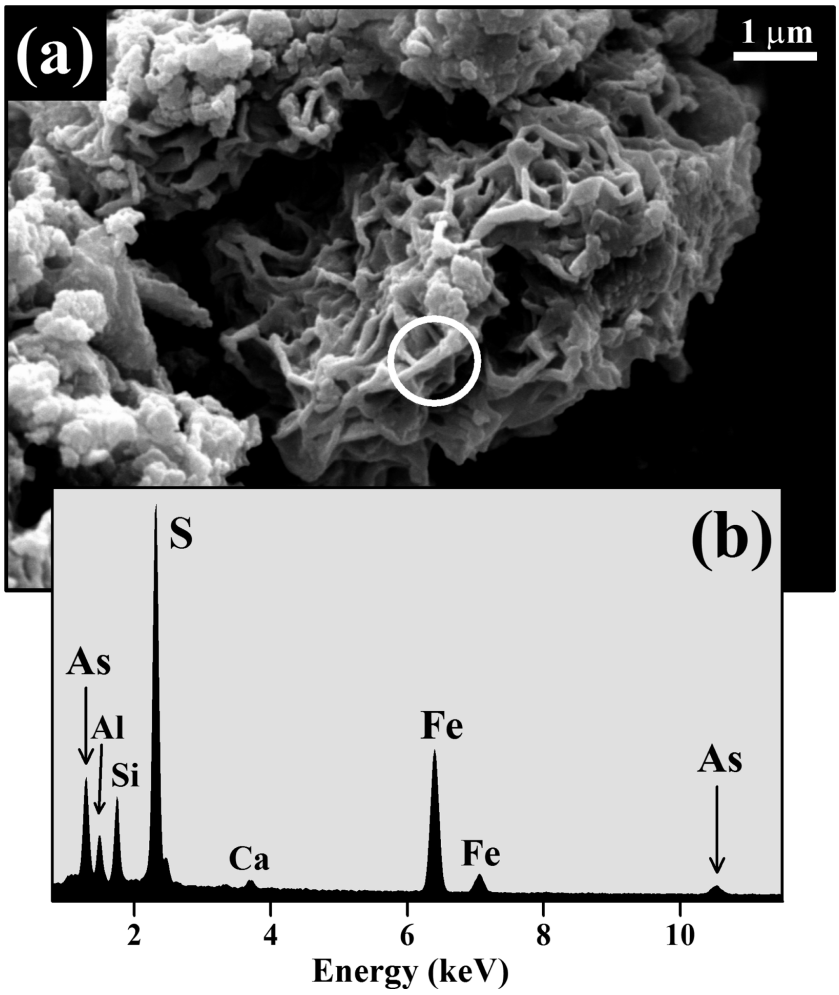

Figure 3.3: a) Scanning electron micrograph and (b) EDX spectra showing an As-bearing FeS particle formed after 10 weeks in the biotic high SO4 treatment from Burton et al. (2014).

Chapter 4

Materials and Methods

4.1 Sample Collection and Water Quality Measurements

During January 12th through 14th 2016, Shahrzad Saffari, Eric Levitt, and Dr. Ming-Kuo Lee of Auburn University, traveled to the study area in Florida. Four new wells were drilled using hollow-stem auger (HAS)/mud rotary. The drilled cores were collected in aluminum bags, sealed, and carried in the cooler with dry ice. These solid samples were frozen and kept at freezer at CASIC building in Auburn University.

Two of these four new wells are injection wells (I-1 and I-2), with 4 inches in diameters, and two other wells, are monitoring wells (M-1 and M-2) and they are 2 inches in diameter. The total depth of these wells is 20-25 feet and the casing material is PVC. Two injection wells were installed in the area of high dissolved As concentration inside the property, and they are almost 5-6 feet apart from their relative monitoring wells. Simple volume balance calculations show that the total injection volume of 3000 gallons will displace all pore water residing in the aquifer (with thickness of 20 feet and porosity of 0.35) within 5-6 feet away from injection points. In addition, the calculations showed that dissolution of 5 Kg of $FeSO_4$ in 1000 gallon of water (the strong solution), would create a solution with Fe concentration of almost 485 $\frac{mg}{L}$, which is not much higher than the secondary drinking water standard of 0.3 $\frac{mg}{L}$ (considering the dilution in the groundwater and consequent pyrite precipitations). During Febraury 15th to 19th the team met at Florida site again for injection event. Our injection solution consisted of 1000 gallon of a strong solution and 2000 gallon of weak solution. The strong solution contained higher concentration of $FeSO_4$ than the weak solution. The injection solutions contained:

- 60 lb. of molasses per 1,000 gal. of water
- 5 kg of $FeSO_4$ per 1000 gal. of water in the strong solution and 5 kg of $FeSO_4$ in 2000 gal. of water in the weak solution
- 2 lb. of agricultural grade fertilizer per 1,000 gal of water

Table 4.1 and Table 4.2 show the detailed information about the four newly installed wells and the injection solution respectively. The ingredients were mixed in a 250 gallon plastic tank and carried out to the site. The injection solution was then gravity fed to the wells. The tank was refilled each time with the ingredients. Each day the tank was emptied and refilled several times, and the whole process of injections took 4 days.

Solid sediment samples precipitated from groundwater were collected from bottom of the wells using a peristaltic pump. The solid samples were collected in a 50 ml centrifuge vials and then were frozen on dry ice to preserve the redox state of chemical species in the groundwater system. The same procedure was used for the microbiology samples. Microbiology samples were sealed in aluminum bags and were frozen, after being collected in the 50 ml centrifuge vials.

Table 4.1: Construction details for all injection and monitoring wells.

	Injection Wells	Monitoring Wells
Installation Method	hollow-stem auger (HSA)/mud rotary	HSA/mud rotary
Diameter of wells	4 inches	2 inches
Total depth of wells	20-25 feet bgs	20-25 feet bgs
Screened interval	0-5 to 20-25 feet bgs (total interval of 20 feet)	10-15 to 20-25 feet bgs (total interval of 10 feet)
Grouted interval	0 to 0.5-1 feet bgs	0 to 1-1.5 feet bgs
Casing diameter	10 inches	8 inches
Cased depth	1.5 feet ags to 0.5-1 feet bgs	1.5 feet ags to 1-1.5 feet bgs
Casing material	PVC	PVC
Injection interval	0-5 to 20-25 feet bgs	N/A

Table 4.2: Details about the injection solution for each injection well.

Injection volume	1000 gallons in I-2, 2000 gallons in I-1
Total injection volume	3000 gallons
Total daily design flow rate	Gravity feed, approximately 1 gallon per minute (gpm)
Fluid injected (Weak)	2000 gallon injection in I-1: 60 lbs of molasses; 2.5 Kg of $FeSO_4 \cdot 7\,H_2O$; 2 lbs of all Purpose 10/10/10 fertilizer per 1,000 gallons of water
Fluid injected (Strong)	1000 gallon injection in I-2: 30 lbs of molasses; 2.5 Kg of $FeSO_4 \cdot 7\,H_2O$; 1 lb of all purpose 10/10/10 fertilizer per 500 gallons of water

Groundwater samples from the aquifer were collected using the peristaltic pump. The wells were purged, until all the water quality parameters readings were stable and three well volumes of water were removed. Doing so, insured that the stationary groundwater inside the well casing is flushed out, and fresh groundwater samples were collected, which represent the geochemical characteristics of the aquifer.

While purging the wells the YSI 556 hand-held multi-parameter probes were measuring the water quality parameters including temperature, pH, dissolved oxygen, ORP, and electrical conductivity. When the readings for these parameters were stable the numbers were recorded. In YSI 556, the pH and the ORP electrodes are built together as a single probe and the ORP is read relative to the standard SHE, therefore, there is no need for converting the ORP readings to Eh values.

The water samples were collected in a clean beaker for each well, then filtered using a 0.45 micron filter, using a clean syringe and purged into three 30 mL vials. Another sample was first filtered with the 0.45 micron filter then filtered through As speciation cartridges to determine As speciation. Four vials were labeled as Arsenic speciation, ICP-MS (the inductively coupled plasma mass spectrometry), IC (Ion Chromatography), and dissolved organic carbon (DOC). The Arsenic speciation and ICP-MS samples were acidified using 5% nitric acid for preserving the trace metal and cation analysis using ICP-MS (Since May 19th sampling event 70% nitric acid was used to acidify the samples after observing the precipitation of some solids in the previously collected water samples). When using the As speciation filters, the first 5 mL of the filtrate was discarded before collecting the samples. Arsenic speciation cartridges contain an adsorbent that adsorbs the negatively charged As ions [such as As(V), $H_2AsO_4^-$] and allows the uncharged As complexes [As(III), H_3AsO_3] to pass through. The ICP-MS analysis of these two sets of samples will indicate the amount of total As and As(III) concentration in the water. A 250 mL water sample was also collected from each well for sulfur isotope study. After collecting the water samples they were kept with dry ice but remained unfrozen, until they were delivered to refrigerator in CASIC Building, in Auburn.

To measure the dissolved sulfide concentration, a HACH DR2700 spectrophotometer was used in the field, via the standard Methyl Blue Method (USEPA Method 8131). A HACH DR820 colorimeter was used to measure the ferrous iron concentration via 1.10 phenanthroline Method (USEPA Method 8146) in the field. To measure the alkalinity in the field we used the HACH digital titrator test kit, using the standard titration method (USEPA Method 8203).

4.2 Monitoring Schedule

After the injection, the groundwater was monitored weekly for one month, and after that, monthly. A total of 7 wells were sampled weekly, and ten wells were sampled monthly. Other

than the four newly installed wells (I-1, M-1, I-2, and M-2), three wells inside the property (RA-12, LH-2, and LH-10) were sampled weekly. Three wells from outside the property in the groundwater flow down gradient direction were also chosen to be monitored monthly (LH-5, RA-9, and RA-10). From the previously existing wells, those that were named LH are 2 inches in diameter and were used to monitor the surficial aquifer to prevent penetrating the Jackson Bluff confining layer. The RA wells are 6 inch in diameter and they were installed for recovery and injections for the pump and treat process. A parallel groundwater monitoring program was conducted by a commercial lab (Test America Laboratories, Inc.) using unfiltered groundwater samples.

4.3 Geochemical Analyses

The samples labeled with ICP-MS and Arsenic speciation, for all the sampling events were used to analyze the major cations concentration in the groundwater, using the ICP-MS (Agilent 7700) in Auburn University. Ten mL vials were filled with these samples and were ran under high He mode, to minimize the interferences with As and Fe atomic mass. The commercial lab ran ICP-MS and IC on the unfiltered samples.

Solid samples of groundwater precipitates were analyzed using XRF and XRD instruments, to identify the elements and the crystals inside the sediments collected from the bottom of the wells. XRD analyses was conducted using the Brucker D2 Phaser X-ray Diffraction spectrometer and the XRF analyses were done utilizing the Bruker X-ray Fluorescent Elemental Tracer IV-ED in the Department of Geocsiences at Auburn University. High energy X-rays bombards the sample and excites the atoms which then releases energy that is specific for each atom and by analyzing this energy XRF is able to identify the elements in the sample and quantify them. Major elements of the samples in the range of parts per million (ppm), were measured using XRF. For XRD analysis, samples were run from two theta values of 7 degrees to 65 degrees with a 0.02 degree step interval. DIFRAC.EVA software was used to determine the mineral composition of our samples. In an XRD analysis

the areas under the peak reflect the amount of each phase present in the sample which can give us an estimation of the quantity of the minerals.

4.4 Hydrogeologic Modeling

The hydrogeological modeling of the groundwater flow and contaminant transport was conducted by U.S. Geological Survey groundwater model MODFLOW (McDonald & Harbaugh, 1988) and MT3DMS (Zheng, 1990). Visual Modflow Classic and Visual Modflow Flex are two industry-standard programs in characterizing the groundwater hydrogeology of an aquifer by Schlumberger Water Services, and were used in this study to conduct the graphic interface modeling. The numerical models of groundwater flow at the site were generated by Starnes (2015), using the measured field hydrogeologic parameters and the data provided in previous studies (Starnes, 2015). The model generated by Starnes (2015) was modified to be able to represent the conditions of the aquifer after injection of 3000 gallons of injection solution in one year.

Chapter 5

Results

5.1 Field Measurements

Tables 5.1-5.7 list the in-situ measurements that were conducted during the monitoring events, for each well. In-situ measurements are presented in Table 4.1 during all the sampling events in 2016. The average water temperature in all seven wells has increased, from February until May. The average temperature for all the wells before the injections was 19.3 °C and the median groundwater temperature was 19.6 °C with a standard deviation of 1.33. As the weather got warmer as a result of seasonal changes the average temperature reached to 22.8 °C, the median was 22.7 °C with the standard deviation of 0.71 (Figure 5.1).

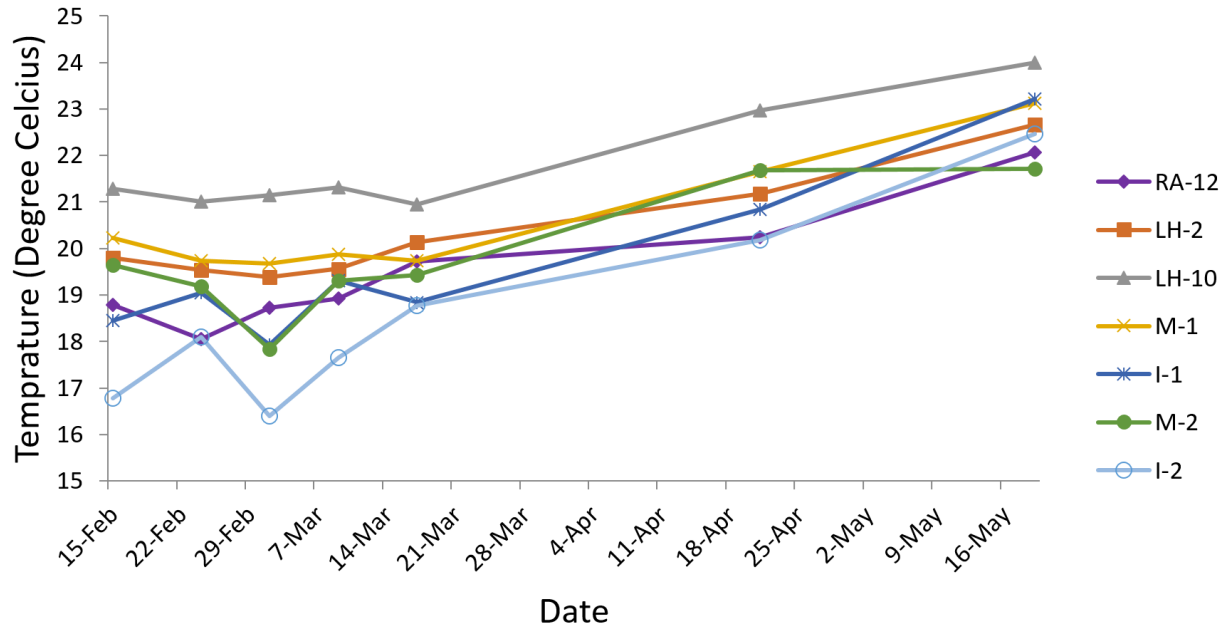

Figure 5.1: Plot showing temperature during the sampling events, three month after the injections.

Table 5.1: Field measurements during the first three months for well RA-12.

Date	Temperature (°C)	pH	ORP (mV)	Conductivity (mS/cm)	DO (mg/L)	Alkalinity (mg/L)	Fe(ferrous) (mg/L)	Dissolved sulfide (ug/L)
15-Feb	18.79	5.53	49.5	0.25	0.13	26	1.37	23
24-Feb	18.05	5.27	5.9	0.2	0.11	26	1.32	39
2-Mar	18.72	6.4	73.4	0.2	0.26	23	1.14	24
9-Mar	18.93	5.46	137.4	0.21	0.27	25	0.81	12
17-Mar	19.72	5.29	-23	0.21	0.4	25	1.29	87
21-Apr	20.24	5.54	-15.7	0.2	0.21	25	1.37	481
19-May	22.06	5.59	45.1	0.15	0.28	32	1.34	52

Table 5.2: Field measurements during the first three months for well LH-2.

Date	Temperature (°C)	pH	ORP (mV)	Conductivity (mS/cm)	DO (mg/L)	Alkalinity (mg/L)	Fe(ferrous) (mg/L)	Dissolved sulfide (ug/L)
15-Feb	19.8	5.45	15.5	0.11	0.17	16	0.49	36
24-Feb	19.54	5.66	-25	0.11	0.12	22	0.46	32
2-Mar	19.39	5.67	21.3	0.11	0.11	17	0.65	240
9-Mar	19.56	5.34	69	0.11	0.1	16	0.68	284
17-Mar	20.14	5.4	-51	0.11	1.15	17	0.68	239
21-Apr	21.18	5.55	-64.3	0.12	0.21	22	0.75	1173
19-May	22.67	5.35	14.4	0.11	3.34	16	0.79	319

Table 5.3: Field measurements during the first three months for well LH-10.

Date	Temperature (°C)	pH	ORP (mV)	Conductivity (mS/cm)	DO (mg/L)	Alkalinity (mg/L)	Fe(ferrous) (mg/L)	Dissolved sulfide (ug/L)
15-Feb	21.28	7	-69	0.43	0.23	200	1.58	57
24-Feb	21.01	7.09	-87	0.44	0.06	390	1.71	50
2-Mar	21.14	5.99	-21.8	0.46	0.09	200	1.7	95
9-Mar	21.31	6.72	-79.6	0.46	0.17	200	1.65	756
17-Mar	20.95	6.58	-149	0.41	1.96	200	1.37	651
21-Apr	22.97	6.59	-15.5	0.43	0.09	230	1.28	777
19-May	24	6.12	-104.5	0.46	0.07	230	1.03	3402

Table 5.4: Field measurements during the first three months for well M-1.

Date	Temperature (°C)	pH	ORP (mV)	Conductivity (mS/cm)	DO (mg/L)	Alkalinity (mg/L)	Fe(ferrous) (mg/L)	Dissolved sulfide (ug/L)
15-Feb	20.22	5.59	8.3	0.13	0.13	24	0.78	128
24-Feb	19.73	7.82	-203.5	1.08	0.06	0.98	100.98	1530
2-Mar	19.67	4.33	20.6	1.05	0.07	0.98	93.84	2652
9-Mar	19.88	4.46	-62.3	0.89	0.72	21	52.53	4029
17-Mar	19.73	4.6	-135.3	0.81	1.91	26	47.43	9027
21-Apr	21.65	4.91	-95.2	0.24	0.1	51	10.71	1071
19-May	23.13	4.99	-26.6	0.25	2.16	48	10.92	2688

Table 5.5: Field measurements during the first three month after the injections for well I-1.

Date	Temperature (°C)	pH	ORP (mV)	Conductivity (mS/cm)	DO (mg/L)	Alkalinity (mg/L)	Fe(ferrous) (mg/L)	Dissolved sulfide (ug/L)
15-Feb	18.45	6.24	125.7	0.15	1.47	53	0.47	44
24-Feb	19.05	8	-142.1	2.3	0.07	0.98	56.49	6321
2-Mar[i]	17.93	4.78	-37	1.43	0.16	110	141.27	357
9-Mar	19.3	4.73	-22.1	0.61	0.08	65	41.31	561
17-Mar	18.84	5.53	-103.5	0.29	1.8	67	21.93	561
21-Apr	20.84	6.04	-86.5	0.13	0.05	48	5.61	306
19-May	23.21	6.13	-16.7	0.18	0.15	71	2.1	462

[i] During the March 2nd sampling event another YSI 556 multi-probe was used for measuring the field parameters in I-1.

Table 5.6: Field measurements during the first three month after the injections for well M-2.

Date	Temperature (°C)	pH	ORP (mV)	Conductivity (mS/cm)	DO (mg/L)	Alkalinity (mg/L)	Fe(ferrous) (mg/L)	Dissolved sulfide (ug/L)
15-Feb	19.64	5.69	55	0.18	0.13	23	0.76	128
24-Feb	19.18	8.22	-159.8	0.56	0.12	48	43.47	84
2-Mar	17.83	4.75	-15.4	1.08	0.12	56	78.54	918
9-Mar	19.3	5.04	-66.2	0.71	0.16	61	42.84	4539
17-Mar	19.43	5	-151.8	0.48	1.62	66	31.11	6681
21-Apr	21.68	5.48	-111.1	0.19	0.11	50	8.67	3111
19-May	21.71	5.49	-85.5	0.19	0.07	58	2.73	1407

Table 5.7: Field measurements during the first three month after the injections for well I-2.

Date	Temperature (°C)	pH	ORP (mV)	Conductivity (mS/cm)	DO (mg/L)	Alkalinity (mg/L)	Fe(ferrous) (mg/L)	Dissolved sulfide (ug/L)
15-Feb	16.78	6.21	125.5	0.21	1.01	58	0.23	18
24-Feb	18.09	8.32	-236.2	0.67	0.11	43	54.18	504
2-Mar	16.39	5.81[ii]	-20	0.24	0.2	74	30.09	204
9-Mar	17.65	5.85	-69	0.22	0.09	78	10.71	459
17-Mar	18.77	6.13	-158.1	0.21	1.2	79	8.16	765
21-Apr	20.18	6.3	-69	0.19	0.1	78	4.08	714
19-May	22.47	6.33	-77.5	0.23	0.25	79	2.04	102

[ii] March 2nd for measuring pH in I-2 a second YSI 556 multi-probe was used.

The pH values for the seven wells before the injections ranged from 5.45 to 7, the average pH for February 15th was 5.96 and the median was 5.69 with the standard deviation of 0.52. The next week (February 24th), one week after the injections, the pH for the four new wells (M-1, I-1, M-2, and I-2) increased significantly to around 8 (Figure 5.2). Three other monitoring wells (LH-2, LH-10, and RA-12) did not show a significant change in pH the following week after the injections. From the second week after the injections the pH in the four new wells decreased again and it reached even lower than the pre-injection values. After the dramatic drop in the second week the pH values for the new wells started to increase slightly for the following weeks.

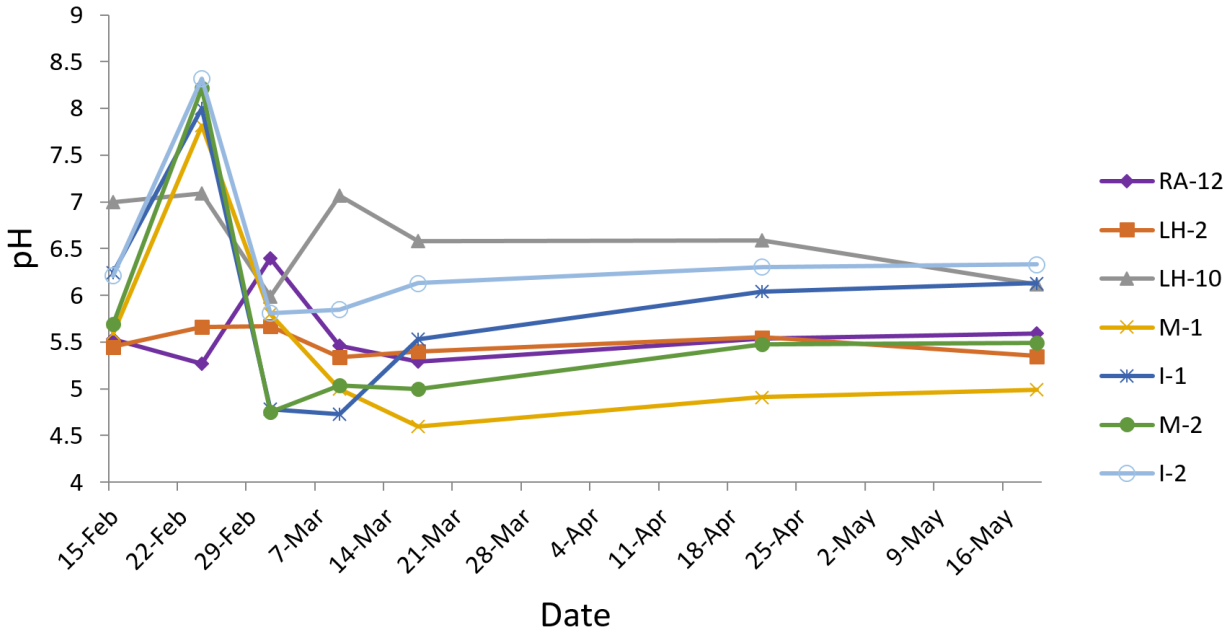

Figure 5.2: Plot showing pH data for all the seven wells during the sampling events, three month after the injections.

Before the injections, ORP was measured for all the seven wells, ranging from -69 mV in LH-10 to 126 mV in I-1. The average ORP before the injection was 44.4 mV, the median was 49.5 mV with the standard deviation of 63.6. The week after injections the ORP had decreased significantly in all the wells, and the average value for all the wells was -121 mV

with the standard deviation of 83.2. ORP values have fluctuated a lot during our monitoring events. That appears to be the result of the high organic carbon present after injections in our sampling wells that could affect the ORP probe. After dramatic fluctuations during the first four weeks after the injections, the ORP began to rise slightly. However the average ORP for all the wells is still -35.9 mV which indicates a reducing condition (Figure 5.3).

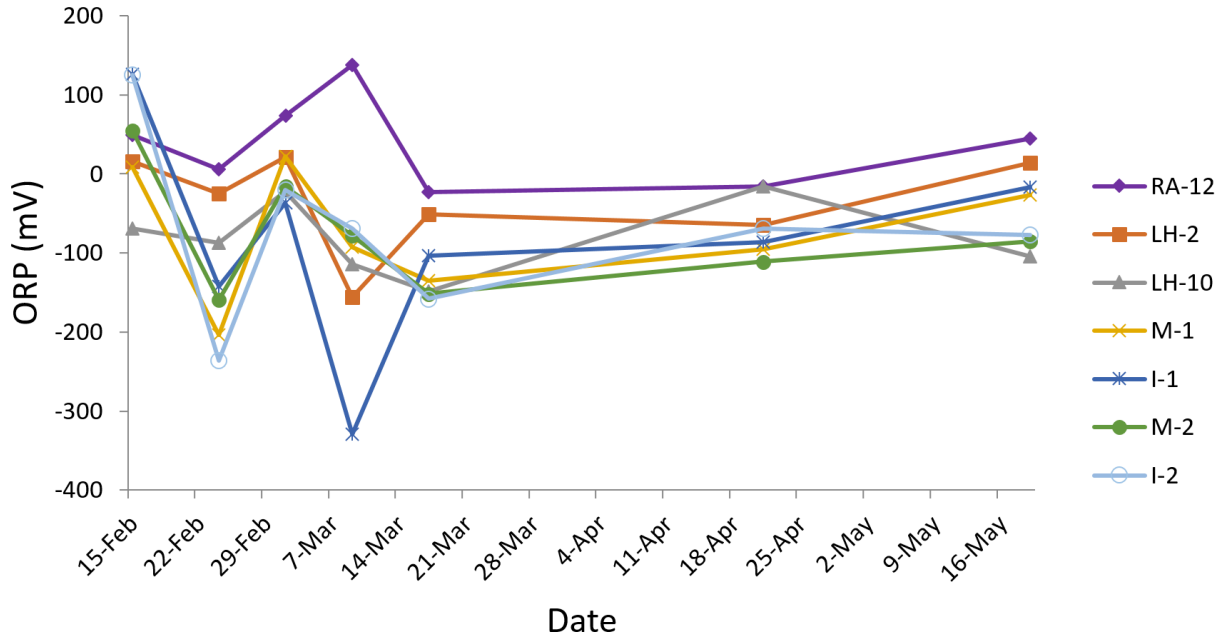

Figure 5.3: Plot showing ORP data for all the seven wells, during the sampling events, three month after the injections.

Conductivity data for RA-12, LH-2, and LH-10 do not show big changes during the sampling events. However the newly installed wells indicate a dramatic increase following the first week after the injections (Figure 5.4). The highest conductivity was recorded in I-1 in February 24th sampling event with 2.3 $\frac{mS}{cm}$. I-2 showed less increase than I-1 however it had its largest amount in the same day. After the first week the conductivity dropped, and since March 17th it has been almost stable.

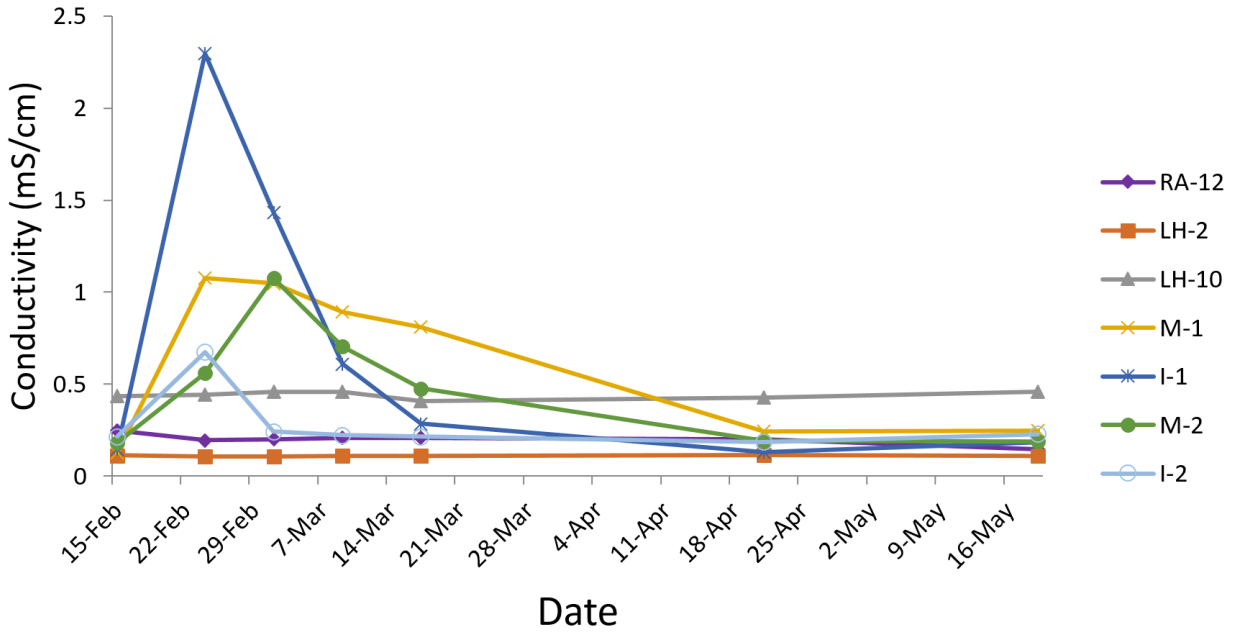

Figure 5.4: Plot showing conductivity data for the seven wells during the sampling events, three month after the injections.

The average dissolved oxygen (DO) concentration in the groundwater the week before the injections was 0.46 $\frac{mg}{L}$. The median was 0.17 $\frac{mg}{L}$ with a standard deviation of 0.5. For the four new wells DO concentration was high before the injections and it decreased after the injections, dramatically. In the other three wells DO concentration was low before and after the injections and it did not change significantly with the injections (Figure 5.5). Since April 21st sampling event a rapid increase in DO levels was observed in M-1 and LH-2, while the other wells have experienced a very slight increase in DO concentrations.

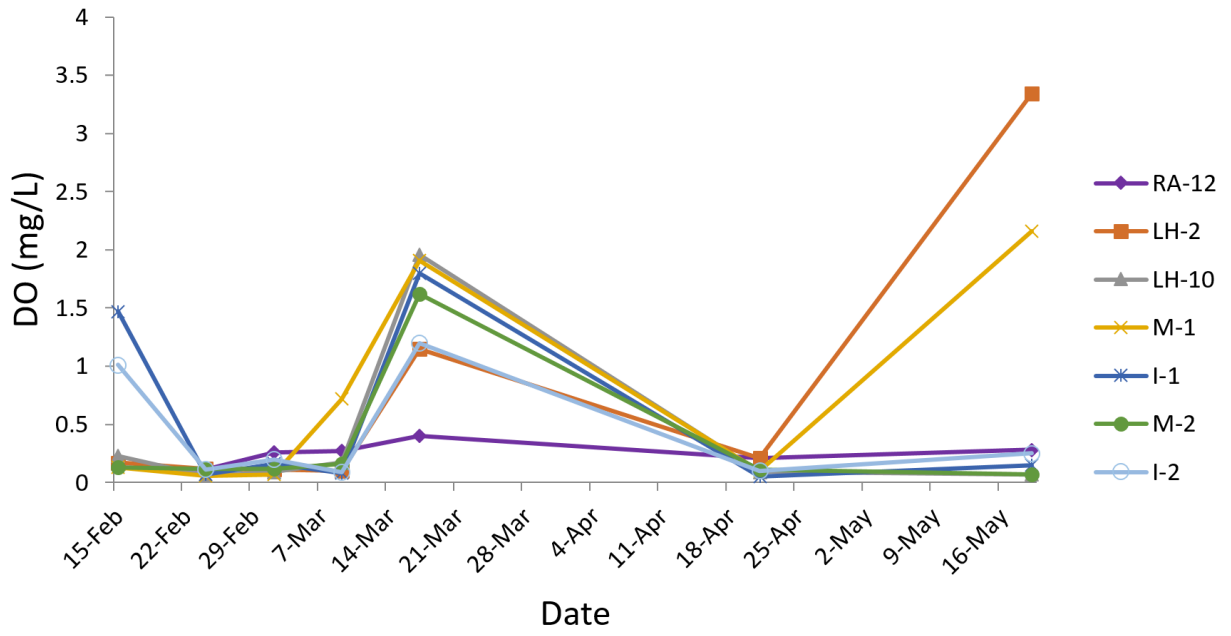

Figure 5.5: Plot showing dissolved oxygen (DO) data for all the seven wells, with three month after the injections.

Ferrous iron was measured in the field and it ranged from 0.23 in I-2 to 1.58 $\frac{mg}{L}$ in LH-10, before the injections. The average was 0.81 $\frac{mg}{L}$, the median 0.76 $\frac{mg}{L}$, and the standard deviation was 0.46 for pre-injection conditions. The first week after the injections the ferrous iron concentration began to increase in all the four new wells, M-1 and I-2 experienced their highest concentration of ferrous iron in February 24th, and I-1 and M-2 had their maximum concentration in March 2nd. The highest ferrous iron concentration recorded was in I-1 with 141.3 $\frac{mg}{L}$ the second week after the injections (Figure 5.6). The other three wells do not show significant response to the injection, and their ferrous iron concentration remained fairly constant.

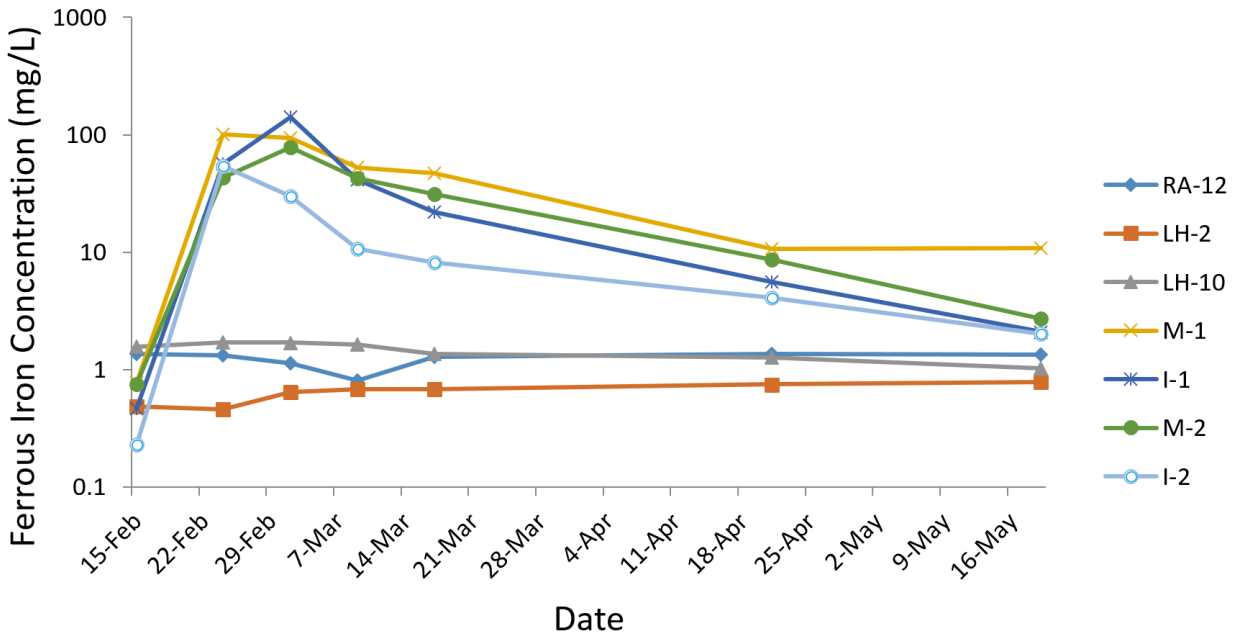

Figure 5.6: Plot showing ferrous iron (field measured) data within three month after the injections (Y-axis is in logarithmic scale).

Dissolved sulfide in groundwater samples was measured in the field during all the sampling events. The average dissolved sulfide in the wells, before the injections was 62 ug/L, the median was 44 ug/L with the standard deviation of 43.4. After the injections RA-12 and LH-2 did not indicate significant changes in dissolved sulfide concentration, LH-10 however, showed an increase toward the April and May sampling events. The four newly installed wells indicated dramatic increases after the injections. I-1 had its highest dissolved sulfide concentration in February 24th, I-2 showed a peak during the first week after the injections, but it had the highest amount of dissolved sulfide in March 17th. M-1 had the highest dissolved sulfide concentration among all wells and all the sampling events, with 9027 ug/L in March 17th. M-2 shows the same trend but in lower concentration than M-1 (Figure 5.7).

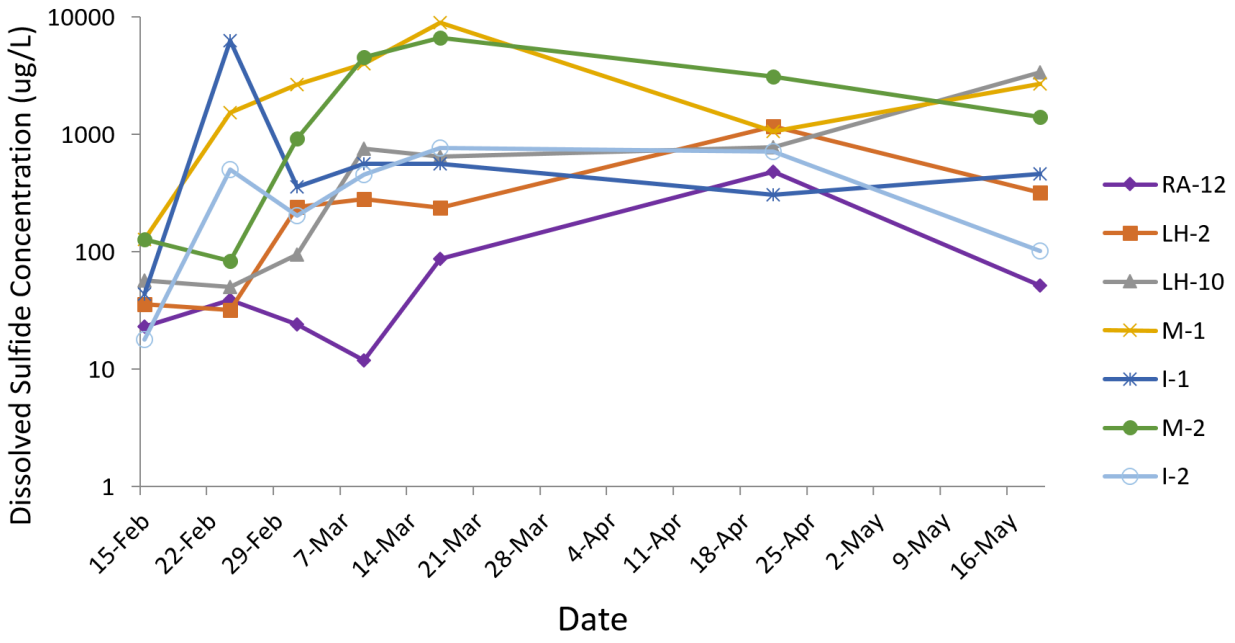

Figure 5.7: Plot showing dissolved sulfide data within three month after the injections (Y-axis is in logarithmic scale).

5.2 ICP-MS Results-Cations

Tables 5.8 through 5.15 are showing the ICP-MS results for major cations in each well three months after the injections. Table 5.16 shows the geochemistry analysis of our injection solutions, strong solution was injected into I-2 and weak solution was injected into I-1. Figures 5.8-5.16 are the charts based on the tables provided.

Table 5.8: Total As concentration ($\frac{mg}{L}$) in groundwater samples.

Date	RA-12	LH-2	LH-10	M-1	I-1	M-2	I-2
15-Feb	0.133	0.245	0.253	0.317	0.123	0.343	0.123
24-Feb	0.124	0.179	0.201	0.245	4.830	0.052	6.155
2-Mar	0.123	0.158	0.227	0.151	9.134	0.080	3.425
9-Mar	0.122	0.147	0.097	0.184	5.327	0.064	1.705
17-Mar	0.140	0.143	0.110	0.018	2.644	0.051	0.794
21-Apr	0.122	0.090	0.044	0.019	0.537	0.018	0.137
19-May	0.167	0.218	0.009	0.022	0.312	0.009	0.119

Table 5.9: As (III) concentration ($\frac{mg}{L}$) in groundwater samples.

Date	RA-12	LH-2	LH-10	M-1	I-1	M-2	I-2
15-Feb	0.125	0.229	0.248	0.276	0.055	0.291	0.085
24-Feb	0.096	0.146	0.195	0.249	5.089	0.051	5.089
2-Mar	0.084	0.142	0.211	0.123	8.368	0.088	3.252
9-Mar	0.107	0.13	0.086	0.138	4.666	0.054	1.433
17-Mar	0.132	0.136	0.091	0.017	2.442	0.035	0.482
21-Apr	0.114	0.081	0.035	0.011	0.443	0.009	0.102
19-May	0.141	0.205	0.007	0.016	0.187	0.008	0.118

Table 5.10: Total Fe concentration ($\frac{mg}{L}$) in groundwater samples.

Date	RA-12	LH-2	LH-10	M-1	I-1	M-2	I-2
15-Feb	1.385	0.418	1.506	0.686	0.311	0.59	0.311
24-Feb	1.32	0.447	0.871	106.474	483.417	10.712	120.943
2-Mar	1.279	0.622	1.756	91.313	195.186	86.459	21.635
9-Mar	1.276	0.586	1.7	70.739	68.267	52.333	12.436
17-Mar	1.321	0.659	1.27	57.505	28.121	29.789	8.97
21-Apr	1.351	0.63	1.162	9.393	4.192	7.827	1.3
19-May	1.35	0.668	1.339	10.386	2.591	6.548	2.96

Table 5.11: Mg concentration ($\frac{mg}{L}$) in groundwater samples.

Date	RA-12	LH-2	LH-10	M-1	I-1	M-2	I-2
15-Feb	6.668	1.542	3.801	1.835	1.905	3.018	3.586
24-Feb	5.095	1.634	3.34	16.971	28.557	11.638	8.091
2-Mar	5.08	1.65	3.948	15.944	18.57	17.067	3.815
9-Mar	5.197	1.579	4.181	14.944	7.535	10.696	3.56
17-Mar	5.207	1.534	4.253	12.257	3.978	6.827	3.57
21-Apr	4.026	1.644	4.992	2.422	1.508	2.819	3.355
19-May	3.255	1.15	7.499	2.554	2.351	2.542	3.179

Table 5.12: Al concentration ($\frac{mg}{L}$) in groundwater samples.

Date	RA-12	LH-2	LH-10	M-1	I-1	M-2	I-2
15-Feb	1	0.068	0.016	0.076	0.078	0.154	0.196
24-Feb	0.865	0.06	0.035	3.337	12.512	0.664	1.51
2-Mar	0.855	0.061	0.013	1.54	2.523	1.883	0.363
9-Mar	0.766	0.068	0.026	1.26	0.694	0.918	0.142
17-Mar	0.764	0.535	0.021	0.964	0.281	0.563	0.127
21-Apr	0.888	0.076	0.024	0.358	0.188	0.239	0.135
19-May	0.619	0.121	0.02	0.396	0.094	0.158	0.106

Table 5.13: Na concentration ($\frac{mg}{L}$) in groundwater samples.

Date	RA-12	LH-2	LH-10	M-1	I-1	M-2	I-2
15-Feb	20.966	8.987	18.578	7.227	3.939	11.671	8.484
24-Feb	15.509	9.276	12.605	12.776	15.395	15.351	9.775
2-Mar	15.225	9.223	18.497	12.523	11.388	15.058	7.624
9-Mar	14.969	9.017	14.154	11.131	6.378	13.746	6.633
17-Mar	14.424	8.94	15.3	9.731	3.134	11.61	6.027
21-Apr	12.136	9.272	14.315	7.754	2.294	9.606	5.001
19-May	8.75	10.055	13.009	4.985	2.644	8.732	4.06

Table 5.14: Ca concentration ($\frac{mg}{L}$) in groundwater samples.

Date	RA-12	LH-2	LH-10	M-1	I-1	M-2	I-2
15-Feb	18.668	9.967	72.757	14.445	25.16	19.354	33.253
24-Feb	18.141	9.903	33.495	77.491	78.223	83.183	31.596
2-Mar	18.062	10.18	76.082	70.652	68.241	109.076	28.443
9-Mar	19.194	9.532	58.053	77.575	34.987	62.003	29.735
17-Mar	18.321	9.763	73.63	62.195	29.214	42.904	31.136
21-Apr	21.746	9.576	84.691	14.565	19.016	14.202	30.289
19-May	13.668	7.936	98.872	15.468	27.745	14.427	35.221

Table 5.15: K concentration ($\frac{mg}{L}$) in groundwater samples.

Date	RA-12	LH-2	LH-10	M-1	I-1	M-2	I-2
15-Feb	0.144	0.883	0.986	0.865	0.263	0.67	1.034
24-Feb	0.126	0.871	0.989	110.028	318.372	10.65	64.372
2-Mar	0.156	0.879	1.01	103.224	183.369	61.789	5.641
9-Mar	0.18	0.854	1.035	100.275	68.848	51.842	2.85
17-Mar	0.162	0.819	1.01	80.701	20.44	34.476	2.613
21-Apr	0.235	0.927	1.044	20.841	1.566	9.739	0.271
19-May	0.107	0.698	1.643	17.621	0.967	6.282	0.223

Table 5.16: Chemical composition of the injection solutions. Strong injection solution was injected in I-2 and the weak solution was injected into I-1.

Analyte	Strong Solution ($\frac{mg}{L}$)	Weak Solution ($\frac{mg}{L}$)
Al	0.48	0.24
As	0.0055	0.0028
Ca	56	53
Chloride	200	210
Dissolved Organic Carbon	1800	1900
Fluoride	0.2	0.22
Fe	680	300
Mg	31	28
Total Nitrate as N	0.076	0.124
Nitrite as N	0.021	0.021
Orthophosphate as P	0.1	0.1
K	350	320
Na	17	16
Sulfate	1100	610
Total Alkalinity as CaCO3	0.98	0.98
Total Dissolved Solids	5400	4600

Before the injections, the average total As concentration in all the seven wells was 0.22 $\frac{mg}{L}$, the median was 0.25 $\frac{mg}{L}$ with the standard deviation of 0.09. The highest amount of total As, before the injections, belonged to M-2 with 0.34 $\frac{mg}{L}$. The first two weeks after the injections total As concentration increased in the two injection wells. The highest increase occurred in I-1 and the As concentration in this well rose to 9.13 $\frac{mg}{L}$ the second week after the injections. Arsenic concentration began to decrease from the third week, in these wells, and almost three months after the injections, the average As concentration is below the

background levels. Arsenic concentration in the two monitoring wells has begun to decrease since the first week after the injections. The samples from the May monitoring event indicate that As levels, in two close-by wells (M-2 and LH-10), have decreased to 0.008 $\frac{mg}{L}$ which is below the EPA drinking water standard of 0.01 $\frac{mg}{L}$ (Figure 5.8). As (III) concentrations almost follow the same trend as the total As concentration in all the wells (Figure 5.9). The commercial Laboratory (Test America Laboratories, Inc.) analyzed the unfiltered samples for As (Figure 5.10), and the trend is almost the same as the filtered samples, but with slightly higher concentrations.

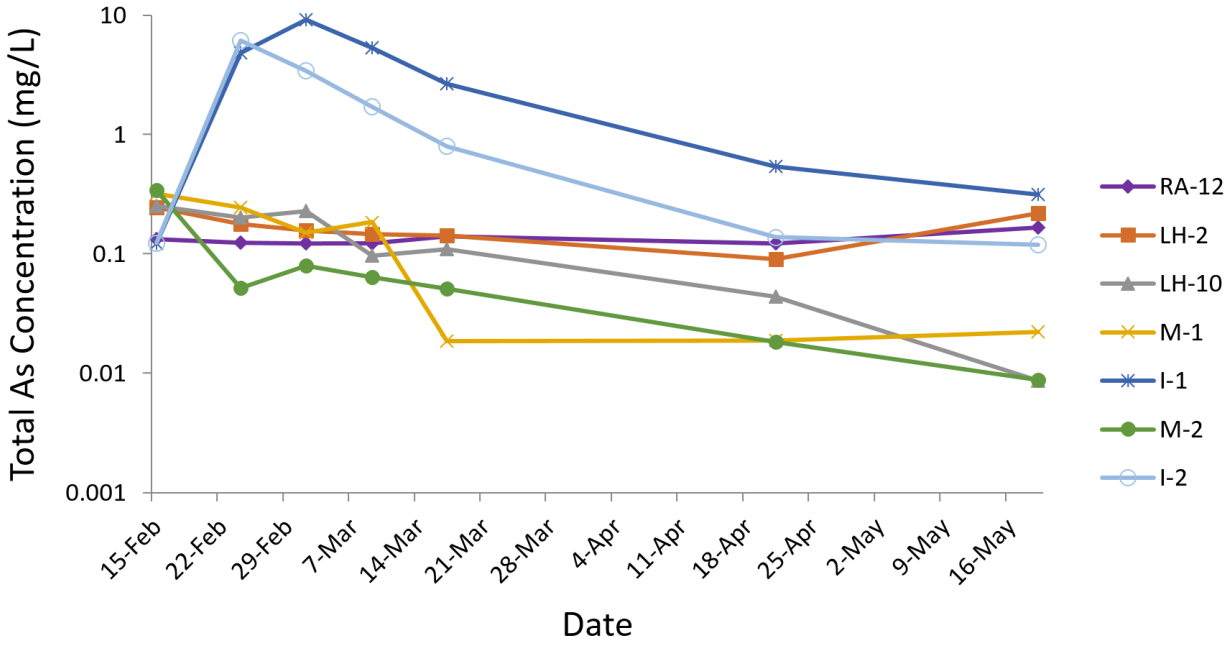

Figure 5.8: Plot showing the changes in total As concentration in the groundwater samples (Y-axis is in logarithmic scale. Data are shown in table 5.8).

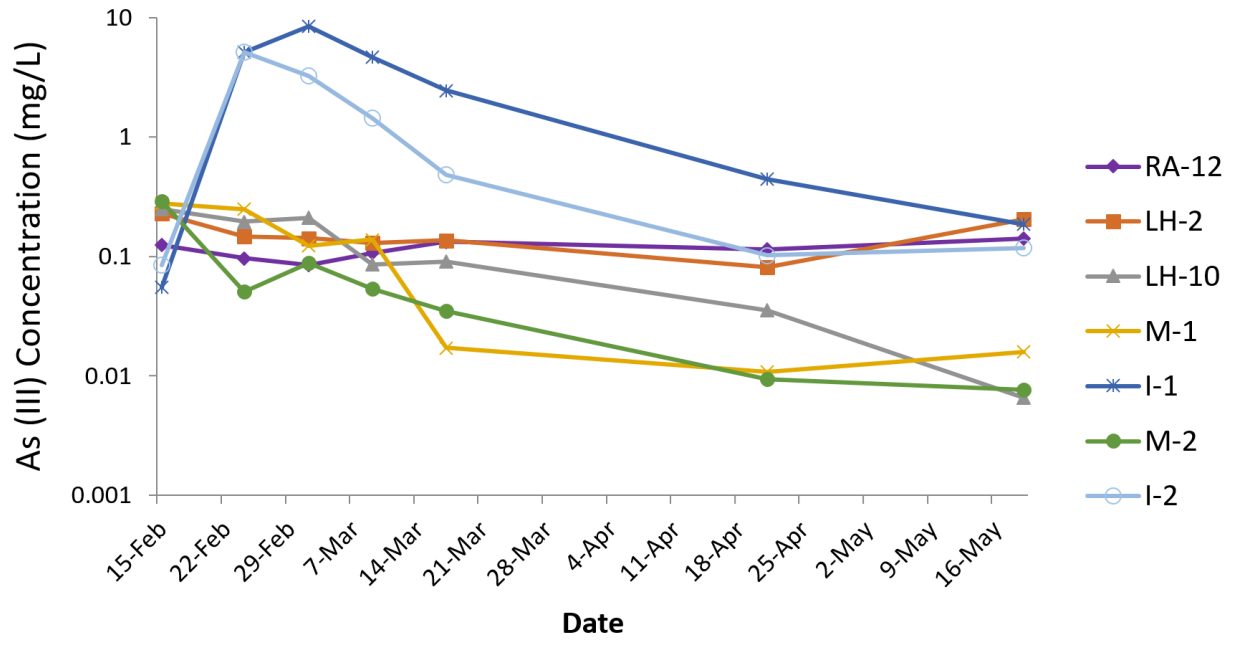

Figure 5.9: Plot showing the changes in As (III) concentration in the groundwater samples (Y-axis is in logarithmic scale. Data are shown in table 5.9)).

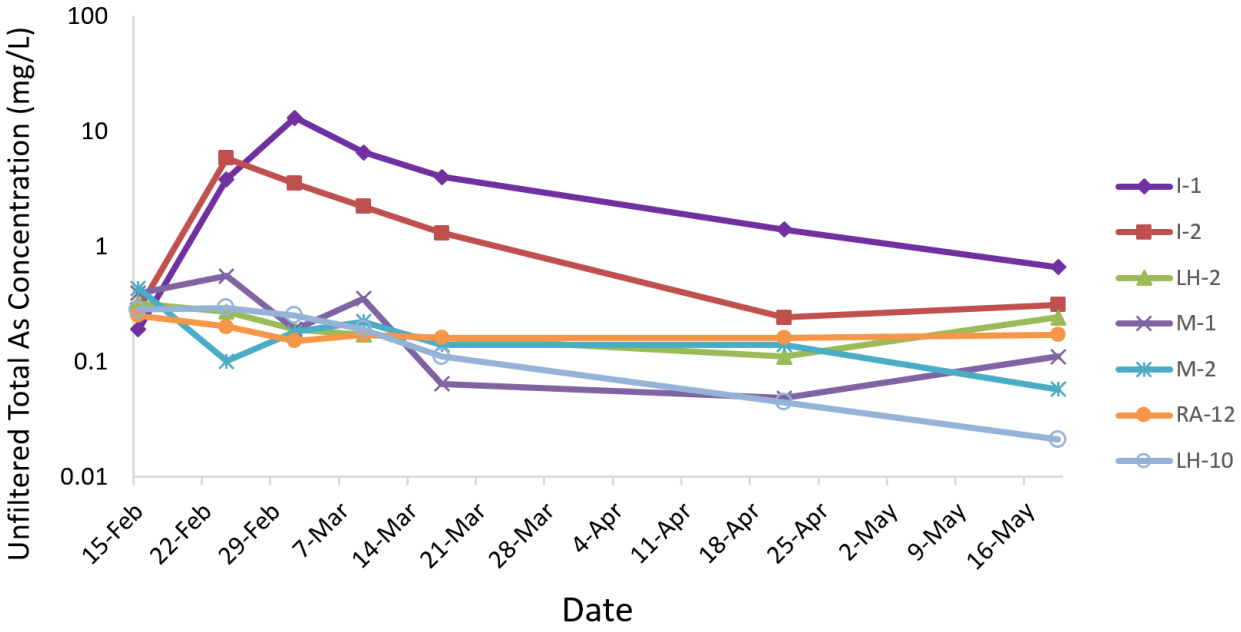

Figure 5.10: Plot showing the changes in unfiltered As in the groundwater samples (from Test America results)(Y-axis is in logarithmic scale).

Figure 5.11 shows the total Fe concentration in groundwater at the site. The average Fe concentration before the injections was 0.74 $\frac{mg}{L}$, the median was 0.59 $\frac{mg}{L}$, and the standard deviation was calculated to be 0.46. The first week after the injections the Fe concentrations increased drastically in all four new wells. The Fe concentrations began to decrease dramatically since the second week after the injections in these wells. The highest Fe concentration was recorded in I-2 with 121 $\frac{mg}{L}$, the week after the injections. The other three wells do not show very significant changes in Fe concentrations after the injections.

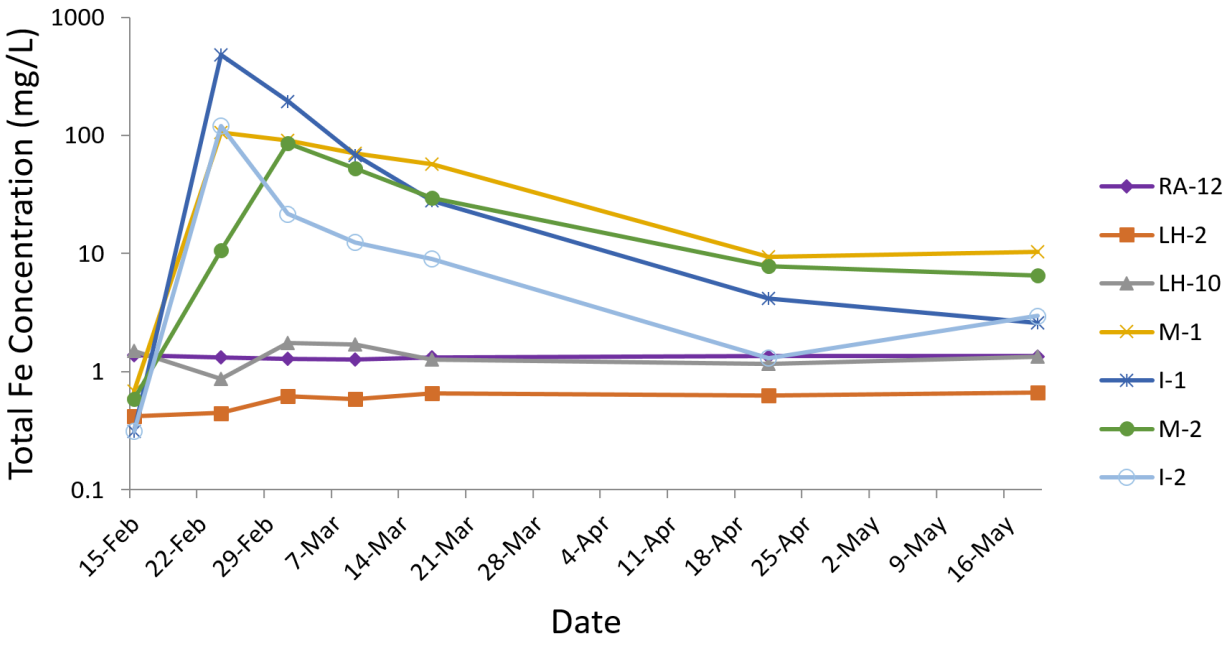

Figure 5.11: Plot showing the changes in Fe concentration in the groundwater samples (Y-axis is in logarithmic scale. Data are shown in table 5.10).

Aluminum concentrations averaged 0.23 $\frac{mg}{L}$ for the week before the injections. The median is 0.08 $\frac{mg}{L}$ with the standard deviation of 0.32. RA-12 had the highest level of Al before the injections with 1 $\frac{mg}{L}$. The first week after the injections four newly installed wells show a dramatic increase in Al concentrations, which starts to decrease from the following week. The other three wells do not show very noticeable changes in regard to injections. RA-12 Al concentrations has decreased since the first week (Figure 5.12).

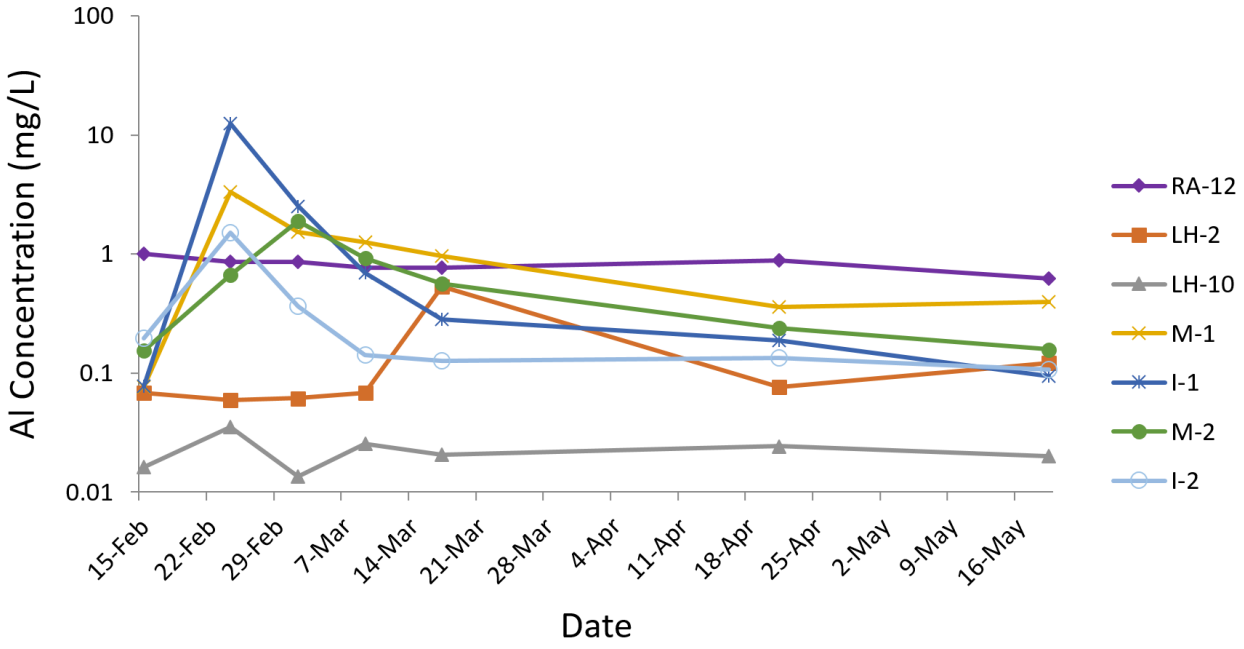

Figure 5.12: The changes in Al concentration in the groundwater samples (Y-axis is in logarithmic scale. Data are shown in table 5.12).

The average Mg concentration before the injections was 3.19 $\frac{mg}{L}$. The median in this week was 3.02 $\frac{mg}{L}$, while the standard deviation was 1.64. RA-12 had the highest levels of Mg before the injections with 6.67 $\frac{mg}{L}$. Mg concentrations increased in the four newly installed wells the first week after the injections (Figure 5.13). The Mg levels started to decrease from the second week after the injections in these wells. The Mg levels in the other three wells changed differently. In RA-12 the Mg has decreased to half its background concentrations, while LH-10 Mg concentration has increased since the second week after the injections, and LH-2 does not show any significant changes in Mg concentrations. The average Na concentration in the groundwater samples before the injections was 11.4 $\frac{mg}{L}$, the median was 8.98 $\frac{mg}{L}$, and the standard deviation was calculated to be 5.73. The four new wells show a slight increase the week after the injections, but since the third week after the injections Na levels seem to be stabilized in all the wells (Figure 5.14). Figure 5.15 shows the changes in concentration of Ca in groundwater in the study area. The average concentration

of Ca in the groundwater before the injections was 27.7 $\frac{mg}{L}$, median was 19.35 with the standard deviation of 19.7. The highest Ca concentration belonged to LH-10 with 72.8 $\frac{mg}{L}$. Ca concentrations in the M-1, I-1, M-2 new wells have increased after the injections. M-2 shows the highest Ca concentration the second week after the injections with 109 $\frac{mg}{L}$. Ca concentrations in I-2, LH-2, and RA-12 did not change significantly in response to injections. LH-10 Ca concentration after some fluctuations during the first few weeks began to increase even more than the background levels. The average K concentration in groundwater before the injections was 0.69 $\frac{mg}{L}$, median was 0.86 $\frac{mg}{L}$ with the standard deviation of 0.33. The highest K concentration was observed in I-2 with 1.03 $\frac{mg}{L}$, before the injections. The week after the injections the K concentration in all four new wells increased dramatically. The highest K concentration belonged to M-1 the first week after the injections with 110 $\frac{mg}{L}$. The K concentrations began to decrease from the second week in these wells. LH-2 and RA-12 do not show a very significant response to the injections, however the K concentration in LH-10 has increased from April sampling event (Figure 5.16).

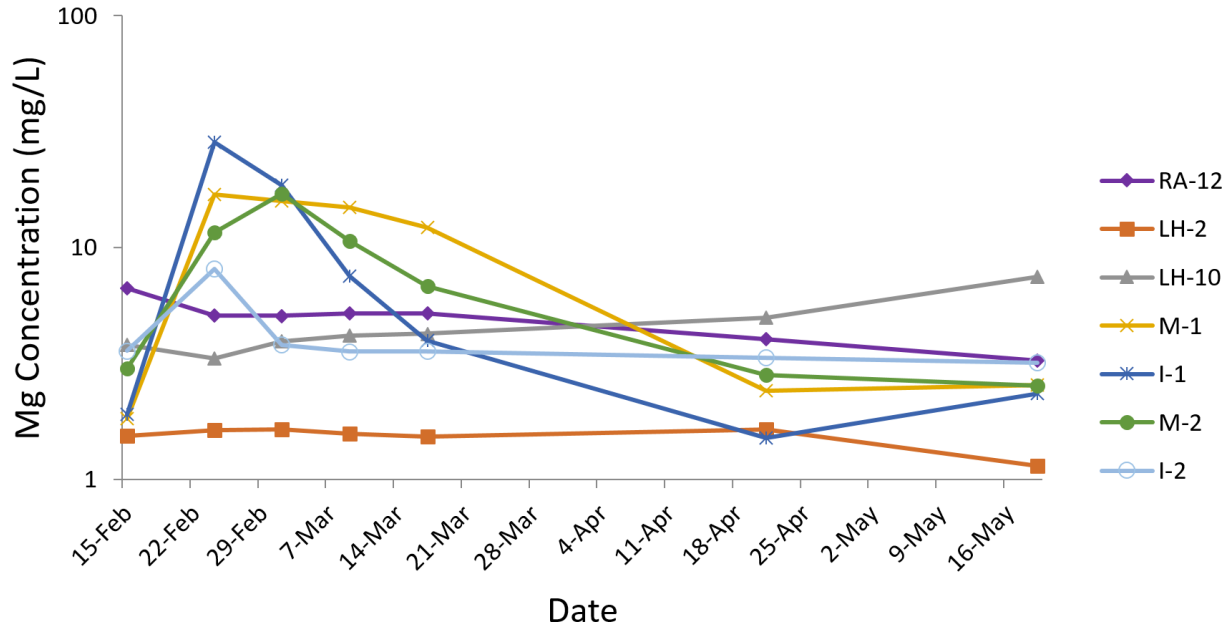

Figure 5.13: Plot showing the changes in Mg concentration in the groundwater samples (Y-axis is in logarithmic scale. Data are shown in table 5.11).

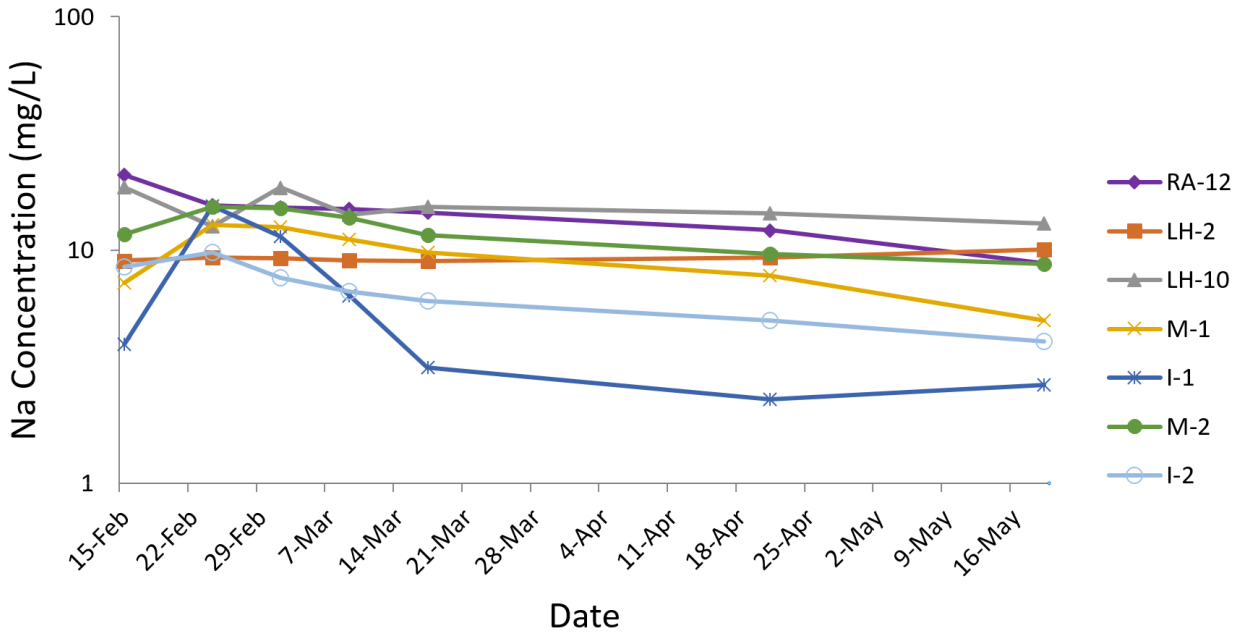

Figure 5.14: Plot showing the changes in Na concentration in the groundwater samples (Y-axis is in logarithmic scale. Data are shown in table 5.13).

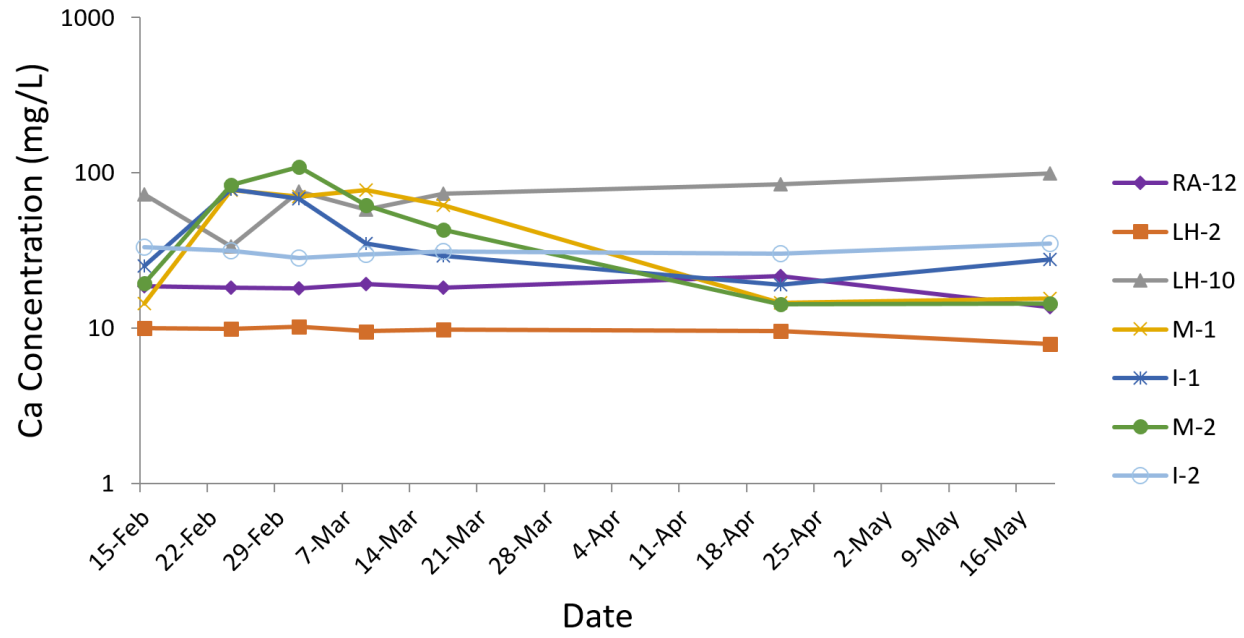

Figure 5.15: Plot showing the changes in Ca concentration in the groundwater samples (Y-axis is in logarithmic scale. Data are shown in table 5.14).

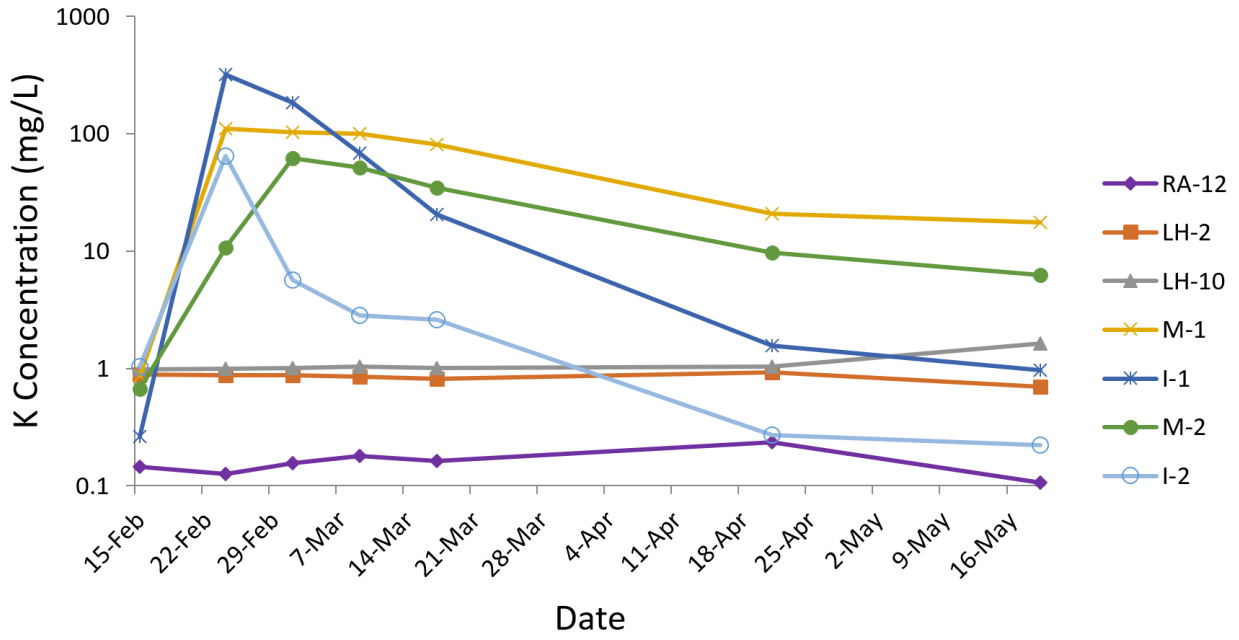

Figure 5.16: Plot showing the changes in K concentration in the groundwater samples (Y-axis is in logarithmic scale. Data are shown in table 5.15).

5.3 Anions

The average DOC of the groundwater before the injection was 11.54 $\frac{mg}{L}$. Median was 10 $\frac{mg}{L}$ with a standard deviation of 6.19. A week after the injections DOC levels increased in the four newly installed wells drastically and decreased after the second week. The other three wells did not show a significant response to the injections, probably due to the fact that the injection solution had not reached those wells yet. However, LH-10 has indicated an increase in DOC contents since March 17th. DOC levels in the four new wells have decreased significantly and are close to the pre-injection conditions with the average of 38.7 (Figure 5.17).

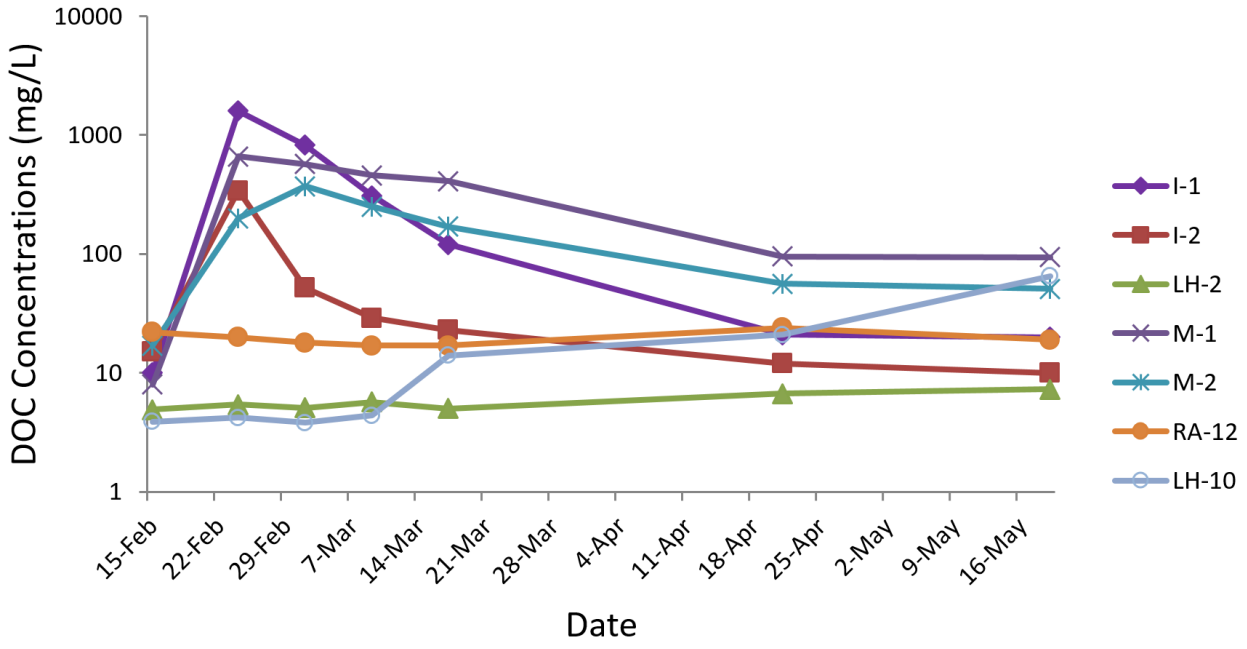

Figure 5.17: DOC level changes in the groundwater during the sampling events (Y-axis is in logarithmic scale).

Phosphorus concentrations were measured by orthophosphate concentration in the groundwater system. The average concentration of P before the injections was 0.12 $\frac{mg}{L}$. The median was 0.1 $\frac{mg}{L}$ and the standard deviation was 0.04. The P concentrations increased in the two injections wells and M-1 one week after the injections. The highest P concentration was recorded in I-1 with 22 $\frac{mg}{L}$ on February 24th. The P levels decreased to the background levels afterward. LH-2 also had raised levels of P the week after the injections which has retrieved to the background levels since the second week (Figure 5.18). Total Dissolved Solids (TDS) was measured and it is in correlation with conductivity. Higher TDS level is usually correlated with higher conductivity. The average TDS measured for the groundwater before the injections was 157 $\frac{mg}{L}$. The median was 160 $\frac{mg}{L}$ and the standard deviation was 55.8. The first week after the injection The TDS levels increased in all four new wells, and started to decrease from the following week. The TDS levels remained steady for the other three wells (Figure 5.19).

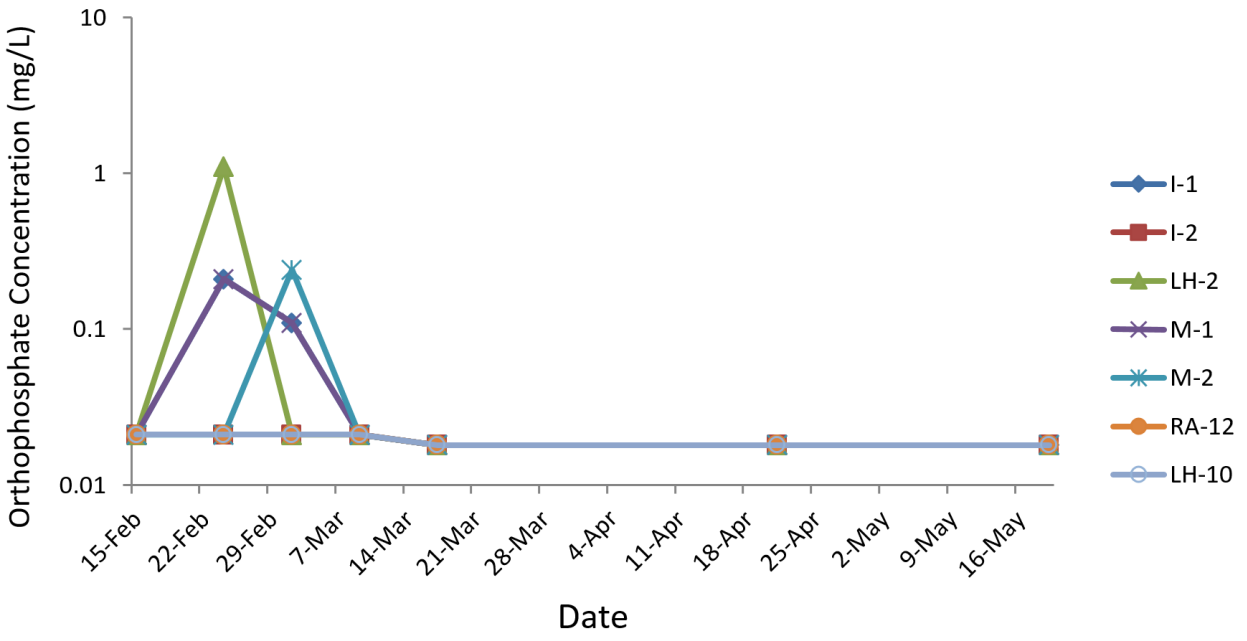

Figure 5.18: Plot of the changes in orthophosphosphate concentrations as P, in the groundwater samples (Y-axis is in logarithmic scale).

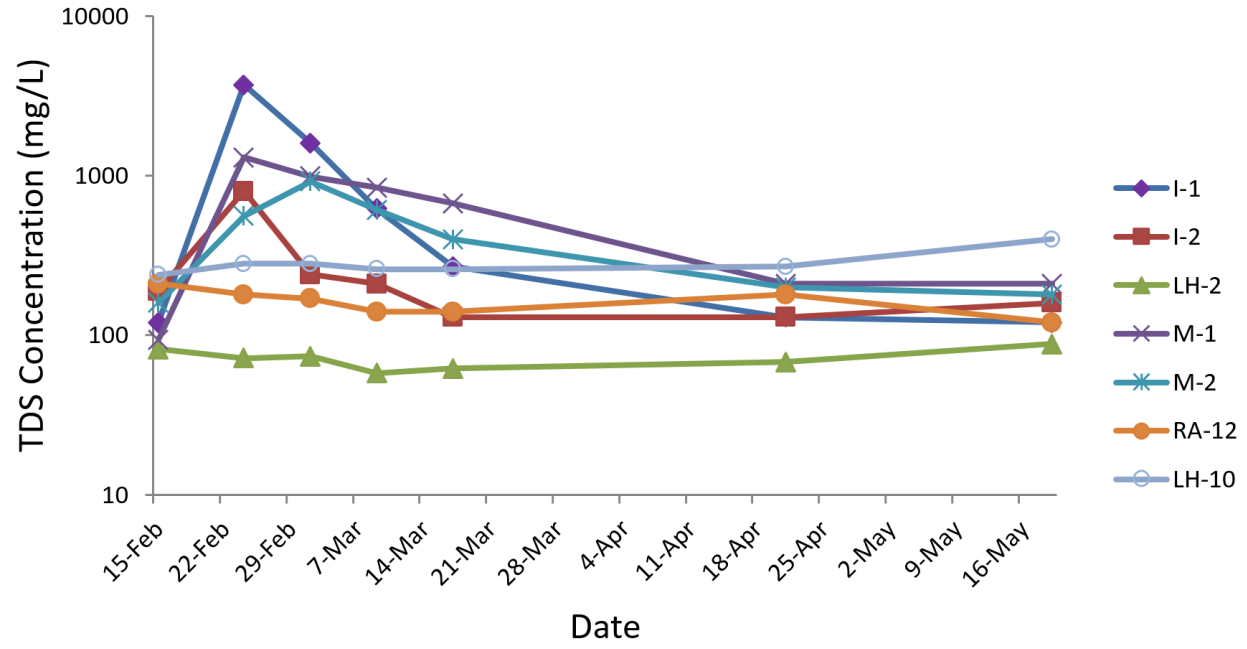

Figure 5.19: Plot of the TDS concentrations in the groundwater samples (Y-axis is in logarithmic scale).

Total Alkalinity was measured as carbonate alkalinity and bicarbonate alkalinity in Test America commercial labs, and the results were added to give the total alkalinity. The average total alkalinity in the groundwater was 57.1 $\frac{mg}{L}$, the median was 26 $\frac{mg}{L}$, and the standard deviation was 60.2. LH-10 had the highest Alkalinity during all the sampling events, before and after the injections (Figure 5.20). The alkalinity values for the four new wells indicated a lot of fluctuations and almost stabilized after the March 17th sampling event (one month after the injections).

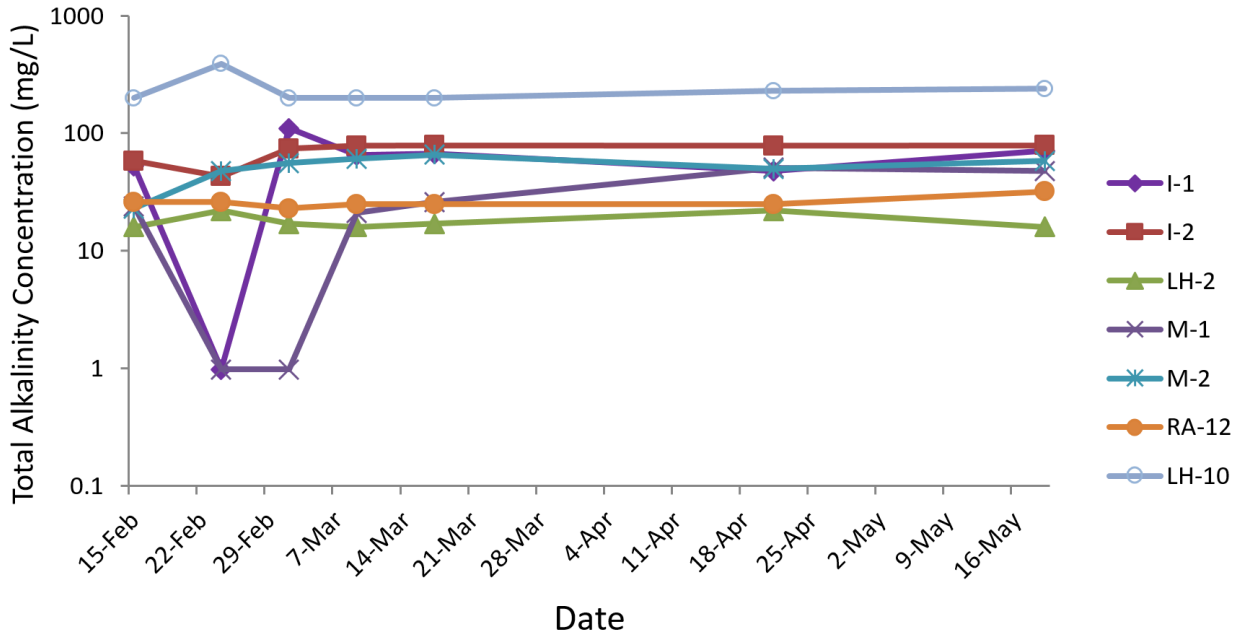

Figure 5.20: Plot of the changes in total alkalinity in the groundwater samples (Y-axis is in logarithmic scale).

The average sulfate concentration before the injections was 21.9 $\frac{mg}{L}$. The median was measured to be 26 $\frac{mg}{L}$ with a standard deviation of 60.2. The following week after the injections, the sulfate concentrations increased drastically in the four new wells (Figure 5.21). Highest sulfate concentration was recorded in I-1 a week after the injections with 800 $\frac{mg}{L}$ sulfate. M-2 had its highest sulfate concentration the second week after the injections. The sulfate concentration began to decrease after March 2nd in these wells. Although RA-12

and LH-2 do not show a significant respond to injections, LH-10 sulfate concentration has decreased since March 17th.

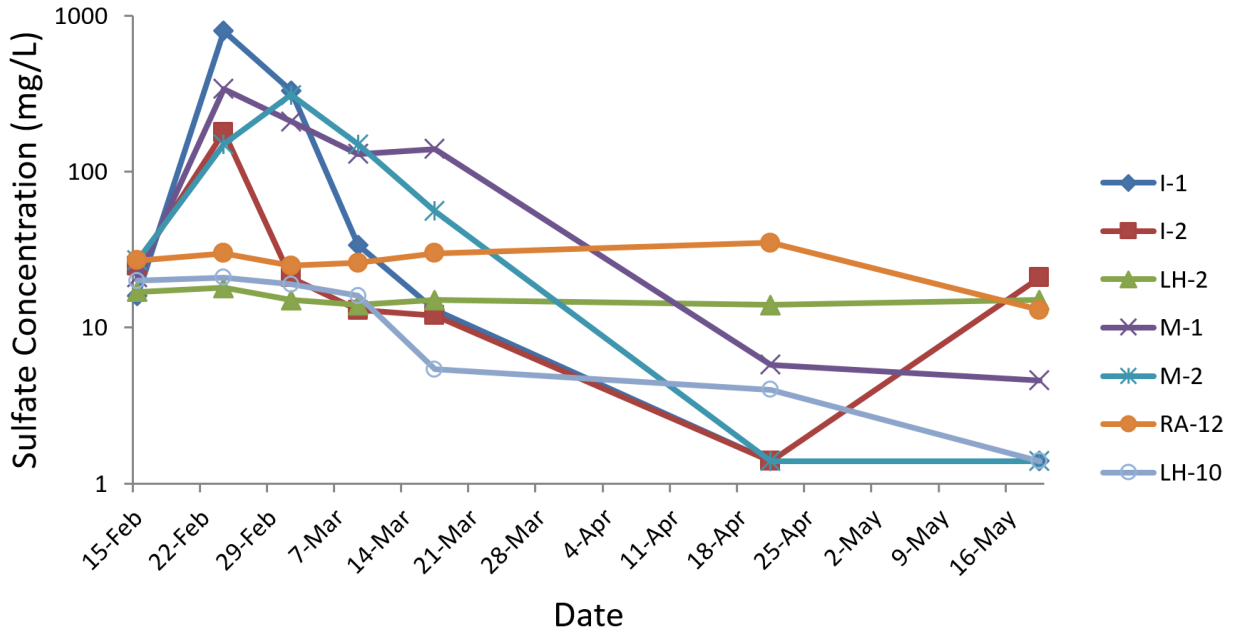

Figure 5.21: Plot of the changes in sulfate concentration in the groundwater samples (Y-axis is in logarithmic scale).

Fluoride (the negatively charged ion of fluorine) average concentration before the injections was measured to be 0.05 $\frac{mg}{L}$. The median was 0.03 $\frac{mg}{L}$ and the standard deviation was 0.05. The first week after the injections the fluoride levels increased dramatically in I-1 and I-2, and slightly in M-1 and M-2. The other three wells did not show significant changes in response to the injections. The increased levels of fluoride decreased to its background levels the second week after the injections (Figure 5.22). The average concentration of chloride (Cl^-)before the injections was 18.6 $\frac{mg}{L}$, median was 17 $\frac{mg}{L}$, and the standard deviation was 9.94. The week after the injections, the four new wells indicated a rise in the chloride concentrations. The increased chloride levels decreased after the second week following the injections. The other three wells showed almost stable chloride concentrations during the whole sampling events (Figure 5.23).

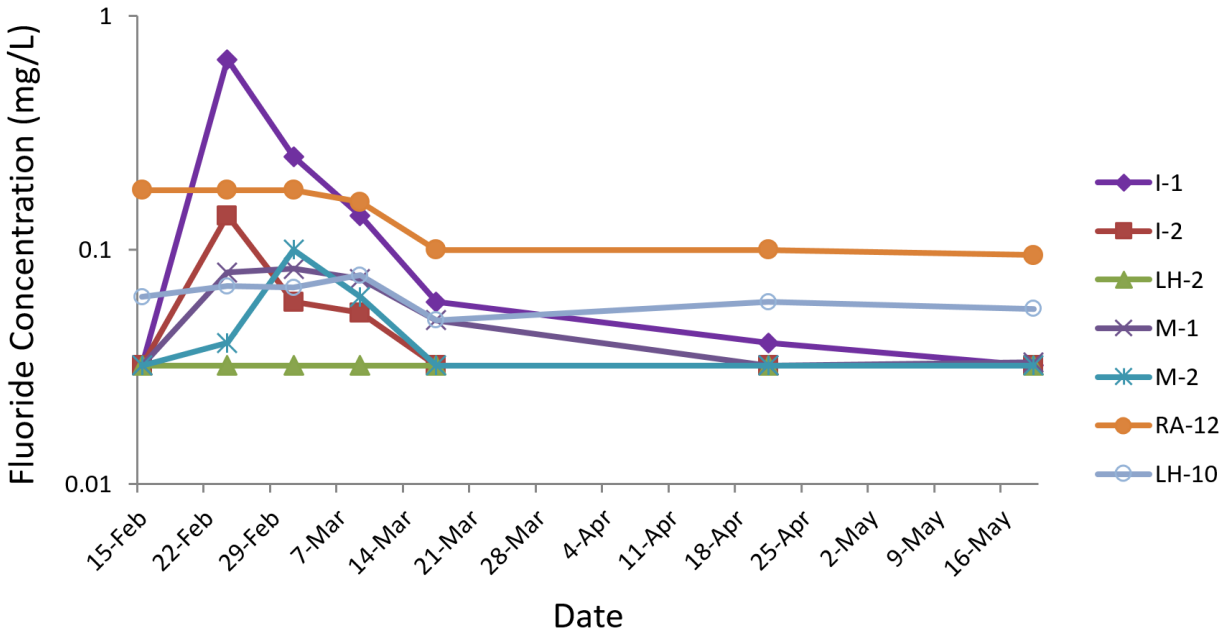

Figure 5.22: Plot of the changes in the Fluoride concentration in the groundwater samples (Y-axis is in logarithmic scale).

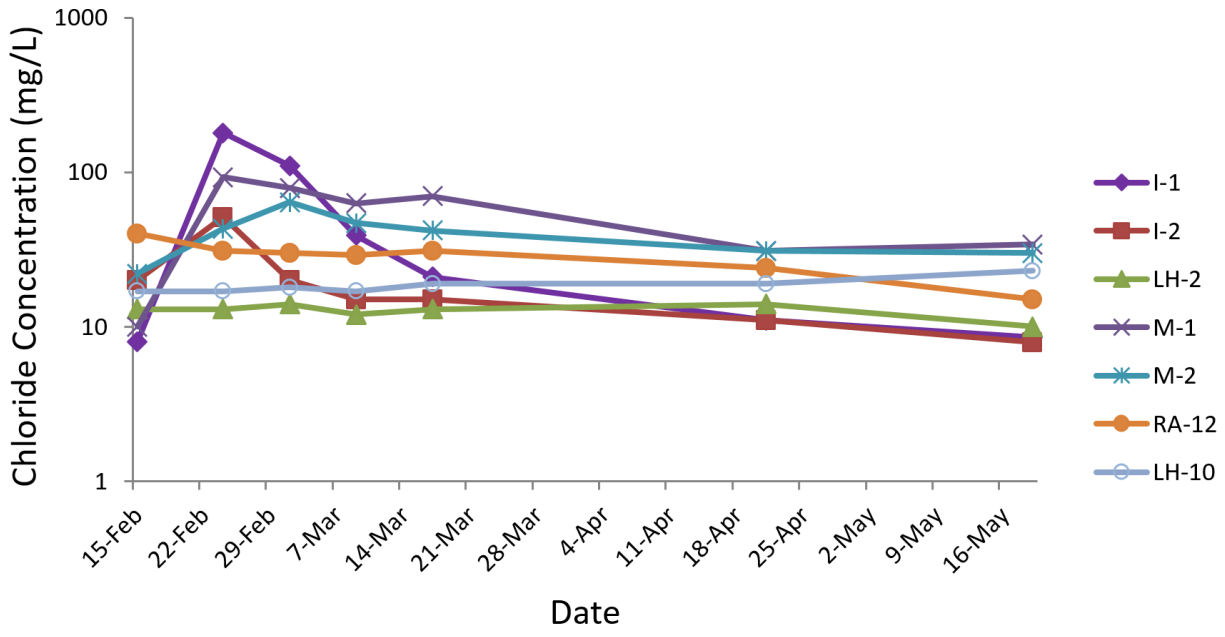

Figure 5.23: Plot of the changes in Chloride concentration in groundwater samples (Y-axis is in logarithmic scale).

Total nitrate average concentration before the injections was 0.049 $\frac{mg}{L}$, median was 0.046 $\frac{mg}{L}$ with the standard deviation of 0.005. The week after the injections the total nitrate concentrations increased significantly in LH-2, M-1, M-2, and I-1. The highest increase occurred in LH-2 with 1.64 $\frac{mg}{L}$ total nitrate, the first week after the injections. The total nitrate levels started to decrease from the second week after the injections and have stabilized, Since March 9th. The other three wells data for total nitrate was almost stable during all the sampling events (Figure 5.24). Nitrite average concentration in the groundwater samples before the injections was reported to be 0.021 $\frac{mg}{L}$, median was 0.021 with the standard deviation of 0. The week after the injections, I-1, LH-2, and M-1 experienced a rapid increase in nitrite levels, which decreased again the second week after the injections and stabilized since March 9th sampling event. The nitrite levels in other four wells did not change after the injections and were almost stable the whole time during all the sampling events (Figure 5.25).

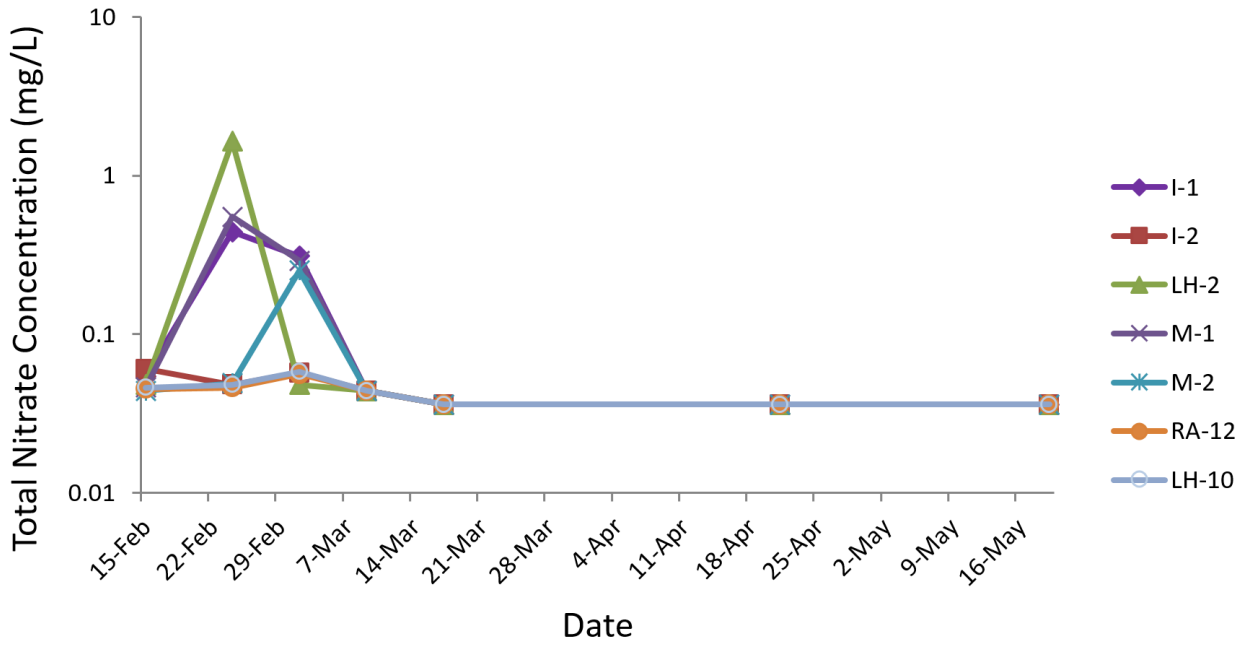

Figure 5.24: Plot of the changes in total nitrate concentrations in groundwater samples (Y-axis is in logarithmic scale).

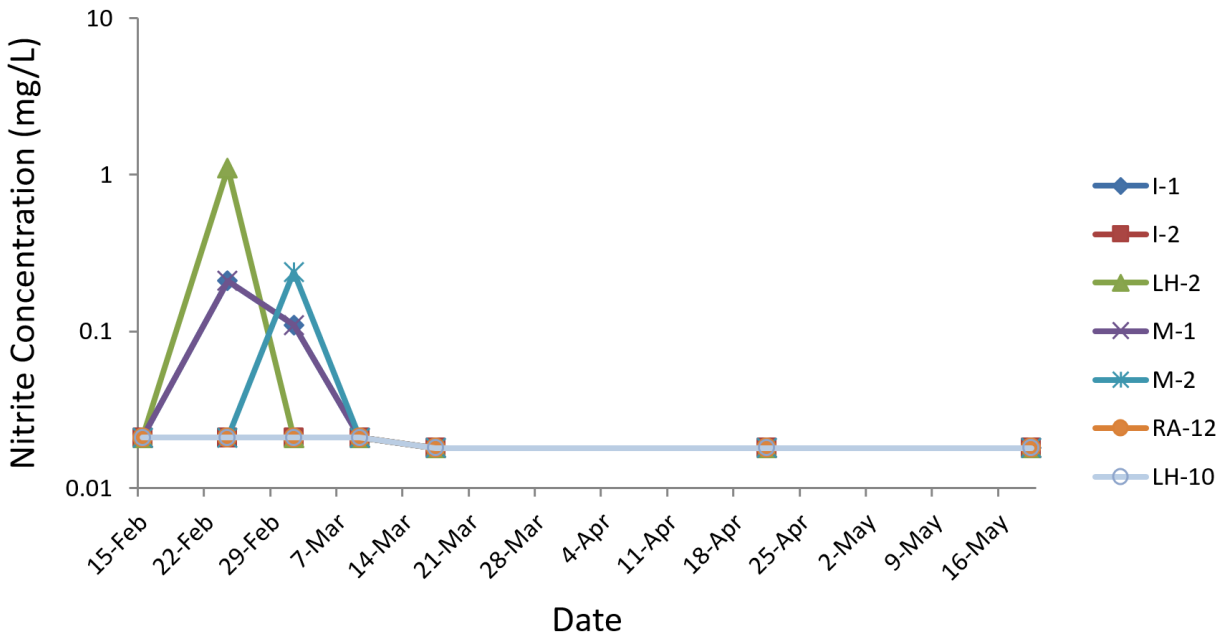

Figure 5.25: Plot of the changes in nitrite concentrations in groundwater samples (Y-axis is in logarithmic scale).

Figures 5.26 to 5.52 are interpolated surfaces created using ArcGIS software that show the distribution of As, Fe, dissolved sulfide, sulfate, in the study area, and their changes through time. The interpolation tool that was used to create these figures was inverse distance weight (IDW), which creates a raster surface from points using an inverse distance technique.

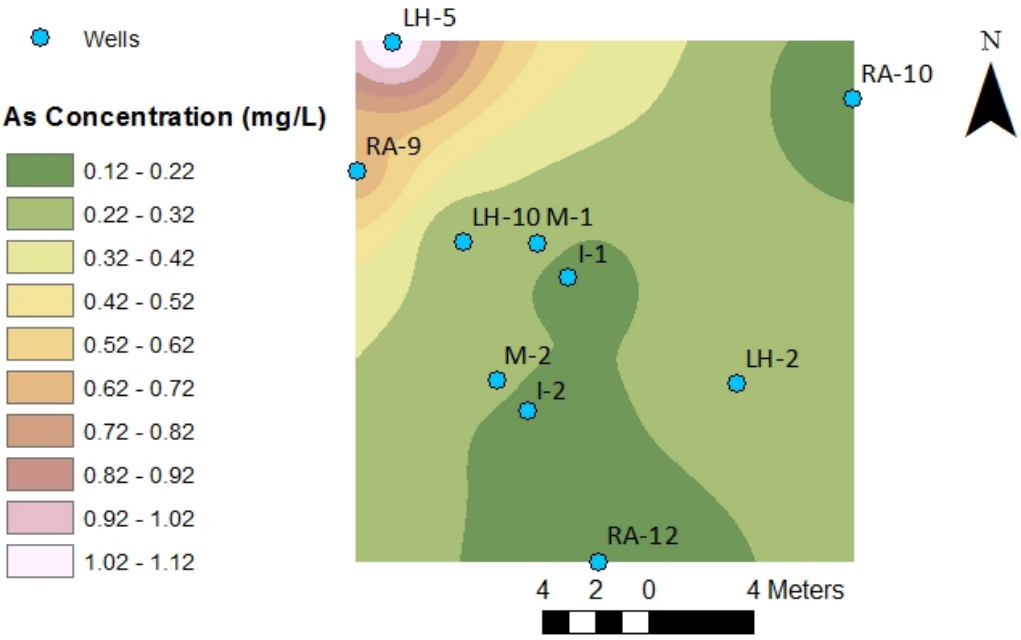

Figure 5.26: Interpolated surface showing the total As distribution in the aquifer for February 15th sampling event.

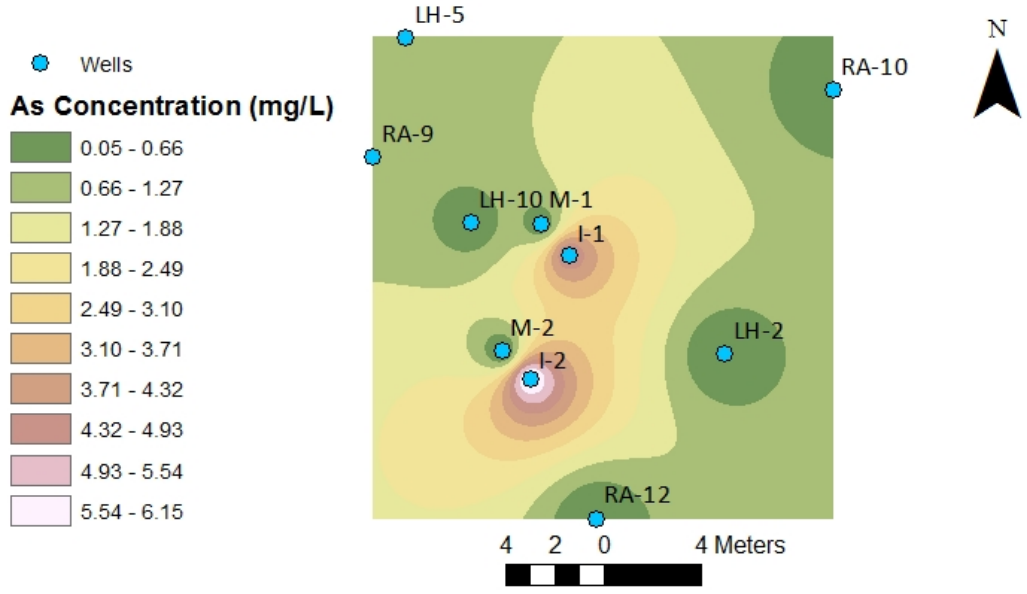

Figure 5.27: Interpolated surface showing the total As distribution in the aquifer for the February 24th sampling event.

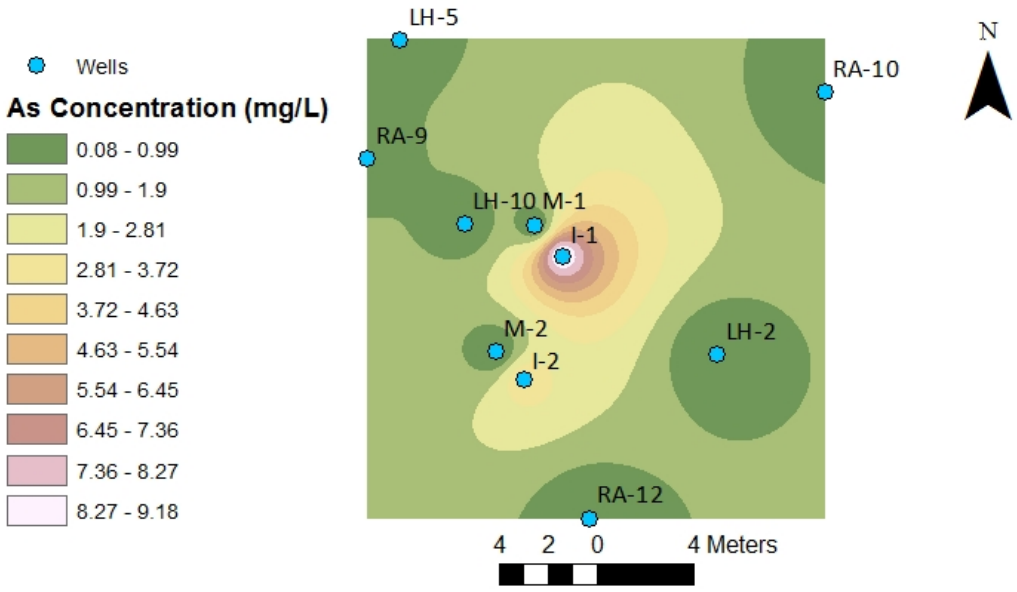

Figure 5.28: Interpolated surface showing total As distribution in the aquifer in the March 2nd sampling event.

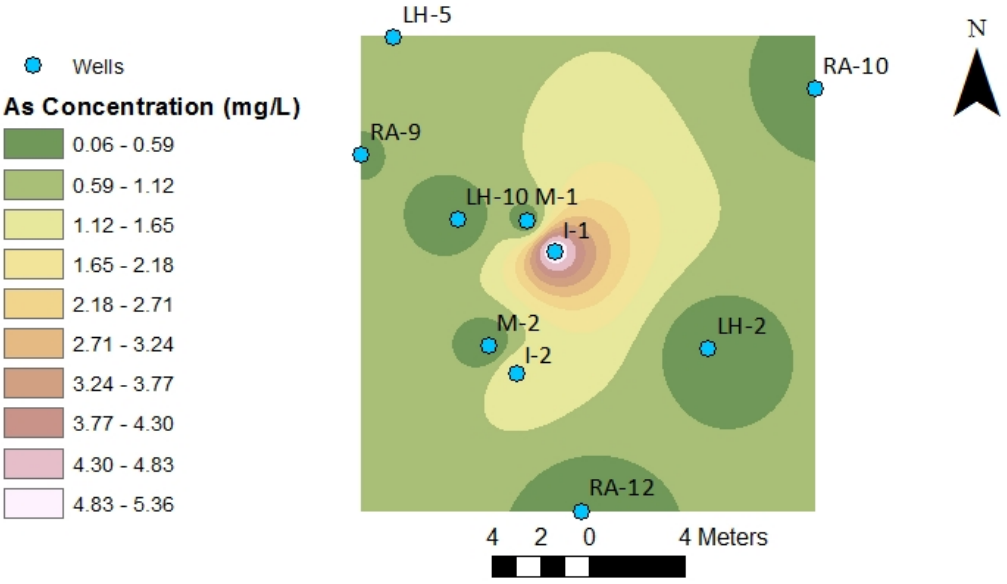

Figure 5.29: Interpolated surface showing the distribution of total As in the aquifer during the March 9th sampling event.

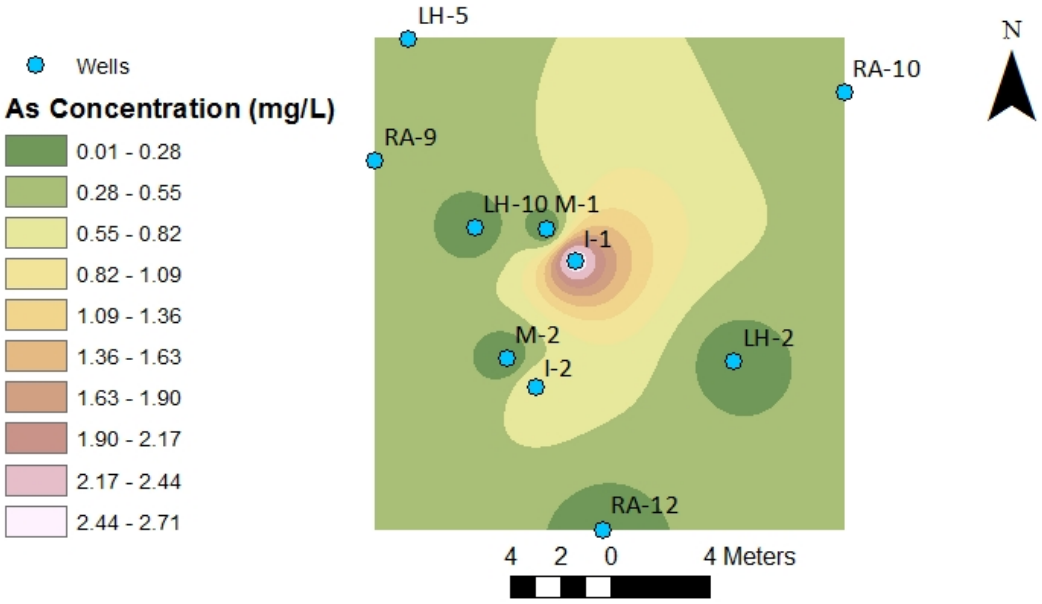

Figure 5.30: Interpolated surface showing the distribution of total As in the aquifer during the March 17th sampling event.

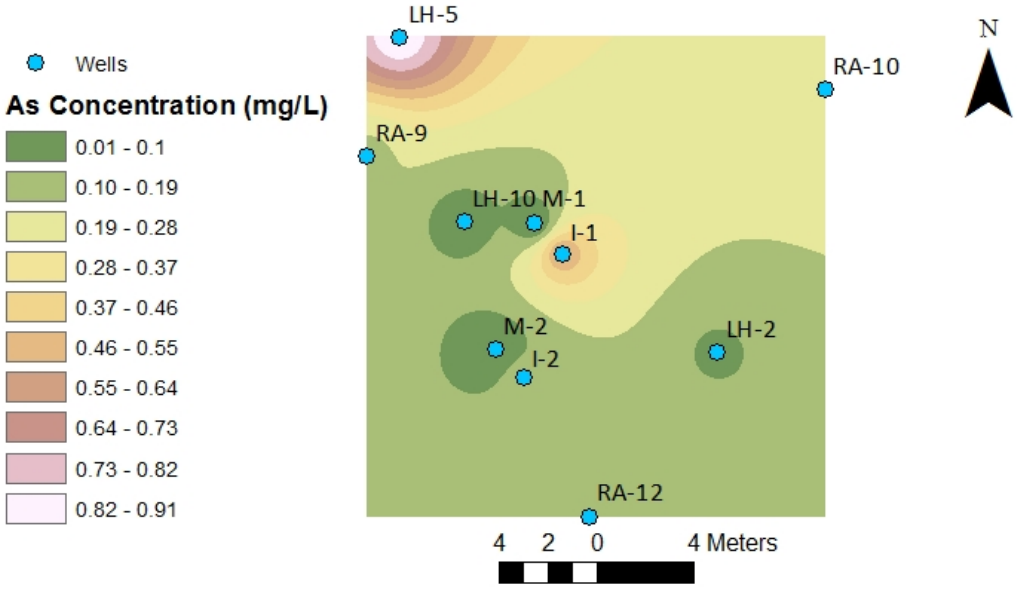

Figure 5.31: Interpolated surface showing the total As distribution in the aquifer during the April 21st sampling event.

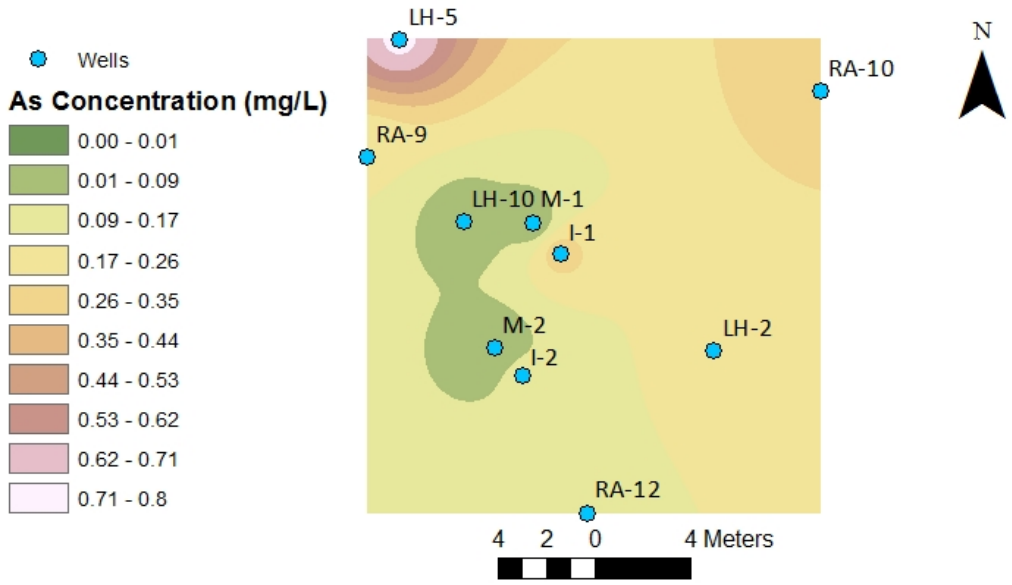

Figure 5.32: Interpolated surface showing the total As distribution in the aquifer during the May 19th sampling event.

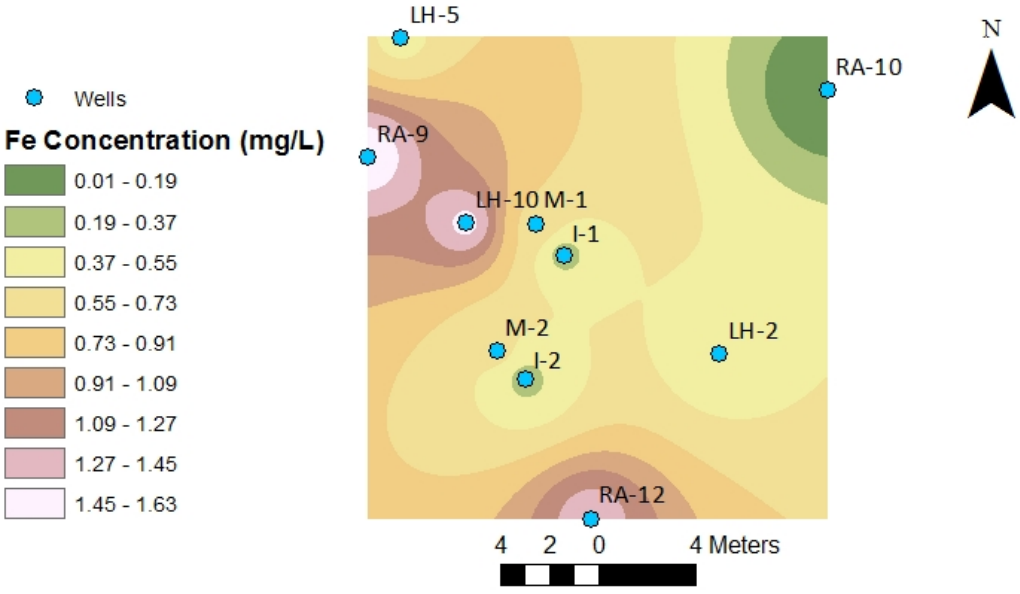

Figure 5.33: Interpolated surface showing the Fe distribution in the aquifer during the February 15th sampling event.

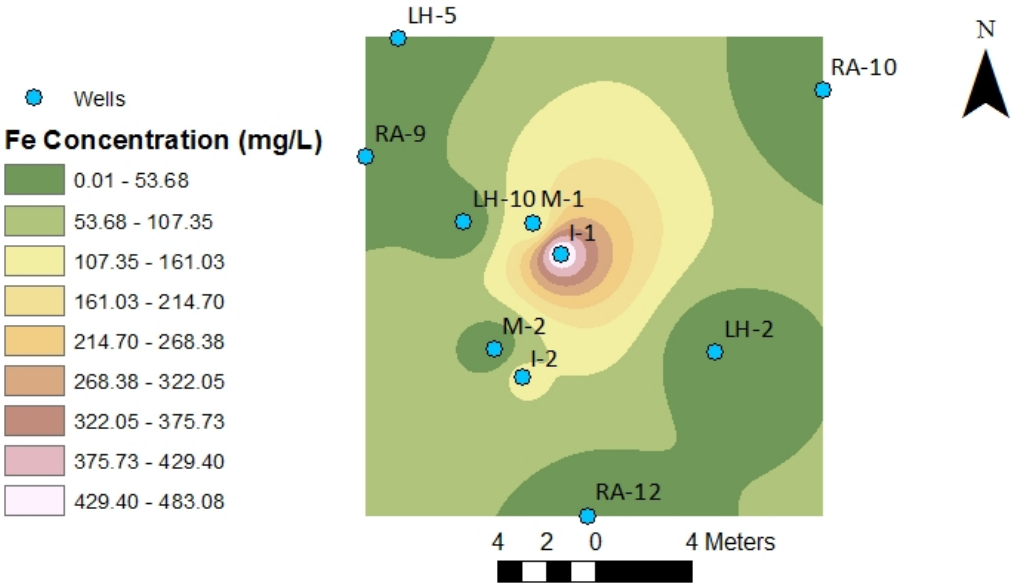

Figure 5.34: Interpolated surface showing the Fe distribution in the aquifer during the February 24th sampling event.

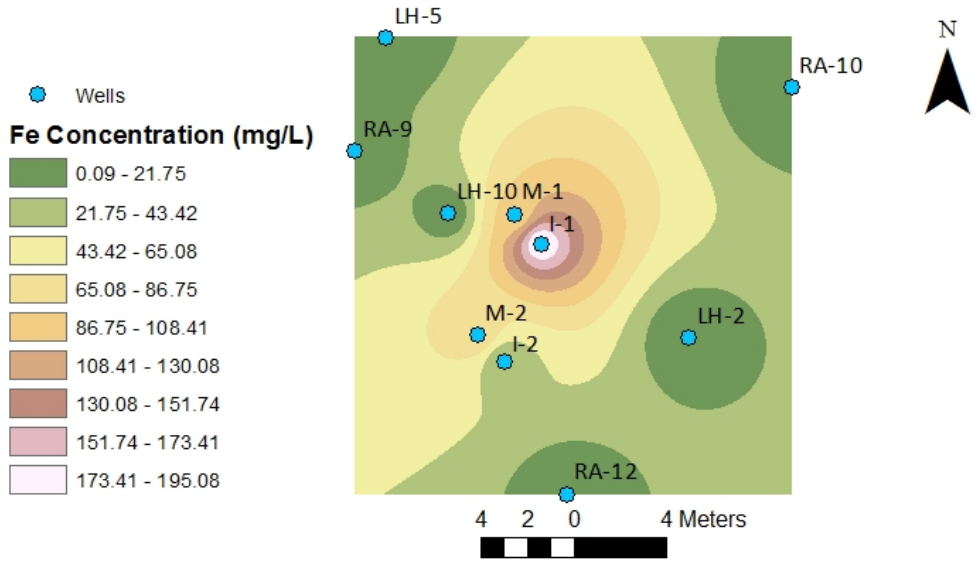

Figure 5.35: Interpolated surface showing the Fe distribution in the groundwater during the March 2nd sampling event.

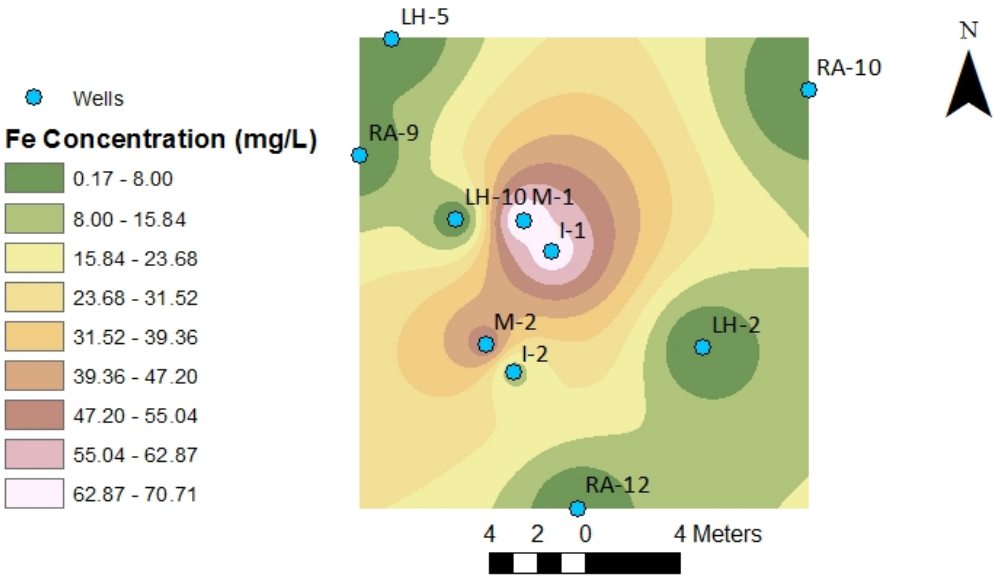

Figure 5.36: Interpolated surface showing the Fe distribution in the aquifer during the March 9th sampling event.

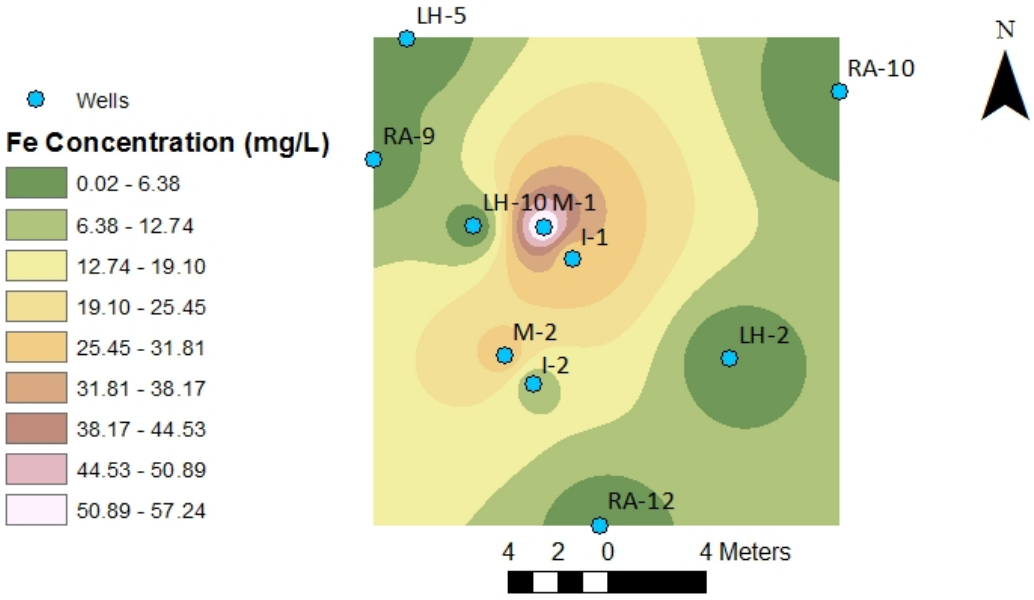

Figure 5.37: Interpolated surface showing the Fe distribution in theaquifer during the March 17th sampling event.

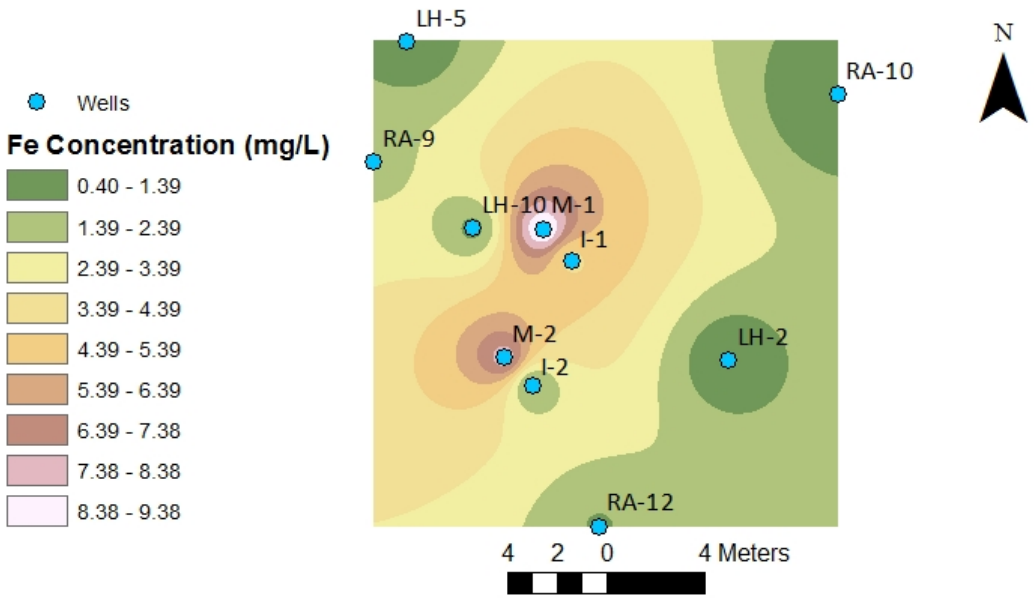

Figure 5.38: Interpolated surface showing the Fe distribution in the aquifer during the April 21st sampling event.

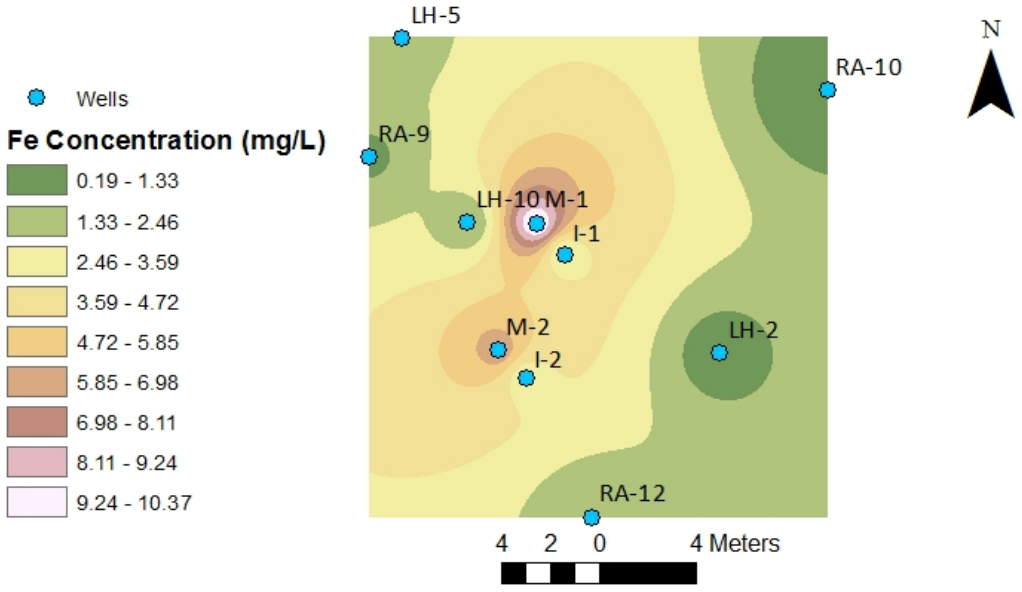

Figure 5.39: Interpolated surface showing the Fe distribution in the aquifer during the May 19th sampling event.

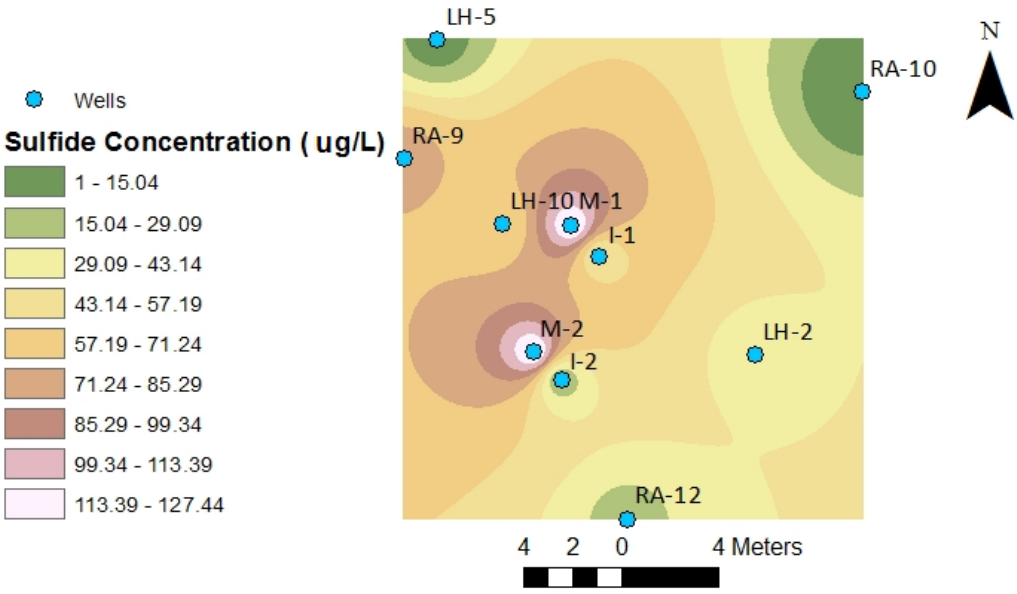

Figure 5.40: Interpolated surface showing the sulfide distribution in the aquifer during the February 15th sampling event.

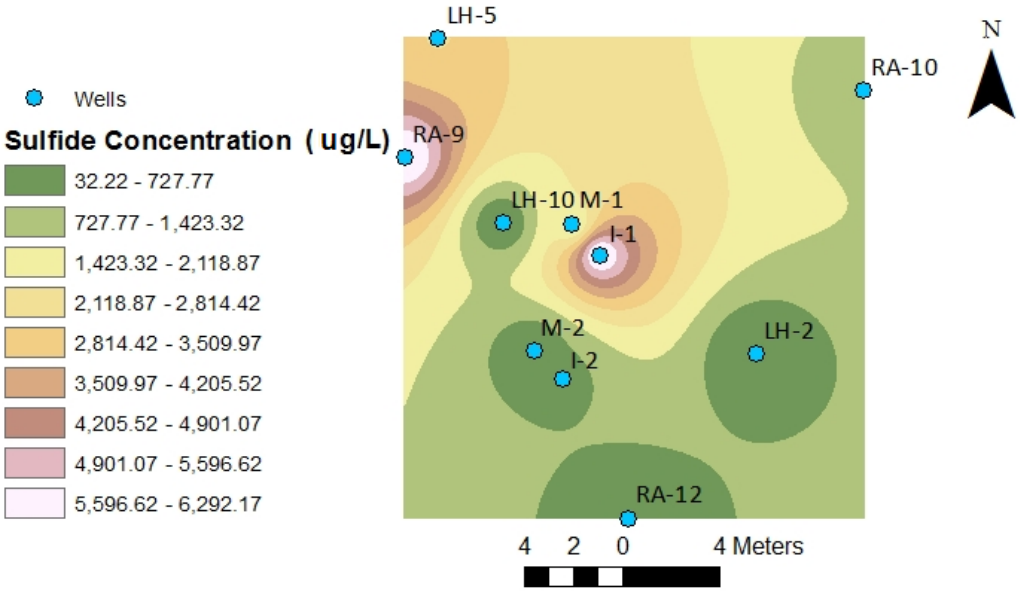

Figure 5.41: Interpolated surface showing the sulfide distribution in the aquifer during the February 24th sampling event.

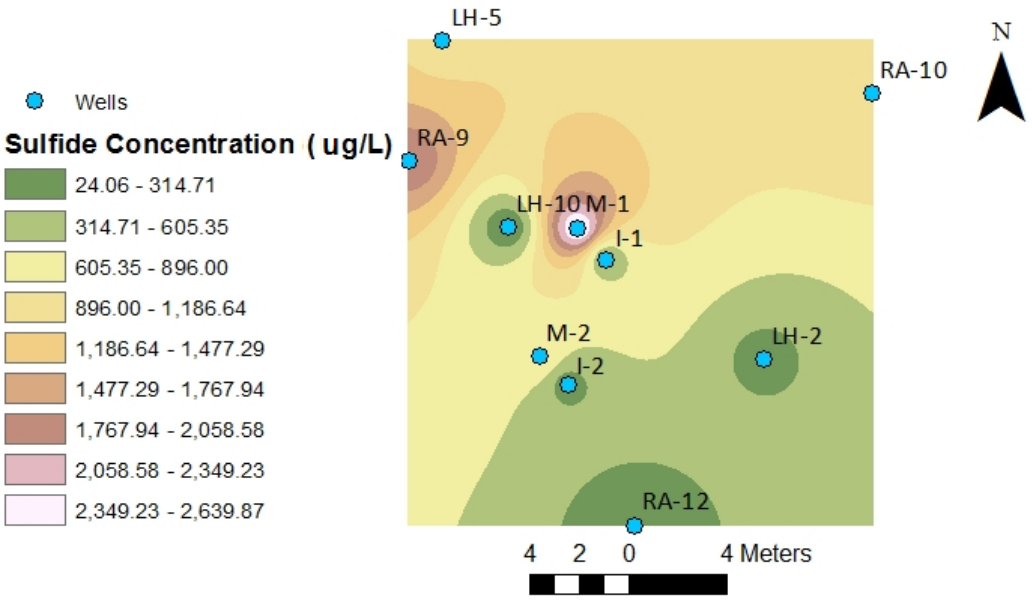

Figure 5.42: Interpolated surface showing the sulfide distribution in the aquifer during the March 2nd sampling event.

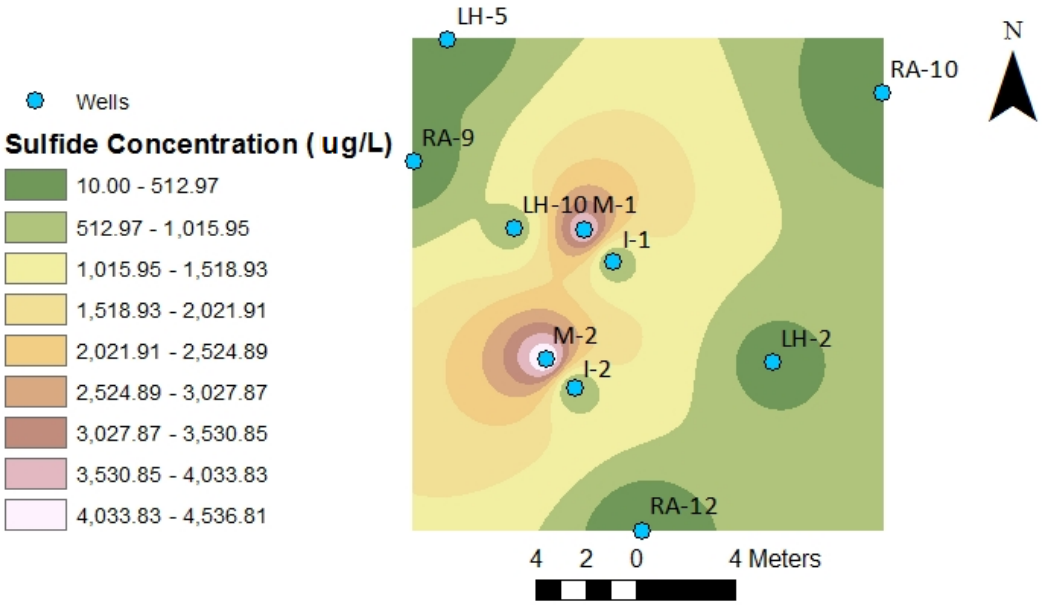

Figure 5.43: Interpolated surface showing the sulfide distribution in the aquifer during the March 9th sampling event.

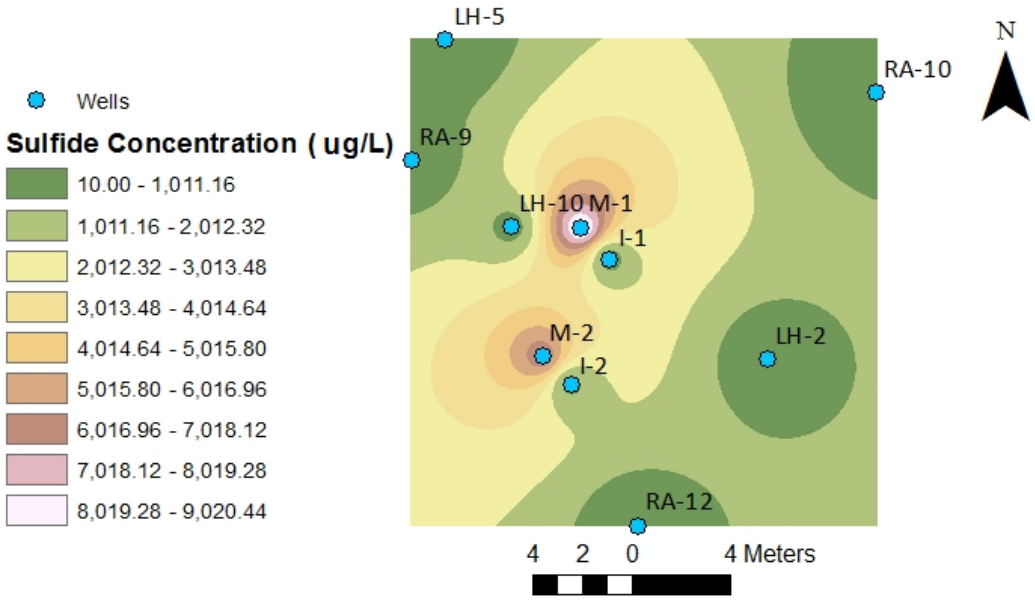

Figure 5.44: Interpolated surface showing the sulfide distribution in the aquifer during the March 17th sampling event.

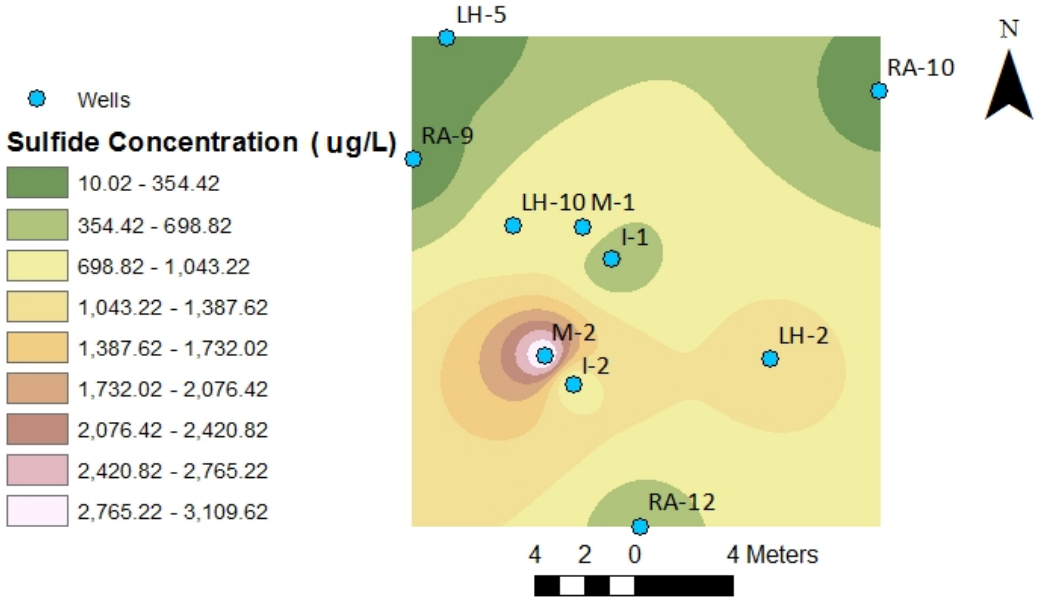

Figure 5.45: Interpolated surface showing the sulfide distribution in the aquifer during the April 21st sampling event.

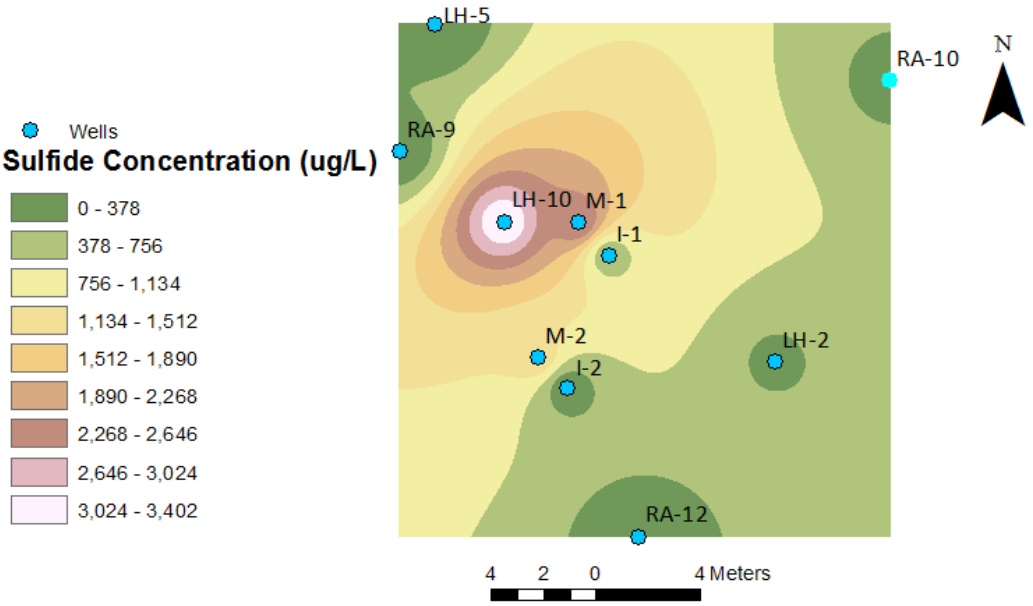

Figure 5.46: Interpolated surface showing the sulfide distribution in the aquifer during the May 19th sampling event.

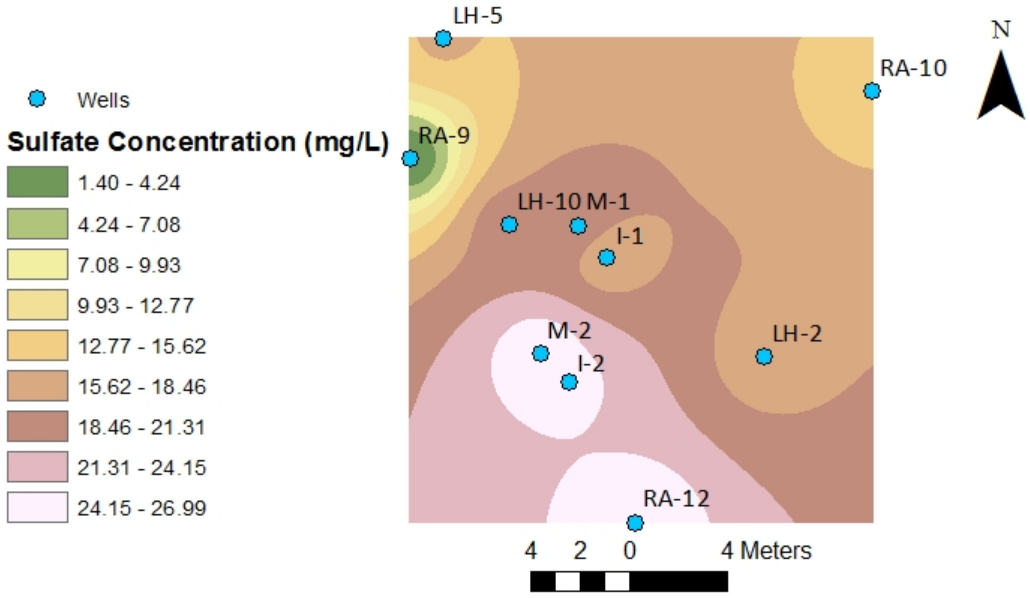

Figure 5.47: Interpolated surface showing the sulfate distribution in the aquifer during the February 15th sampling event.

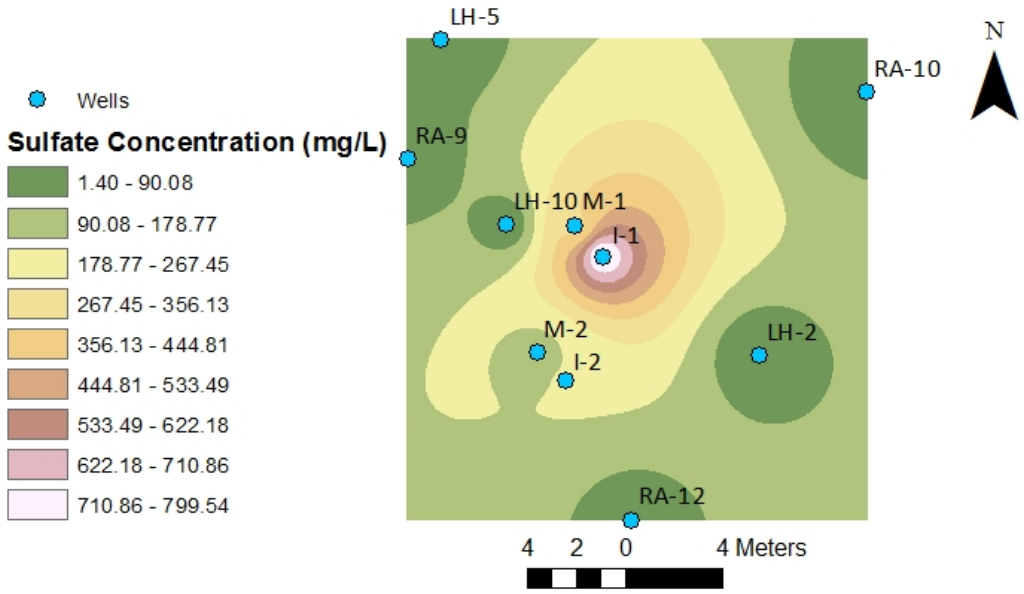

Figure 5.48: Interpolated surface showing the sulfate distribution in the aquifer during the February 24th sampling event.

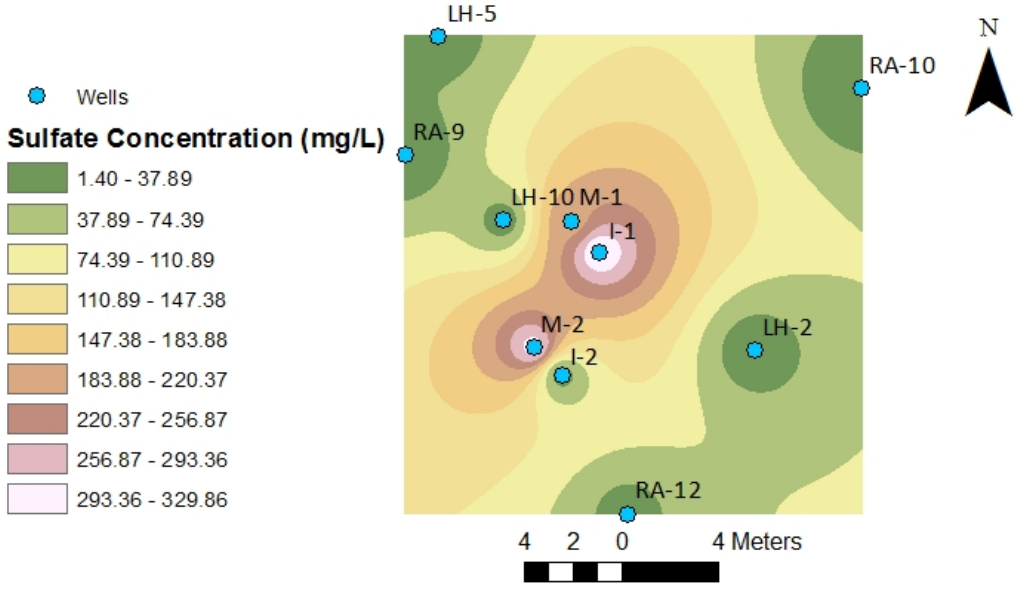

Figure 5.49: Interpolated surface showing the sulfate distribution in the aquifer during the March 2nd sampling event.

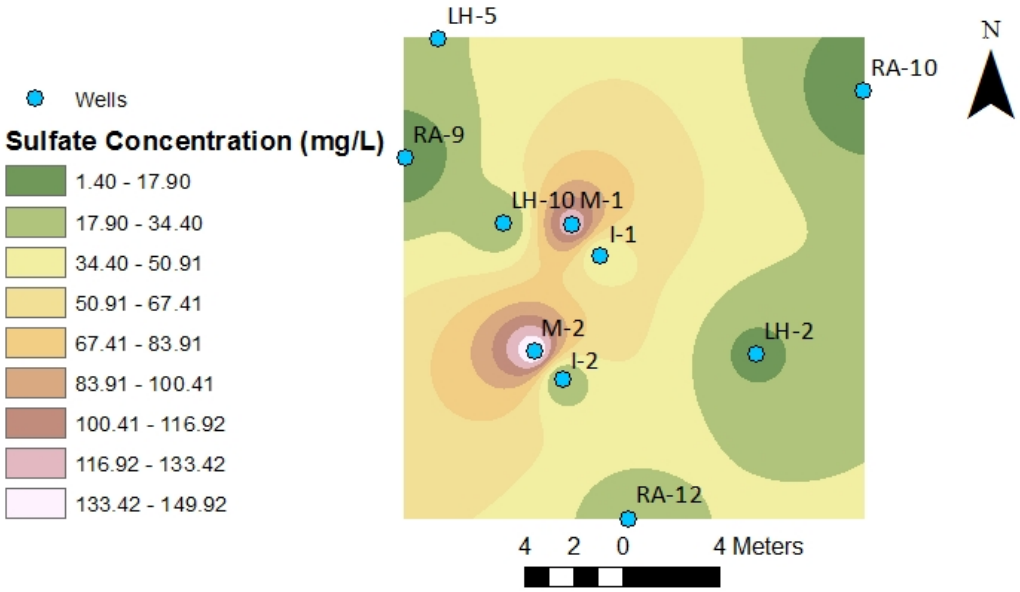

Figure 5.50: Interpolated surface showing the sulfate distribution in the aquifer during the March 9th sampling event.

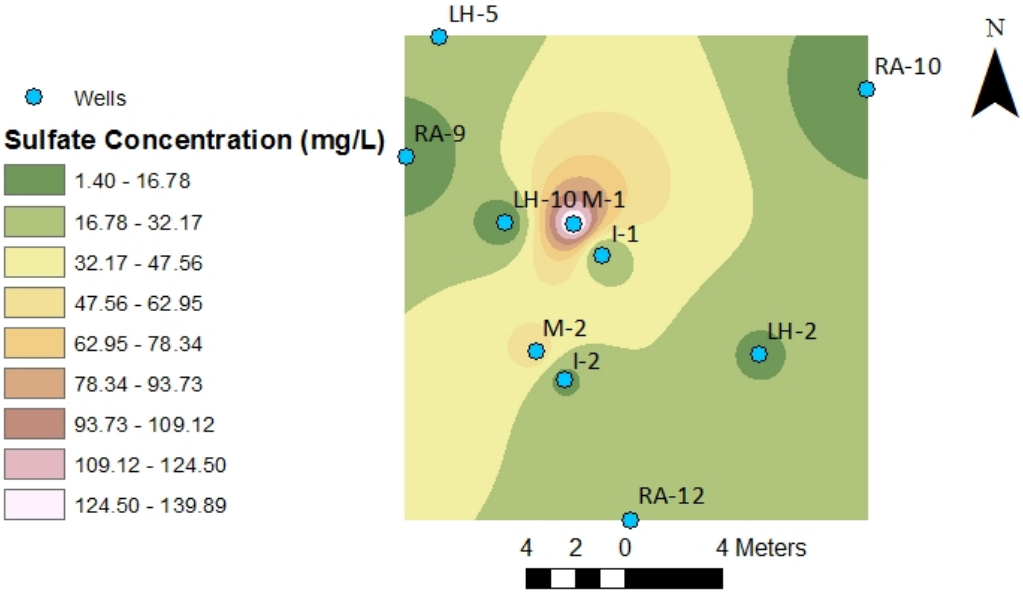

Figure 5.51: Interpolated surface showing the sulfate distribution in the aquifer during the March 17th sampling event.

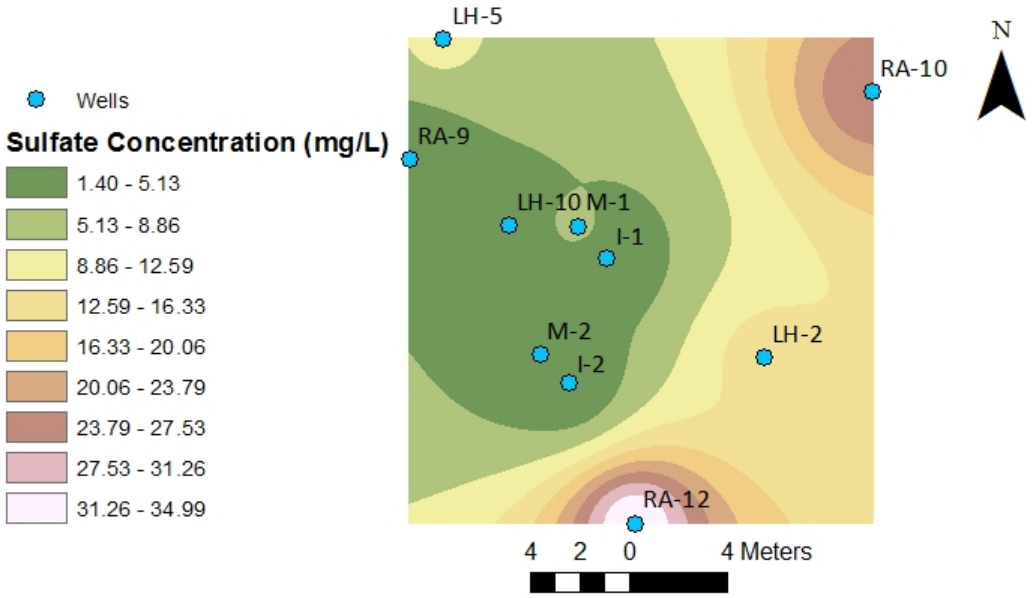

Figure 5.52: Interpolated surface showing the sulfate distribution in the aquifer during the April 21st sampling event.

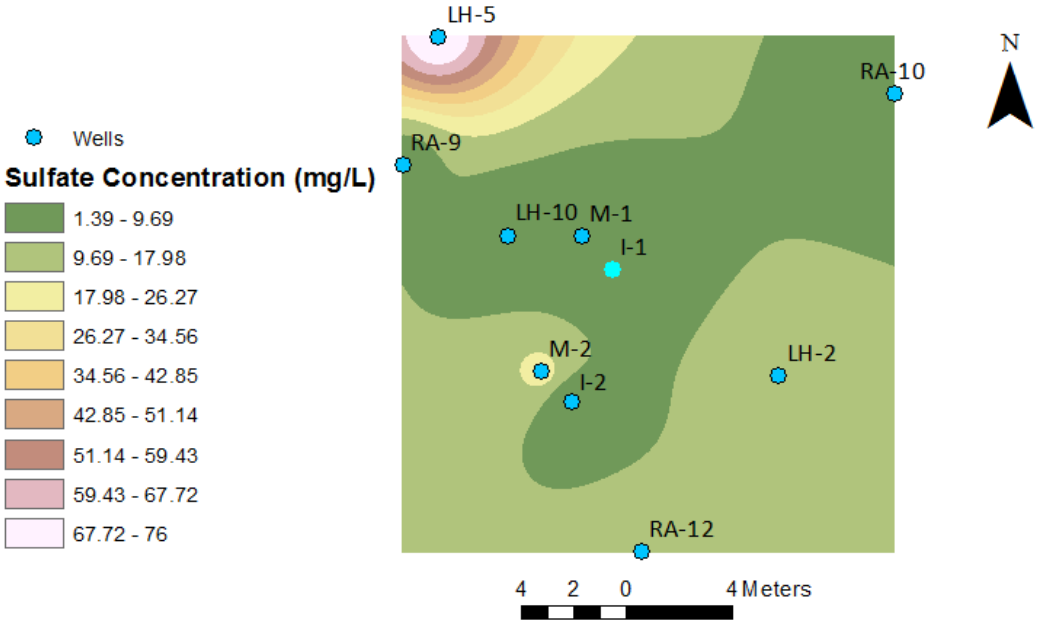

Figure 5.53: Interpolated surface showing the sulfate distribution in the aquifer during the May 19th sampling event.

5.4 Hydrogeologic and geochemical Modeling

In order to better understand the effects of injections on groundwater flow and the transport and fate of the injection solutions in the aquifer the changes in Fe concentration was predicted with MODFLOW and MT3DMS software. Starnes' model (Starnes, 2015) was modified to show how Fe concentration will change through time after the injections. Table 5.17 shows the hydrologic parameters used in creating the model (Starnes, 2015). The flow direction was predicted to have a west-northwest trend by Starnes model and the flow velocity was calculated to be on the order of a few to tens of meter per year.

Table 5.17: Hydraulic Parameters used to create the MODFLOW model.

Input Parameter	Value
Hydraulic Conductivity	0.0014 cm/s
Specific Storage	9.3×10^{-7} $\frac{1}{m}$
Storativity	0.01
Effective Porosity	0.35
Total Porosity	0.35
Dispersivity	10.4 meters
Recharge	66 cm/year
Distribution Coefficient	0 mL/g

Fe concentration was simulated through time to show how injection solution will affect the groundwater after certain amount of time. To do so, two injection wells were assigned in the model as I-1 and I-2. The injection rate was assigned to be 500 gallon per day (GPD), for I-2 and 1000 GPD for I-2 for two days. At the same time a point source was assigned on the same cell with the Fe concentration equal to Fe concentration in the injection solution. Based on laboratory data the weak injection solution, contained 300 $\frac{mg}{L}$ of Fe and the strong solution had 680 $\frac{mg}{L}$, which were assigned to I-1 and I-2 respectively.

Figures 5.54, 5.55, and 5.56 show the predicted Fe concentration 2, 100 and 365 days after the injections, assuming the conservative behavior of the element, thus adsorption and pyrite precipitation is not considered in this model. The model was run with distribution coefficient equal to zero (no adsorption), in order to yield the highest Fe concentration in the groundwater after the injections. The model shows that the plume will move in the general direction of the groundwater flow (northwest) over a period of one year. The first few days, because of the injection of the solution a cone was created in each of the injection wells, and the size of the plume was very small initially with very limited advection and spreading (Figure 5.54). The predicted Fe concentration the 2nd day after the injection, does not match the real measured Fe concentration of the groundwater, perhaps due to oxidation and resuspension of Fe. However, as the time passes the predicted concentrations get closer to the measured concentrations. Almost 100 days after the injections, predicted Fe concentrations in most of the wells are almost the same as the measured concentrations but a little higher. The center mass of plume moved a few feet in the groundwater direction (5.55). The higher predicted concentration can be due to the fact that this model is not considering pyrite formation and any kind of precipitation and adsorption. After one year the model predicts that the center mass of the plume moves almost 20 feet toward northwest direction and the Fe concentration decrease even more, due to advective transport and hydrodynamic dispersion (5.56).

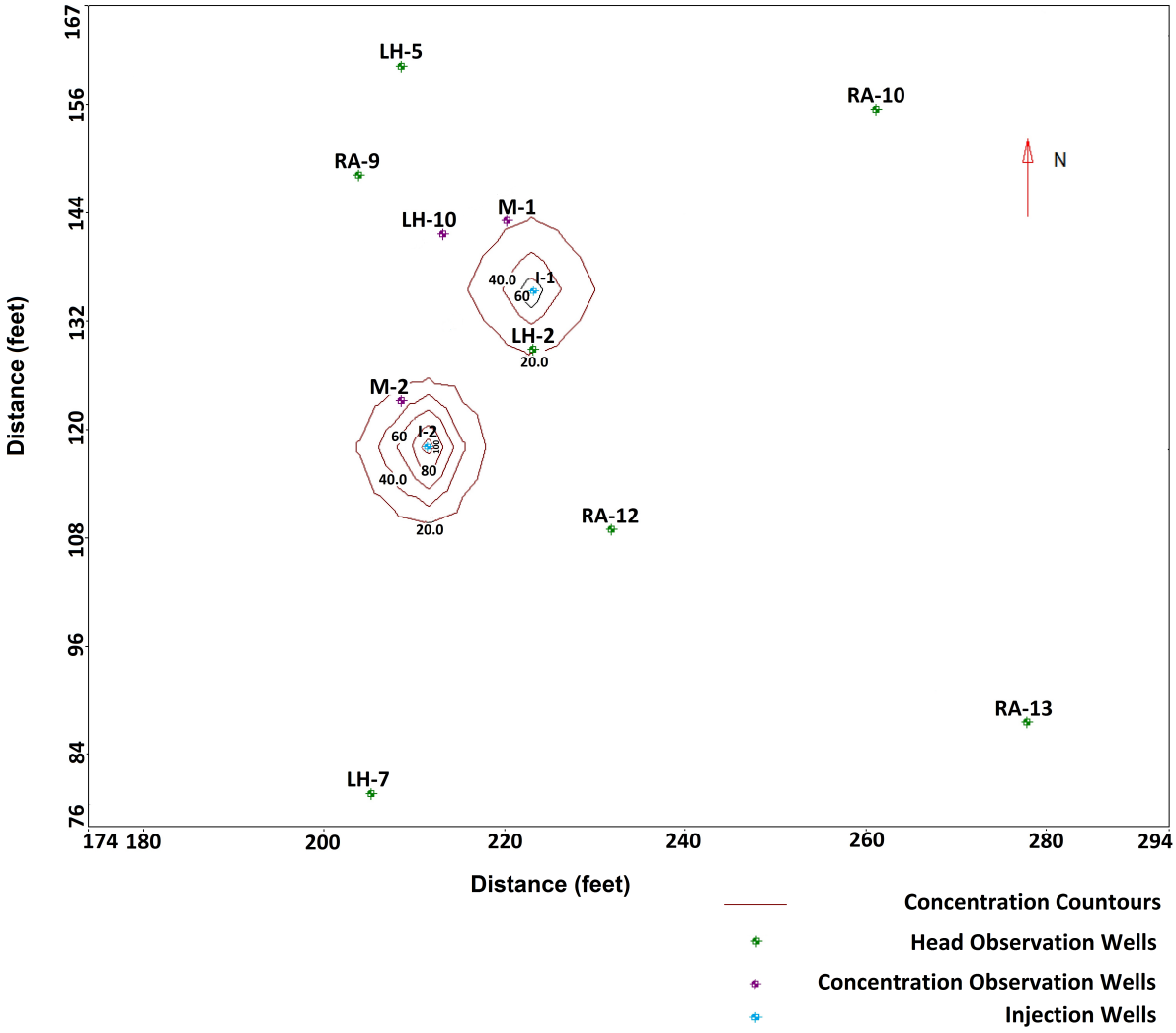

Figure 5.54: The simulated concentration contours of Fe for 2 days after the injections. Concentration contours are in $\frac{mg}{L}$.

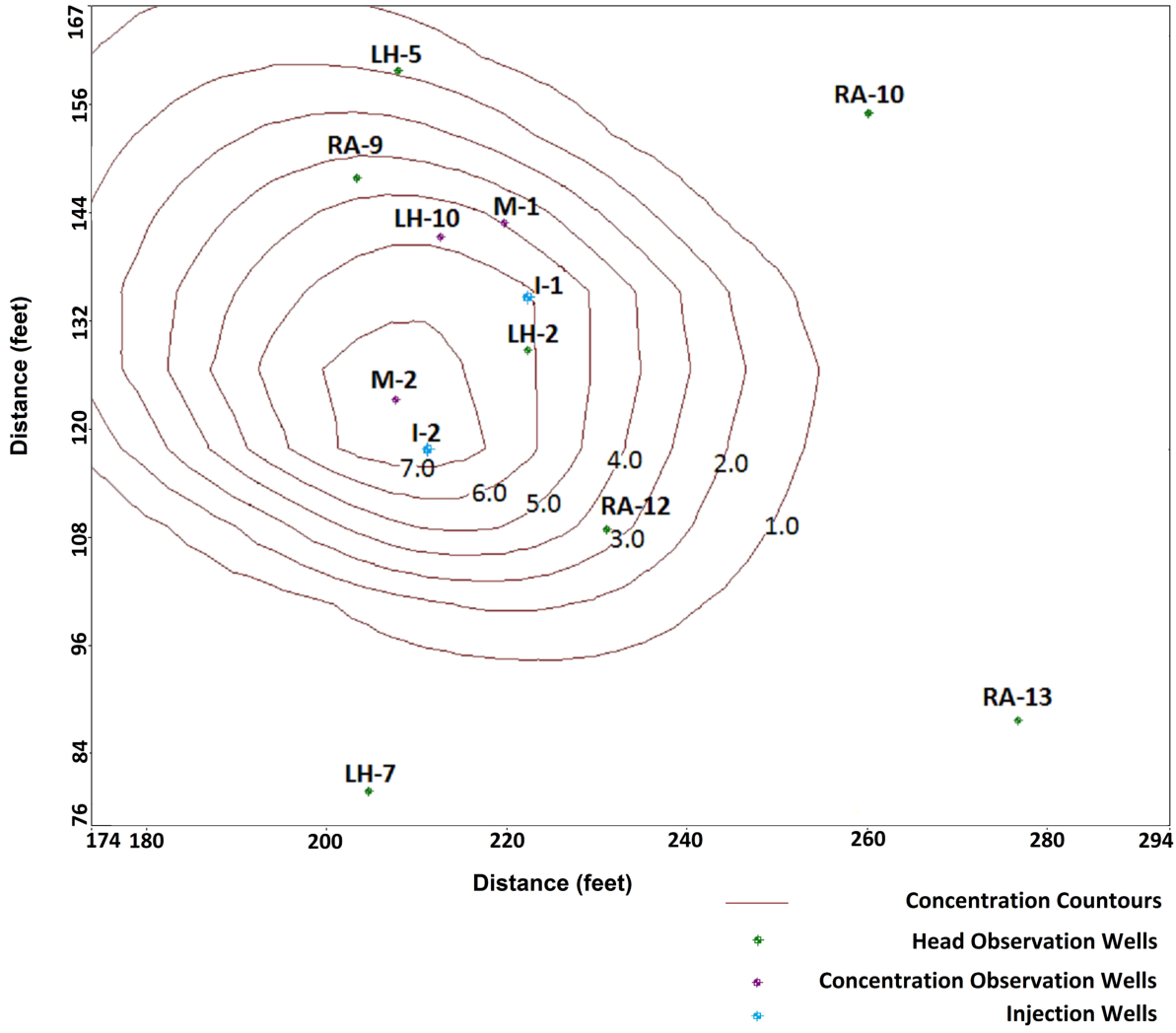

Figure 5.55: The simulated concentration contours of Fe for 100 days after the injections. Concentration contours are in $\frac{mg}{L}$.

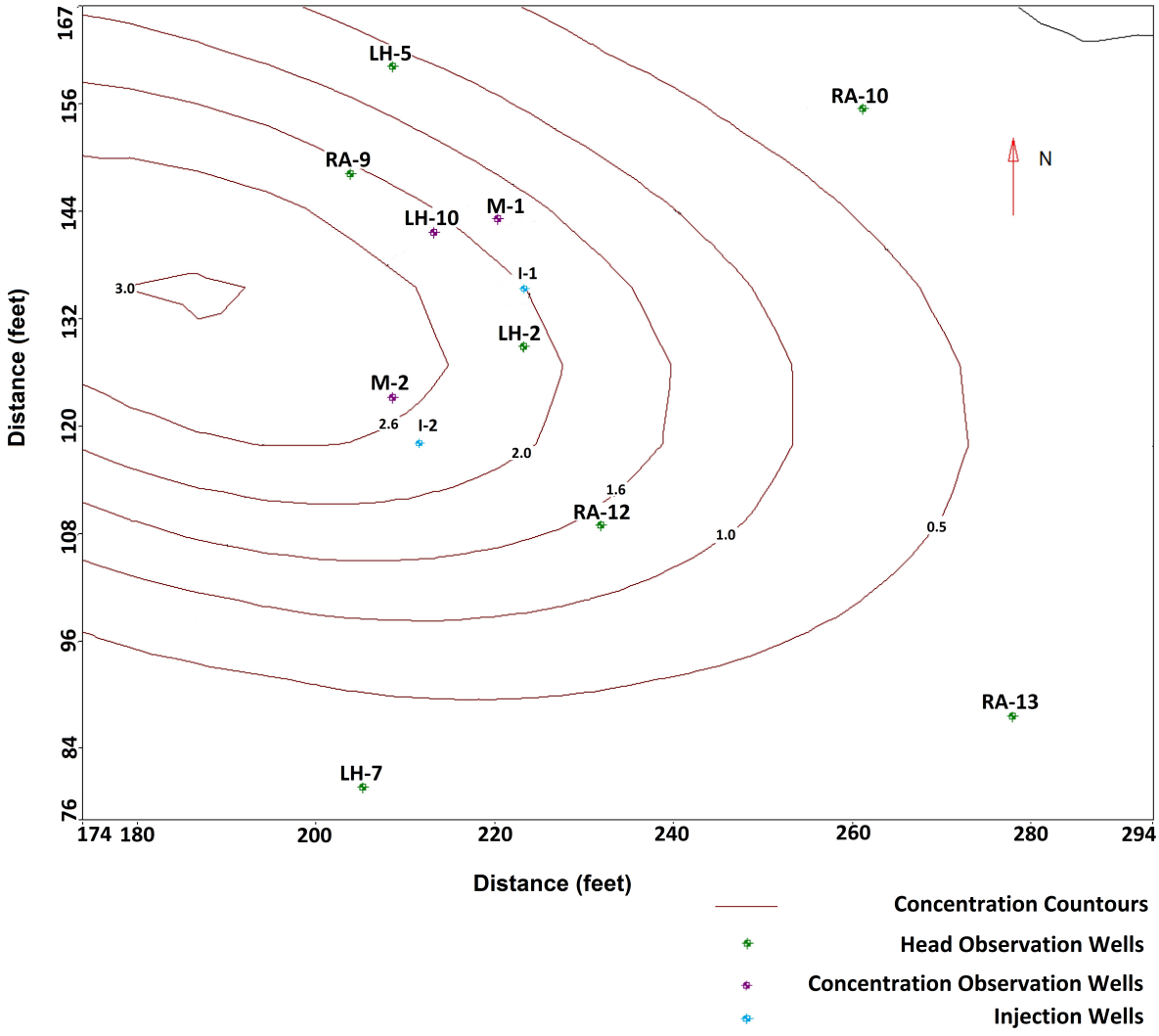

Figure 5.56: The simulated concentration contours of Fe for 365 days after the injections. Concentration contours are in $\frac{mg}{L}$.

Geochemist's workbench (Bethke, 2007) was used to create Eh-pH activity diagrams that show the dominant As species during each sampling event in the presence of Fe and sulfate. Therefore, the stability field of aqueous and solid phases of Fe, As and S, under different pH-Eh conditions are shown (activity of Fe = 10^{-5}, activity of sulfate = 10^{-5}, and activity of As = 10^{-3}). In each diagram pre-injections data are accompanied with the corresponding data for a discrete sampling event. Figure 5.57 shows the pre-injection data

along with the first week after the injections data. Pre-injection data show that most of the wells are in a mildly reducing and slightly acidic condition. The first week after the injections groundwater in all of the wells quickly became more reducing, and groundwater in four new wells were mostly in the slightly basic condition. Most of the groundwater samples plot in the stability field of arsenite [$As(OH)_3$].

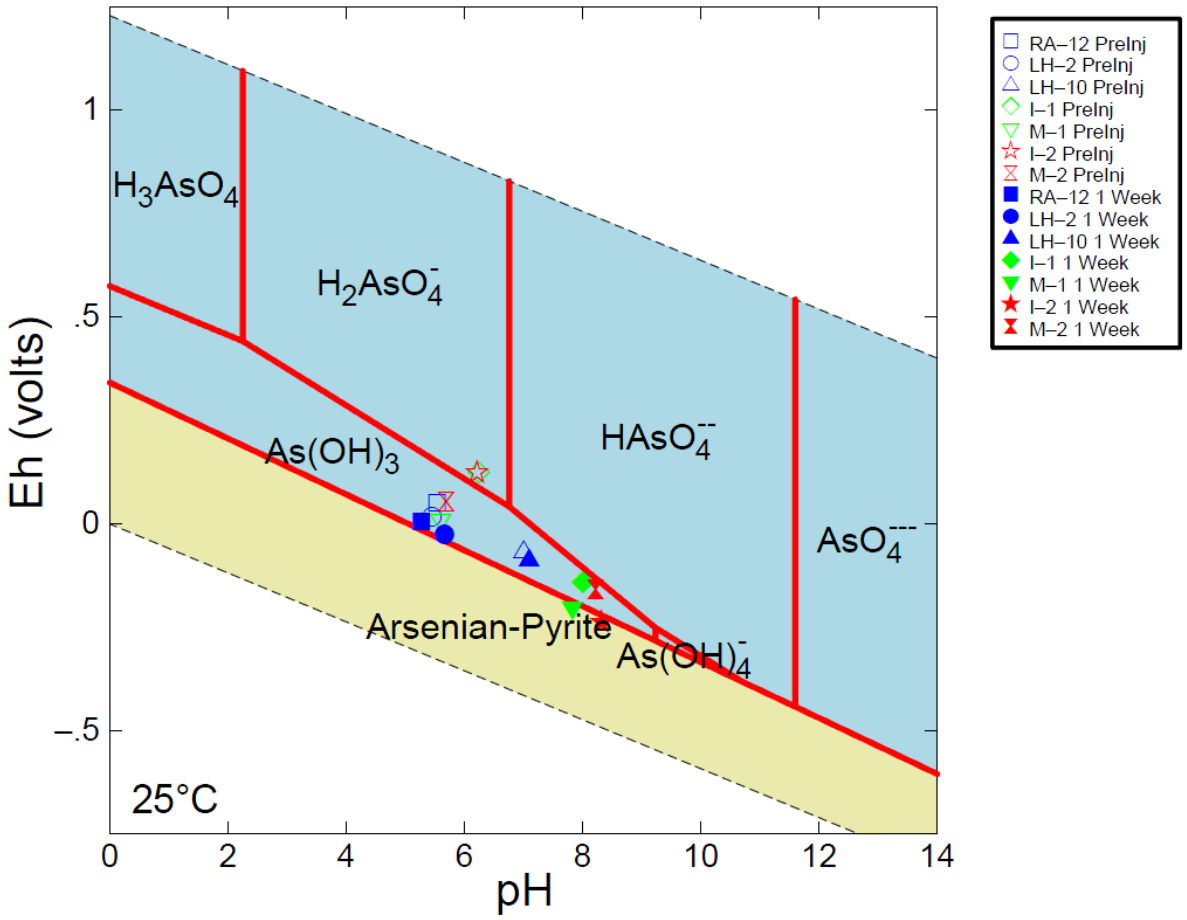

Figure 5.57: Eh-pH diagram indicating the stability field of different As species under different redox condition, in the presence of Fe and sulfate. The Eh and pH data for each well in pre-injections sampling event and the first week after the injections are plotted on the diagram (the blue sections are showing the aqueous phases and the tan-colored area shows the solid phases).

Figure 5.58 shows the Eh-pH diagram with groundwater data for the second week after the injections as well as the pre-injections data. This diagram shows that groundwater in most of the wells is still in the mildly reducing conditions. The geochemical condition have changed to a slightly more acidic condition than was present before the injections in

the second week. Most of the groundwater analyses still plot in the field of $As(OH)_3$ and groundwater in I-1 and M-2 plots in the arsenian-pyrite field.

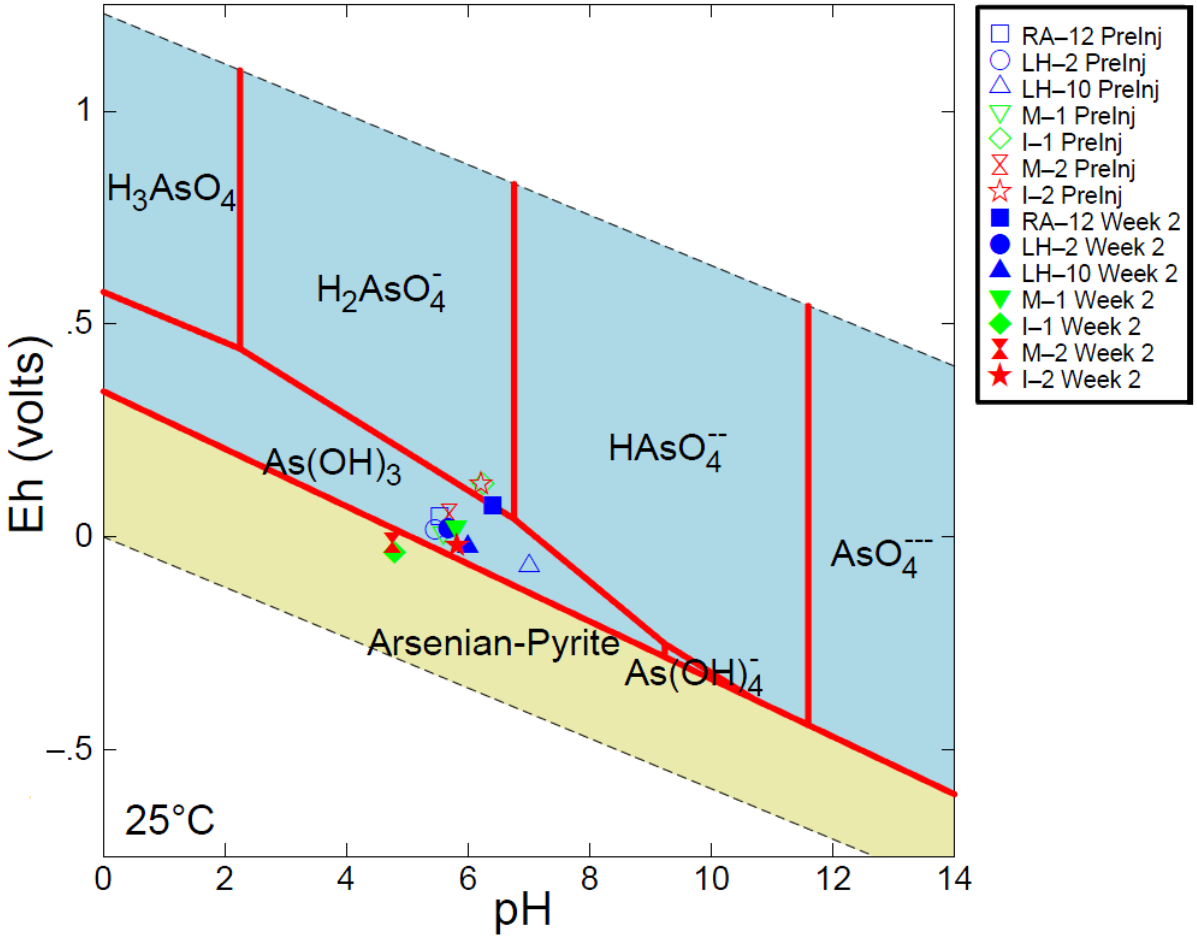

Figure 5.58: Eh-pH diagram indicating the stability field of different As species under different redox condition, in the presence of Fe and sulfate. The Eh and pH data for each well in pre-injections sampling event and the second week after the injections are plotted on the diagram (the blue sections are showing the aqueous phases and the tan-colored area shows the solid phases).

The Eh-pH diagram for the third week (Figure 5.59) shows that the groundwater became more reducing than the week before, but the pH is almost the same as the second week after

the injections. During this sampling event most of the wells (especially the four new wells) are plotted in the arsenian-pyrite stability field. The fourth week after the injections the Eh decreased and caused all of the groundwater samples to be in the arsenian-pyrite stability field (Figure 5.60). During the fifth sampling event, which took place almost two month after the injections, the Eh had increased slightly from the previous month, but the arsenian-pyrite was still the dominant As species (Figure 5.61). Three months after the injections groundwater samples are slightly less reducing than the last sampling event, but they are still more reducing than the pre-injections conditions and most groundwater samples still plot in the field of arsenian-pyrite (Figure 5.62).

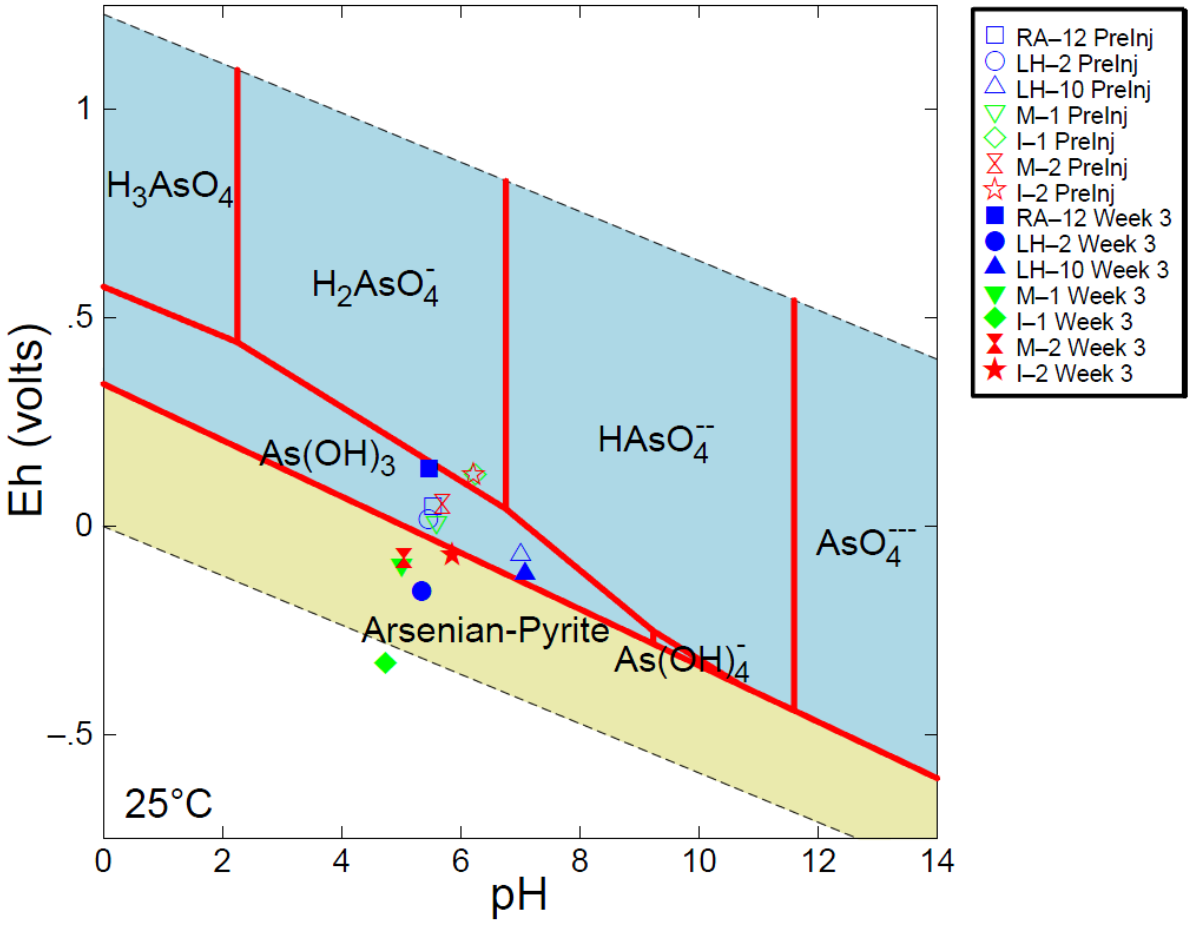

Figure 5.59: Eh-pH diagram indicating the stability field of different As species under different redox condition, in the presence of Fe and sulfate. The Eh and pH data for each well in pre-injections sampling event and the third week after the injections are plotted on the diagram (the blue sections are showing the aqueous phases and the tan-colored area shows the solid phases).

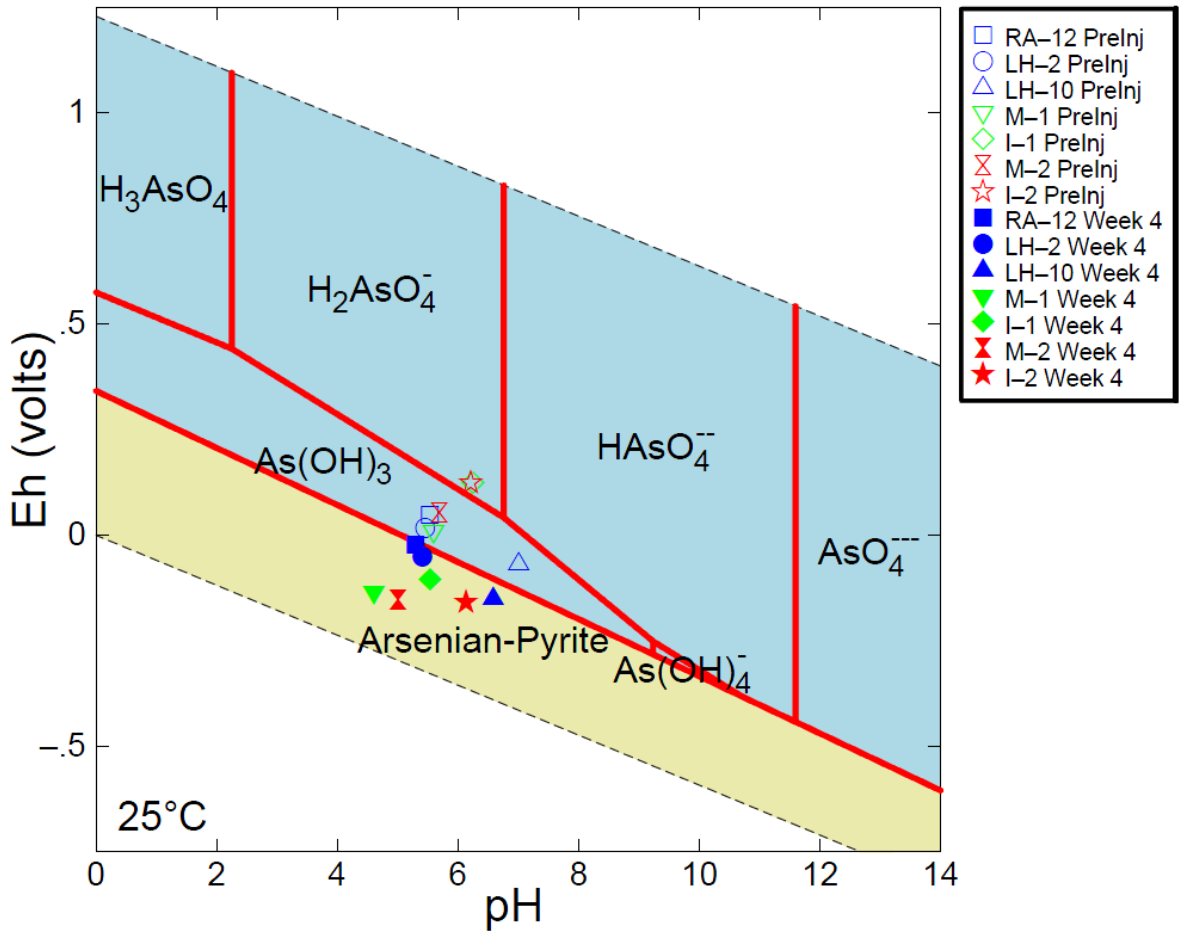

Figure 5.60: Eh-pH diagram indicating the stability field of different As species under different redox condition, in the presence of Fe and sulfate. The Eh and pH data for each well in pre-injections sampling event and the fourth week after the injections are plotted on the diagram (the blue sections are showing the aqueous phases and the tan-colored area shows the solid phases).

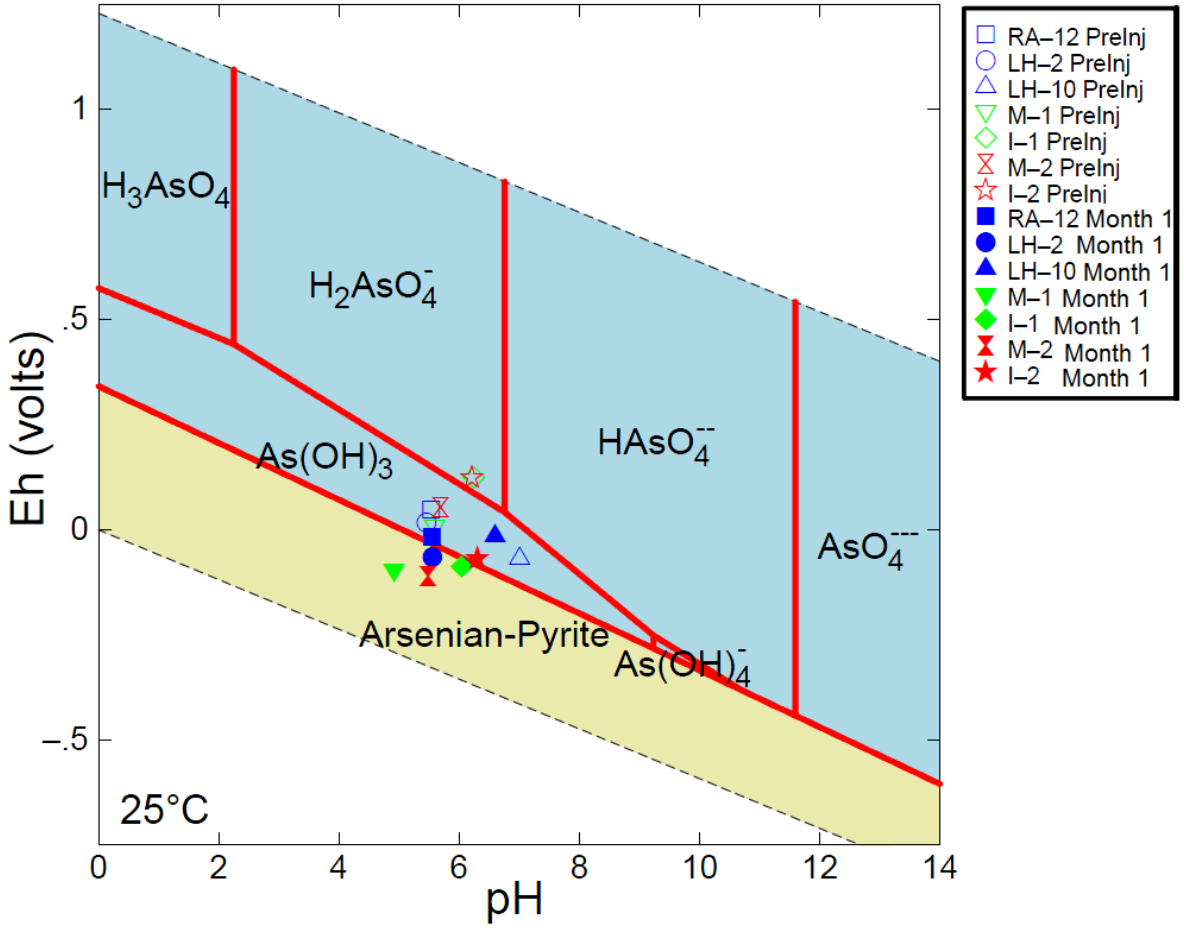

Figure 5.61: Eh-pH diagram indicating the stability field of different As species under different redox condition, in the presence of Fe and sulfate. The Eh and pH data for each well in pre-injections sampling event and the two month after the injections are plotted on the diagram (the blue sections are showing the aqueous phases and the tan-colored area shows the solid phases).

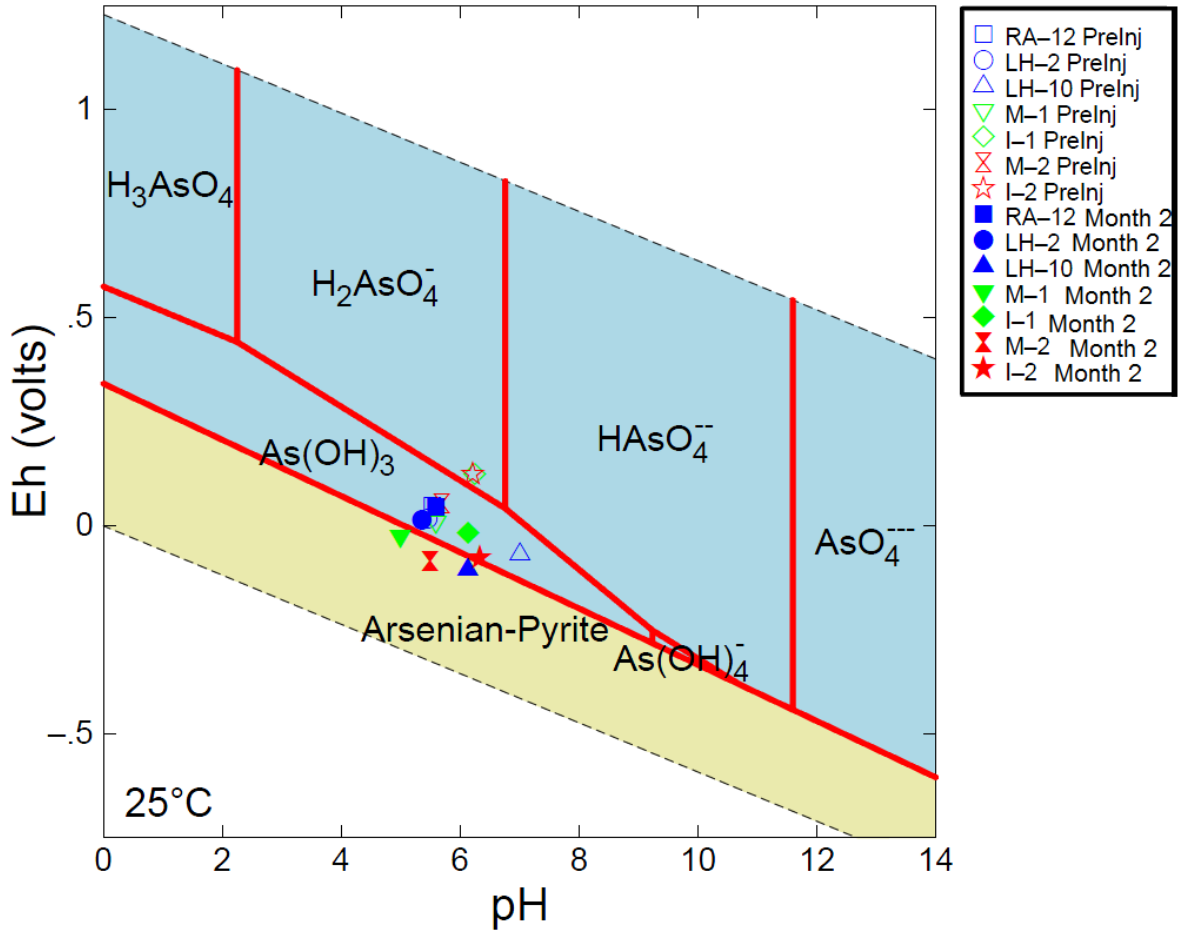

Figure 5.62: Eh-pH diagram indicating the stability field of different As species under different redox condition, in the presence of Fe and sulfate. The Eh and pH data for each well in pre-injections sampling event and the three month after the injections are plotted on the diagram (the blue sections are showing the aqueous phases and the tan-colored area shows the solid phases).

5.5 XRD and XRF Analyses of Groundwater Precipitates

XRD and XRF analyses were conducted on two of the solid samples that were collected from the bottom of the wells (I-2 from April 21st sampling event and M-2 from the March

17th sampling event). XRF analyses of solid samples show peaks for As, Fe, and S (Figure 5.63 and 5.64). Figures 5.65 and 5.66 show XRD results that indicate the presence of arsenian-pyrite in these solid samples that matches arsenian-pyrite from lignite from Czech Republic (Rieder et al., 2007).

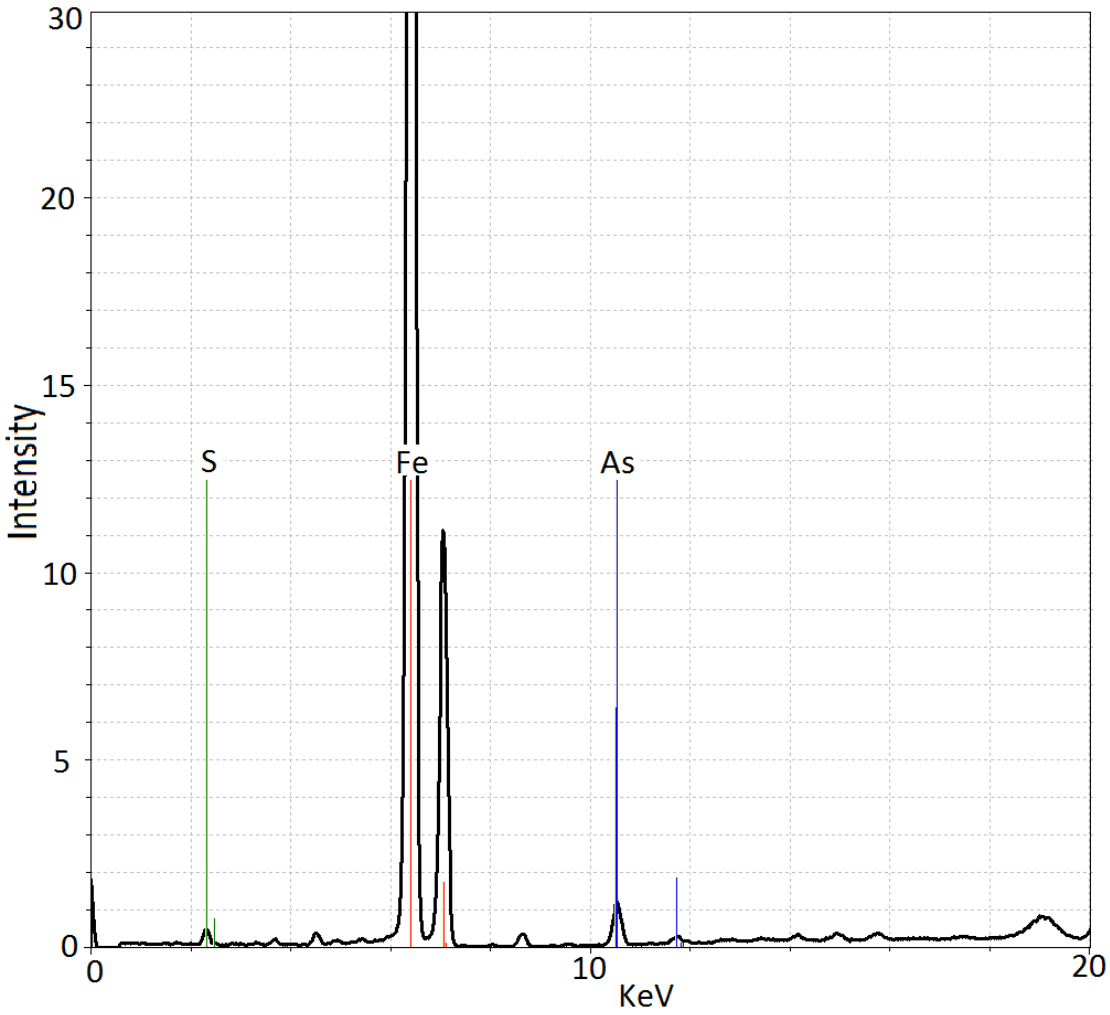

Figure 5.63: XRF spectrum of solid samples from the bottom of I-2 in the April 21st sampling event. The peaks for As, S, and Fe show the presence of these elements in the solid phase in this well.

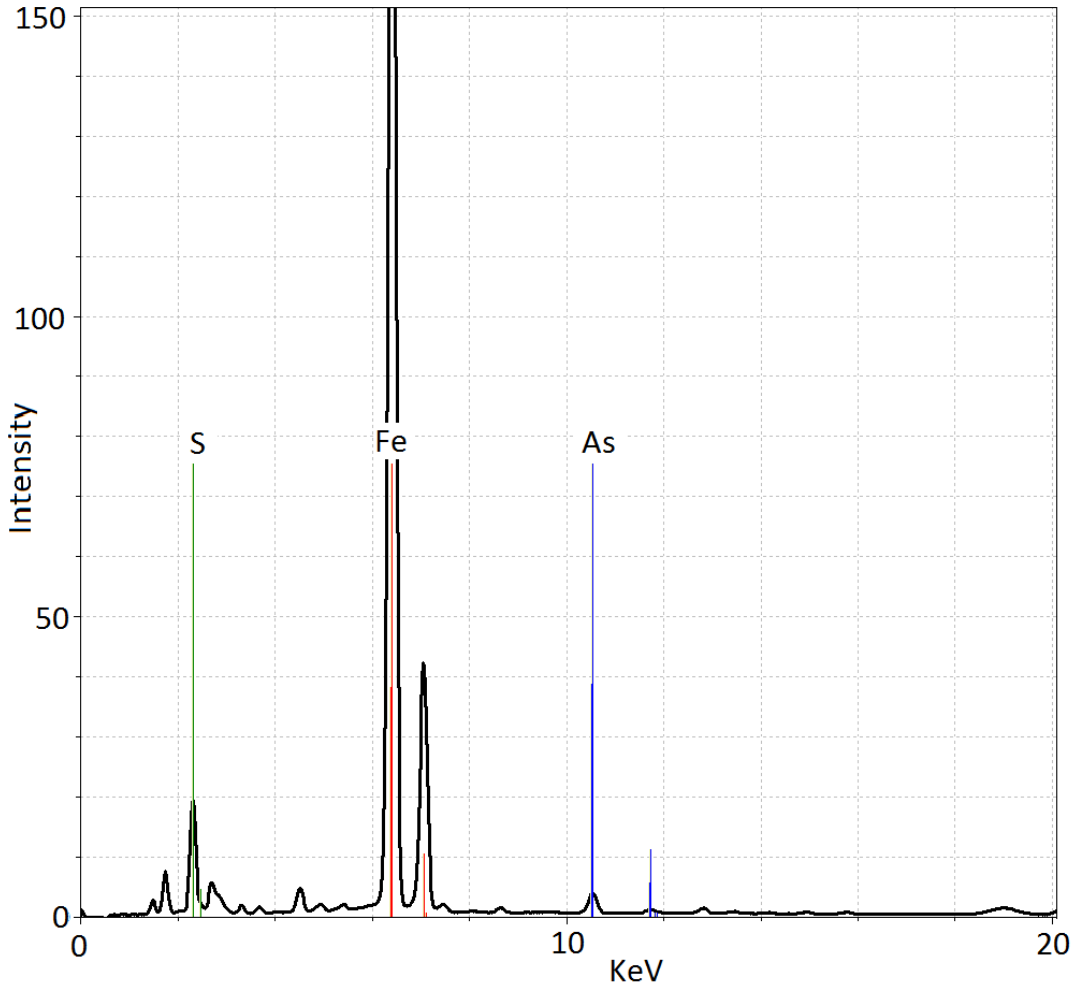

Figure 5.64: XRF spectrum of solid samples from the bottom of M-2 in the March 17th sampling event. The peaks for As, S, and Fe show the presence of these elements in the solid phase in this well.

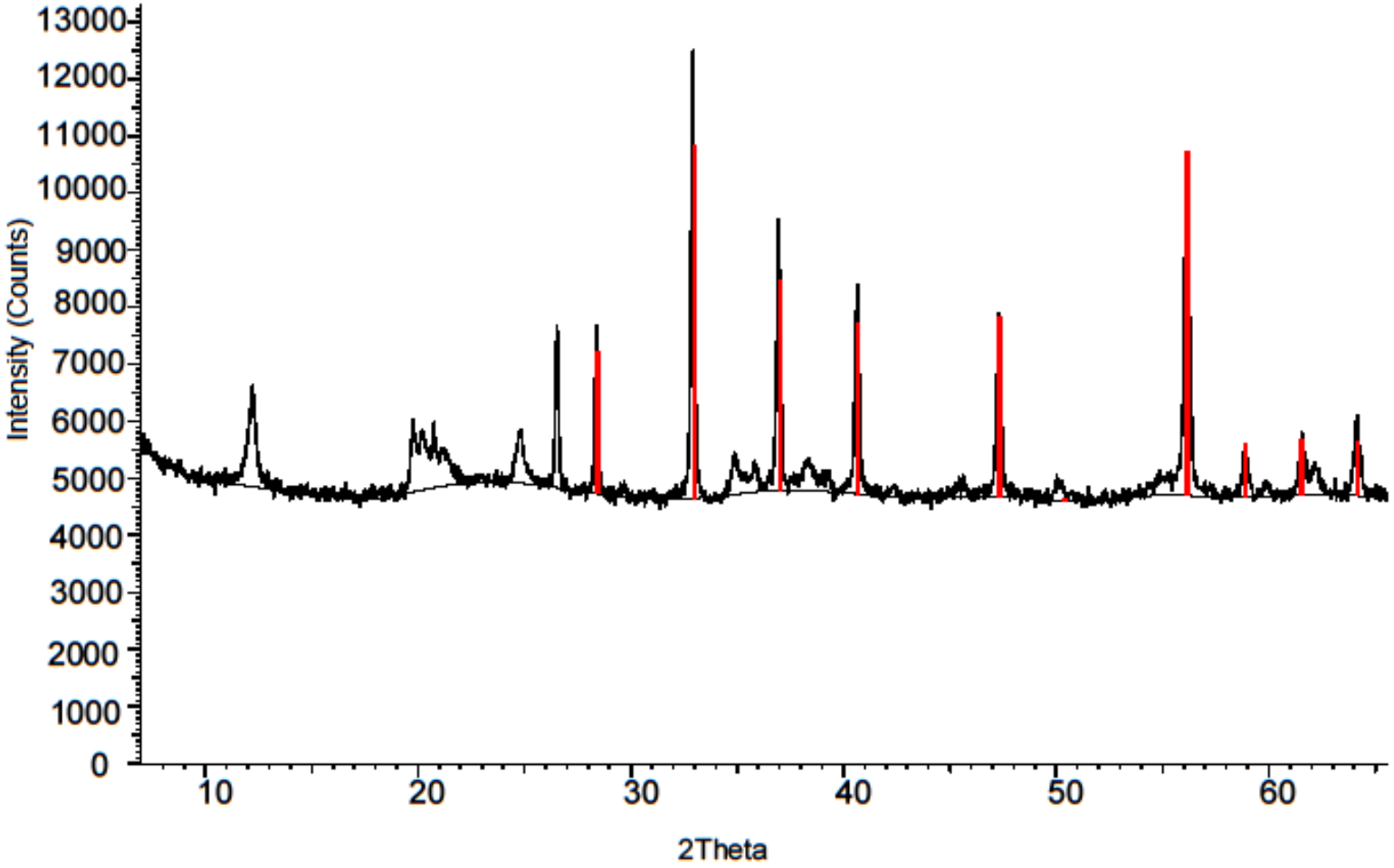

Figure 5.65: XRD spectrum of solid samples from the bottom of I-2 during April 21st sampling event. The red lines are arsenian-pyrite peaks from Rieder et al. (2007).

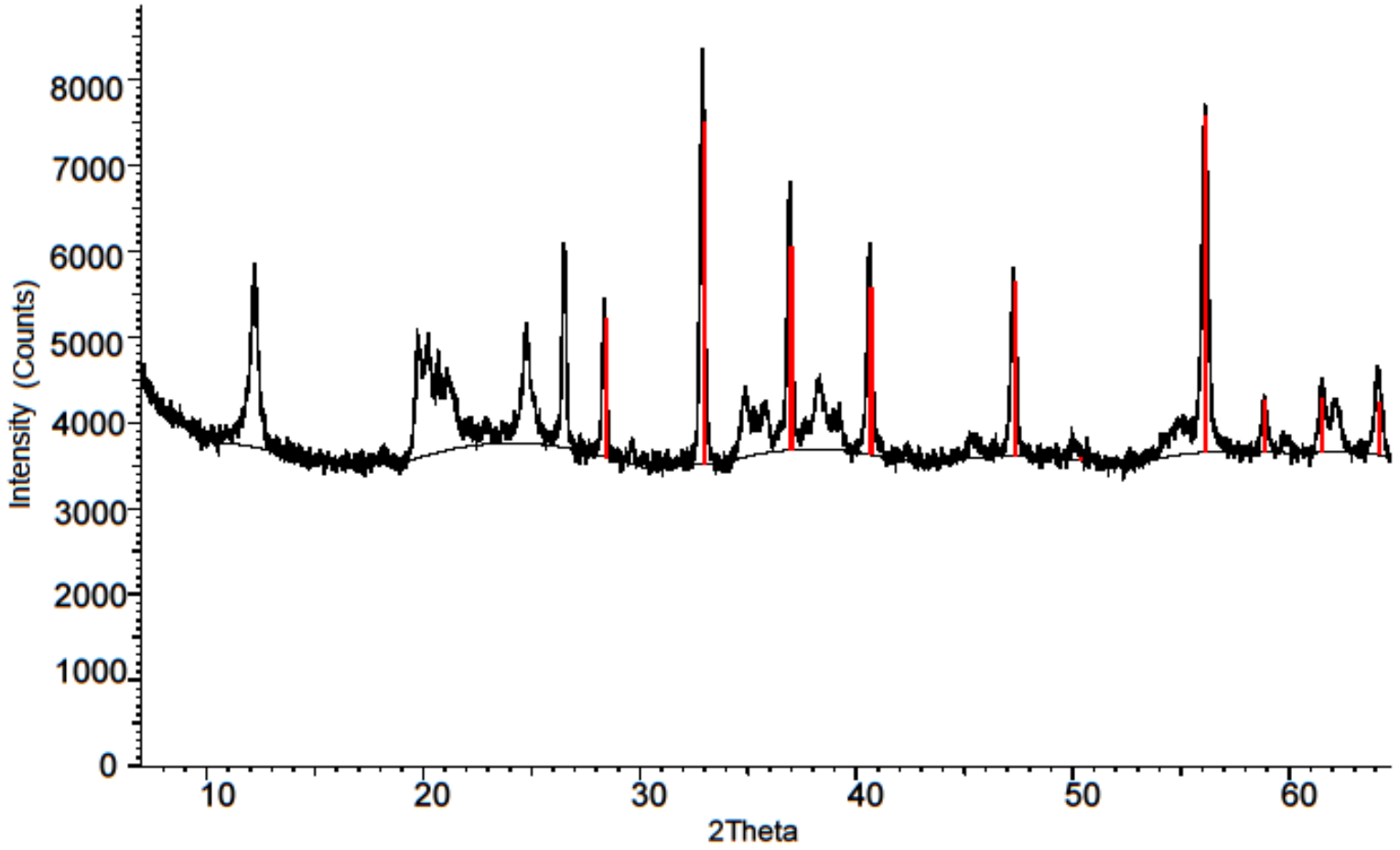

Figure 5.66: XRD spectrum of solid samples from the bottom of M-2 during March 17th sampling event. The red lines are arsenian-pyrite peaks from Rieder et al. (2007).

Chapter 6

Discussion

6.1 Field Measurements of Geochemical Parameters

The increases in temperature are most likely a result of seasonal change in the weather temperature from January to May. The pH values before the injections are slightly below neutral pH, whereas after the injections the pH increased dramatically in all four new wells to around 8. This is probably due to the fact that injections have established a sulfate reducing conditions in which more protons are being removed from the groundwater as SO_4^{2-} is converted into H_2S, causing the pH to increase. The decrease in pH levels the second week after the injections can be due to introduction of oxygen to groundwater by purging and pumping the wells, that can oxidize Fe^{2+}, create $Fe(OH)_3$ and release protons into the groundwater. It is similar to positive feedback effect of generating acid mine drainage. Large fluctuations in the pH from the first couple of weeks after the injections can also be due to the presence of high organic carbons in the groundwater. pH values become stable and return to background levels almost one month after the injections.

ORP values before the injections showed a mildly reducing conditions (44.4±63.6 mV). The week after the injections the ORP values dropped significantly to even more reducing values (-121±83.2 mV) in most of the wells. This is again probably due to the effect of injections on the groundwater and establishment of sulfate reducing conditions in the aquifer. Also from a microbiology stand point perhaps sulfate-reducing bacteria began to out compete Fe-reducing bacteria by dropping the ORP/Eh (Chapelle & Lovley, 1992). The first few weeks after the injections, fluctuations were observed in the ORP data, which perhaps could be due to organic carbon interfering with the ORP probe. Almost three months after the injections, the average ORP for all the wells was negative, suggesting a mildly reducing

conditions in the aquifer, implying that the sulfate-reduction continues at a lower rate. Even though the ORP levels have increased relative to the first week after the injections, the As concentration in the water samples are still decreasing, which is discussed below.

The conductivity increased significantly, after the injections, which is most probably due to the high TDS composition of injection solution and resuspension of solids. With consumption of ions present in the solution (particularly sulfate and Fe), resulting in decrease in TDS, the conductivity began to drop from the second week and stabilized after a month.

DO data for the week before the injections shows an average of 0.46 $\frac{mg}{L}$. The two injection wells had higher DO levels in that week (The highest was I-1 with 1.47 $\frac{mg}{L}$). The week after the injections the DO levels in the four newly installed wells decreased rapidly, due to establishment of more reducing conditions in the groundwater. The slight increase in DO, during the last couple of sampling events, is consistent with the slight increase in ORP, suggesting that the groundwater became less reducing than the first week after the injections. The fluctuations in the DO concentration might also be due to rainfall and water table changes in the groundwater.

Total alkalinity can be defined as the measure of the total amount of chemical bases (e.g., HCO_3^-, CO_3^{2-}, and OH^-). Average of total alkalinity in the groundwater before the injections was 57.1 $\frac{mg}{L}$. The weeks after the injections, we expected to observe high alkalinity in the four new wells, due to having a high amount of dissolved carbonate in the system, but because of low pH-Eh conditions in the groundwater, the dominant carbonate species in the water was carbonic acid and bicarbonate and carbonate concentration was relatively low (Drever, 1997), therefore the alkalinity that was recorded may not be representative of the real alkalinity for the system. Although the alkalinity test was conducted for all the wells in the field during the sampling events, due to problems related to the precision of the field technique, alkalinity results presented in this study are the lab measurements from the commercial lab (Test America Ltd.).

The average ferrous iron concentration before the injections in the groundwater was 0.81 $\frac{mg}{L}$. In the first two weeks after the injections the ferrous iron concentration increased significantly to an average of 49.6 $\frac{mg}{L}$ due to the injection of ferrous iron into the groundwater, and a smaller portion of the extra ferrous iron may have been added due to the reduction of ferric iron to ferrous iron, after the injection which is a result of iron-reducing conditions which occur before sulfate reducing conditions (Chapelle & Lovley, 1992; Rittle et al., 1995; Saunders et al., 2008; Nickson et al., 2000). Fe-reducing bacteria compete with sulfate-reducing bacteria and in a certain redox condition by maintaining dissolved hydrogen, formate and acetate concentrations at low levels, Fe-reducing bacteria can minimize sulfate-reducers activity (Chapelle & Lovley, 1992). By establishment of sulfate reducing conditions and subsequent precipitation of iron sulfides from the groundwater, ferrous iron concentration decreased significantly to an average of 2.99 $\frac{mg}{L}$, three months after the injections. The total iron concentration follows the same trend as the ferrous iron concentration. Figure 6.1 shows ferrous iron concentration compared to total iron in the groundwater.

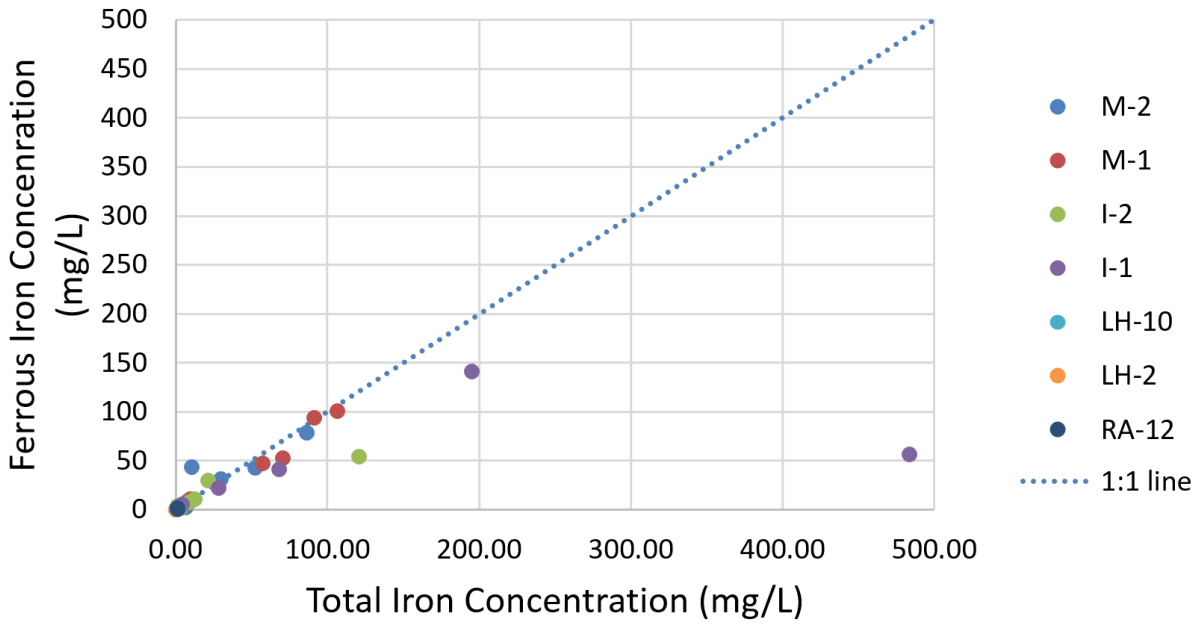

Figure 6.1: Plot showing Concentration of total iron compared to ferrous iron in groundwater. The inaccuracy of our field measurement tests can be the reason for the out lier data point for I-1.

The average dissolved sulfide concentration in the wells was 0.062 $\frac{mg}{L}$, before the injections. It increased significantly the first few weeks after the injections due to injection of sulfate into the groundwater, which had increased the sulfate-reducing bacteria metabolism and by reduction of sulfate to sulfide, the concentration of sulfide increased in the groundwater. Two injection wells experienced their highest levels of sulfide during the February 24th sampling event, and the two monitoring wells had their highest concentrations of sulfide one week later on March 2nd (The highest sulfide concentration recorded for injection wells was 6.32 $\frac{mg}{L}$ in I-1, and for monitoring wells, 9.03 $\frac{mg}{L}$ in M-1). That is probably due to the fact that establishment of sulfate-reducing conditions occurred earlier in the injection wells, and later on it established in the monitoring wells down gradient. Dissolved sulfide concentration has remained high three month after the injections, with an average of 1.204 $\frac{mg}{L}$, suggesting that the sulfate-reduction is still happening in the groundwater system. The

increase in dissolved sulfide concentrations in LH-10 is probably due to diffusion of H_2S gas or hydrodynamic dispersion of the injected plume from the center of the plume with active sulfate-reduction process.

6.2 Laboratory Water Chemistry Analyses

The average total As concentration before the injections was 0.22 $\frac{mg}{L}$. After the injections, as predicted before, the two injection wells experienced an increase in As concentration. The increase in As levels is accompanied with high ferrous iron concentration which can be a result of iron-reducing conditions. Fe-reducing bacteria can use reactive organic carbon and establish a Fe-reducing condition before sulfate-reduction which leads to dissolution of the oxy-hydroxide minerals of iron and release of previously adsorbed As (Nickson et al., 2000; Lowers et al., 2007; Saunders et al., 2008). Another possibility is that phosphate that was added to the groundwater through the fertilizer in the injection solution, can compete with As for adsorption sites and can cause As release in groundwater by being substitute for As on ferric-oxyhydroxide minerals. From the second week after the injections As levels in the two injection wells and three monitoring wells in the down gradient (M-1, M-2, and LH-10) began to drop. The decrease in As concentrations is most probably due to the adsorption and co-precipitation of As on to newly formed iron sulfide minerals such as mackinawite and pyrite. If mackinawite did form initially, it probably reacted quickly with H_2S to form pyrite.As discussed before only pyrite was observed in the solid precipitates formed at the site. So if indeed mackinawite did form initially, it would have reacted with H_2S continuously being produced by sulfate-reducing bacteria to make pyrite. This reaction was proposed by Rickard & Luther (1997):

$$FeS(\text{mackinawite}) + H_2S(aq) = FeS_2(\text{pyrite}) + H_2(g)$$

Arsenic concentrations have also decreased in LH-10 from March 2nd sampling event. Due to the fact that sulfate and ferrous iron concentration in this well have decreased during

the past few sampling events below background levels and the dissolved sulfide concentration has increased significantly,it is possible that groundwater in this well is also experiencing a sulfate-reducing condition. Even if the center of the injected plume had not reached the well at the time of May sampling event, the decrease in As concentration could be the result of diffusion and/or hydrodynamic dispersion, where H_2S is moving faster than the average front of the injection plume. Thus H_2S appears to be reacting with dissolved Fe (or perhaps Fe in solid phases) to make pyrite capable of removing As by sorption and co-precipitation. As (III) concentrations follow the same trends as the total As levels. Figure 6.2 shows concentrations of As (III) compared to total As in the groundwater during all sampling events and indicates that As (III) is the dominant As species in the groundwater.

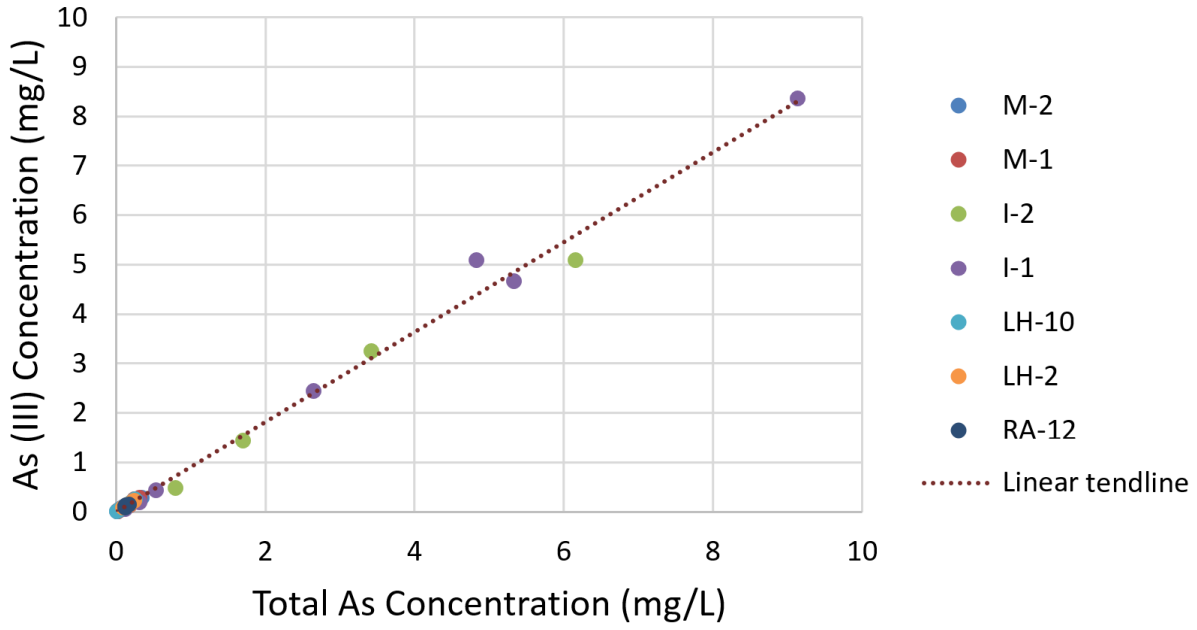

Figure 6.2: Plot showing Concentration of total As compared to As (III) in groundwater.

Al, Mg, Ca, and K concentrations after the injections have increased in the four newly installed wells. During the injection process Al, Mg , Ca, and K bearing clay minerals, such as kaolinite and illite which are reported to be present in the soil may be disturbed and may have created a suspension in the groundwater which can consequently cause the high concentration

of these elements in the wells after the injections (Patel, 1989). Increased amounts of Ca and Mg can also occur because of ion exchange on clay minerals. In addition, the chemical analysis of our injection solution indicates that this solution contained considerable amounts of Al, Mg, Ca, and K (from the fertilizer), which no doubt affected the concentration of these elements in the groundwater for the first few weeks. Concentrations of these major ions return to background levels three to four weeks after the injections (Table 5.16).

The average DOC concentration before the injections was 11.5 $\frac{mg}{L}$ and the week after the injections it went up to 1600 $\frac{mg}{L}$ in I-1. DOC is formed naturally by decay of organic matter. In our groundwater system, adding 180 lb of molasses (a source of organic carbon) to the aquifer caused the initial increase in DOC levels. It can be confirmed by the injection solution chemical analysis which shows that the injections solutions had at least 1800 $\frac{mg}{L}$ of DOC. DOC continued to drop after it reached the peak concentration, indicating active bacterial break down of organic carbon during sulfate reduction (Table 5.16).

The increase in P concentration the week after the injections is most likely due the composition of the fertilizer that was added to the aquifer to increase the bacterial metabolism (Table 5.16). The P concentration decreases as As concentration decreases and indicates that the bacteria consume the P in their metabolism process. However, P can decrease the As adsorption on iron-sulfide minerals, by competing with As for adsorption sites (Pi et al., 2016).

Sulfate concentration is one of the most important reaction path variables in this study, and it is also a common naturally occurring ion in groundwater. The average sulfate concentration in the groundwater was 21.9 $\frac{mg}{L}$, before the injections and the first week after the injections the sulfate concentration increased as high as 800 $\frac{mg}{L}$ (Figure 5.21). This increase is due to the injection of at least 610 $\frac{mg}{L}$ of sulfate through the ferrous sulfate present in our injection solution. The sulfate-reduction condition that was established in the groundwater caused the sulfate to be reduced to sulfide by the bacteria and decreased the sulfate concentrations for the following sampling events. The average sulfate levels were less

than the background levels in April 21st, especially in the four new wells, probably due to consumption of sulfate by sulfate-reducing bacteria.

Fluoride and chloride concentrations have also increased the first week after the injections in the four newly installed wells. The most important factor in this rapid increase is once again in the injection solution, since our injection solution had high concentrations of chloride and fluoride (mostly from the fertilizer). Also the increase in nitrite and total nitrate concentration the week after the injections should be due to the fact that the injection solution contained, at least, 0.21 $\frac{mg}{L}$ of nitrite and 0.076 $\frac{mg}{L}$ of total nitrate (Table 5.16).

6.3 Geochemical Modeling

The activity diagrams for the pre-injections data and the first week after the injections shows that after the injections the conditions in the groundwater has moved toward a more basic and more reducing condition, as it was predicted, after sulfate-reducing conditions had been established. The increase in pH is due to consumption of H^+ in H_2S production during sulfate-reduction process. The fact that most of the groundwater samples plot in the $As(OH)_3$ (arsenous acid) stability field confirms our water chemistry data that shows As (III), a neutral species of As, is the dominant species of As in this groundwater. Data from the second week indicate that although the Eh and pH conditions have changed and have moved slightly toward the background conditions, $As(OH)_3$ is still the dominant As oxidation state in the groundwater. Groundwater became more reducing during the third week after the injections, and groundwater Eh-pH conditions are consistent with the solid As-rich pyrite as the main As host. This shows that As was mostly being sequestered in arsenian-pyrite. This condition continued in the fourth week after the injections. During the fifth sampling event April 21st and the sixth on the May 19th the diagrams show that the conditions are getting less and less reducing and three months after the injections, the arsenian-pyrite is still the dominant As species suggesting the deposition of As along with iron sulfides.

These diagrams suggest that at first As (III) is the dominant species in the groundwater, as the time passes after the injections redox conditions cause the Fe^{2+} to move toward the stability field of pyrite and reacts with the H_2S that has been produced by the bacteria through sulfate-reduction process and precipitate as pyrite. This pyrite can remove trace elements such as As by co-precipitation or adsorption (Saunders et al., 1997). It is possible that realgar and orpiment could precipitate before pyrite based purely on existing thermodynamic data. However, because these minerals are not likely to form in a low temperature condition, and as a result, they have been suppressed in the model that is produced. Model results are consistent with the XRD and XRF data showing that arsenian-pyrite has formed soon after the injections.

Recent research has raised some doubts about the efficiency of using sulfate-reducing bacteria for remediating As-contaminated groundwater, such as the studies that suggest the transformation of FeS to pyrite can be retarded by As sorption, which can subsequently decrease the formation of more stable As sink (Wolthers et al., 2007). In addition, there are studies that has proposed that sulfate-reduction can cause As to form aqueous complexes with aqueous H_2S (Pi et al., 2016) thus potentially enhancing As mobility under sulfate-reducing conditions. Further there are concerns about the possibility of oxidation of As-bearing Fe sulfides and the consequent release of As into groundwater after a biogenic sulfate-reduction ends. Such oxidations could be caused by recharge of groundwater by oxygenated water from rainfall or perhaps a drop in the water table in times of drought. However, recent studies by DeFlaun et al. (2009) and Onstott et al. (2011) show that if Fe-sulfides are oxidized to Fe-oxyhydroxides, the latter will continue to sorb As. The results from this study, to date, have shown that this bioremediation process can be effective. The injection of Fe seems to: 1) Keep As-sulfides or As-H_2S aqueous complexes from forming and 2) cause the formation of pyrite, the most stable Fe-sulfide that also is very effective in removing As. The future progresses in this project can definitely help better understanding the problems and uncertainties in this method, if any.

Chapter 7

Conclusions

In this study an in-situ bioremediation was conducted at an industrially As contaminated site. An injection solution containing water, molasses, ferrous sulfate, and agricultural-grade fertilizer was gravity fed to the groundwater through injection wells. The field measurements and samplings were conducted weekly, for the first month and monthly afterward. The following can be concluded from the results of the geochemical analysis as well as the field measurements.

Field measurements during a three month period suggest that approximately one week after the injections the sulfate-reduction condition was established in the groundwater. The pH and ORP levels are rising back to the background levels three months after the injections. The XRD and XRF results show that arsenian-pyrite formed during this time.

The groundwater geochemistry data indicate that As levels increased at the beginning of the process due to Fe-reducing conditions that mobilizes As from Fe-oxide minerals in the aquifer. It started to decrease after the establishment of sulfate-reducing conditions. Along with decrease in As concentrations, Fe and sulfate concentration have decreased as well, suggesting that bacterial sulfate-reduction is consuming the sulfate and creating H_2S. Ferrous iron reacts with the dissolved sulfide in the groundwater and produces iron sulfide minerals which adsorb and co-precipitate As. Three months after the injections, As levels decreased from 0.25-0.34 $\frac{mg}{L}$ to below the EPA drinking water standard of 0.01 $\frac{mg}{L}$ in M-2 and LH-10, two wells in the down gradient direction. In addition, As levels in most of other wells have decreased to below their background levels. These results and the geochemical modeling indicate that although the redox conditions are returning back to the background levels, the newly formed iron sulfide minerals are still stable and adsorbing As. Pyrite should

be stable under the Eh-pH conditions at the site (conditions that were present before the injections), so it should retain As that is already removed and perhaps continue to remove newer As released from the aquifer materials.

Three months after the injections, the decrease observed in Fe concentration was not as rapid as As decrease, while sulfate concentrations have decreased to less than the background levels, suggesting that Fe concentration in the injection solution may have been higher than necessary and $FeSO_4$ can be replaced to some extent by $MgSO_4$ for the future injections.

The XRF analyses of selected solid samples collected from the injection wells and monitoring wells showed major peaks for Fe, S, and As. XRD analysis of these solid samples also indicate that pyrite and As-bearing sulfide minerals are present in the sediments in the aquifer. These results once again confirm the adsorption of As onto iron sulfide minerals that have been formed due to SRB metabolism. Contaminant transport models are showing how the injected solution affects the groundwater after one year. Fe concentrations will drop to a few $\frac{mg}{L}$ (close to background levels) one year after the injections.

Data generated to date indicate this approach of giving indigenous sulfate-reducing bacteria reactive organic C and $FeSO_4$ has the potential to become a useful in-situ bioremediation process by making pyrite, which some previous studies suggest that is optimal for removing As. In particular, the addition of Fe^{2+} serves to retard H_2S-As aqueous complexing to occur, and at the same time lead to pyrite formation, which removes As.

Monitoring the wells and samplings will continue on a monthly basis to observe the exact changes in As concentration and the stability of sulfide minerals in the study area for one year. The monitoring can determine the efficiency of this method as an cost-effective bioremediation solution for As contaminated aquifers.

References Cited

Abraitis, P., Pattrick, R., & Vaughan, D. (2004). Variations in the compositional, textural and electrical properties of natural pyrite: a review. *International Journal of Mineral Processing*, *74*, 41–59.

Annachhatre, A. P., & Suktrakoolvait, S. (2001). Biological sulfate reduction using molasses as a carbon source. *Water Environment Research*, *73*, 118–126.

Bethke, C. M. (2007). *Geochemical and biogeochemical reaction modeling*. Cambridge University Press.

Bissen, M., & Frimmel, F. H. (2003). Arsenica review. part i: occurrence, toxicity, speciation, mobility. *Acta hydrochimica et hydrobiologica*, *31*, 9–18.

Blanchard, M., Alfredsson, M., Brodholt, J., Wright, K., & Catlow, C. R. A. (2007). Arsenic incorporation into fes 2 pyrite and its influence on dissolution: a dft study. *Geochimica et Cosmochimica Acta*, *71*, 624–630.

Bostick, B. C., & Fendorf, S. (2003). Arsenite sorption on troilite (fes) and pyrite (fes 2). *Geochimica et Cosmochimica Acta*, *67*, 909–921.

Burton, E. D., Johnston, S. G., & Kocar, B. D. (2014). Arsenic mobility during flooding of contaminated soil: the effect of microbial sulfate reduction. *Environmental Science & Technology*, *48*, 13660–13667.

Chapelle, F. (1993). *Ground-water microbiology and geochemistry*. John Wiley & Sons, New York, USA.

Chapelle, F. H., & Lovley, D. R. (1992). Competitive exclusion of sulfate reduction by fe (lll)-reducing bacteria: a mechanism for producing discrete zones of high-iron ground water. *Ground Water*, *30*, 29–36.

DeFlaun, M., Lanzon, J., Lodato, M., Henry, S., Onstott, T. E., Chan, E., & Otemuyiwa, B. (2009). *Anaerobic Biostimulation for the In Situ Precipitation and Long-Term Sequestration of Metal Sulfides*. Technical Report DTIC Document.

Drever, J. I. (1997). *The Geochemistry of Natural Waters: Surface and Groundwater Environments. Prentice Hall*. Englewood Cliffs, New Jersy, USA.

Egal, M., Casiot, C., Morin, G., Elbaz-Poulichet, F., Cordier, M.-A., & Bruneel, O. (2010). An updated insight into the natural attenuation of as concentrations in reigous creek (southern france). *Applied geochemistry*, *25*, 1949–1957.

Farquhar, M. L., Charnock, J. M., Livens, F. R., & Vaughan, D. J. (2002). Mechanisms of arsenic uptake from aqueous solution by interaction with goethite, lepidocrocite, mackinawite, and pyrite: An x-ray absorption spectroscopy study. *Environmental Science & Technology*, *36*, 1757–1762.

Goldberg, S. (2002). Competitive adsorption of arsenate and arsenite on oxides and clay minerals. *Soil Science Society of America Journal*, *66*, 413–421.

Huerta-Diaz, M. A., & Morse, J. W. (1992). Pyritization of trace metals in anoxic marine sediments. *Geochimica et Cosmochimica Acta*, *56*, 2681–2702.

Keimowitz, A., Mailloux, B., Cole, P., Stute, M., Simpson, H., & Chillrud, S. (2007). Laboratory investigations of enhanced sulfate reduction as a groundwater arsenic remediation strategy. *Environmental Science & Technology*, *41*, 6718–6724.

Kirk, M. F., Holm, T. R., Park, J., Jin, Q., Sanford, R. A., Fouke, B. W., & Bethke, C. M. (2004). Bacterial sulfate reduction limits natural arsenic contamination in groundwater. *Geology*, *32*, 953–956.

Kirk, M. F., Roden, E. E., Crossey, L. J., Brealey, A. J., & Spilde, M. N. (2010). Experimental analysis of arsenic precipitation during microbial sulfate and iron reduction in model aquifer sediment reactors. *Geochimica et Cosmochimica Acta*, *74*, 2538–2555.

Kocar, B. D., Borch, T., & Fendorf, S. (2010). Arsenic repartitioning during biogenic sulfidization and transformation of ferrihydrite. *Geochimica et Cosmochimica Acta*, *74*, 980–994.

Kruger, M. C., Bertin, P. N., Heipieper, H. J., & Arsène-Ploetze, F. (2013). Bacterial metabolism of environmental arsenicmechanisms and biotechnological applications. *Applied Microbiology and Biotechnology*, *97*, 3827–3841.

Lee, M.-K., Saunders, J. A., Wilkin, R. T., & Mohammad, S. (2005). Geochemical modeling of arsenic speciation and mobilization: Implications for bioremediation. In *Advances in Arsenic Research: Integration of Experimental and Observational Studies and Implications for Mitigation, ODay et al.(eds.), American Chemical Society Symposium Series* (pp. 398–413). volume 915.

Lowers, H. A., Breit, G. N., Foster, A. L., Whitney, J., Yount, J., Uddin, M. N., & Muneem, A. A. (2007). Arsenic incorporation into authigenic pyrite, bengal basin sediment, bangladesh. *Geochimica et Cosmochimica Acta*, *71*, 2699–2717.

Manning, B. A., & Goldberg, S. (1997). Arsenic (III) and arsenic (V) adsorption on three california soils. *Soil Science*, *162*, 886–895.

McDonald, M. G., & Harbaugh, A. W. (1988). A modular three-dimensional finite-difference ground-water flow model.

Mondal, P., Bhowmick, S., Chatterjee, D., Figoli, A., & Van der Bruggen, B. (2013). Remediation of inorganic arsenic in groundwater for safe water supply: a critical assessment of technological solutions. *Chemosphere*, *92*, 157–170.

Muyzer, G., & Stams, A. J. (2008). The ecology and biotechnology of sulphate-reducing bacteria. *Nature Reviews Microbiology*, *6*, 441–454.

Nickson, R., McArthur, J., Ravenscroft, P., Burgess, W., & Ahmed, K. (2000). Mechanism of arsenic release to groundwater, Bangladesh and West Bengal. *Applied Geochemistry*, *15*, 403–413.

Omoregie, E. O., Couture, R.-M., Van Cappellen, P., Corkhill, C. L., Charnock, J. M., Polya, D. A., Vaughan, D., Vanbroekhoven, K., & Lloyd, J. R. (2013). Arsenic bioremediation by biogenic iron oxides and sulfides. *Applied and environmental microbiology*, *79*, 4325–4335.

Onstott, T. C., Chan, E., Polizzotto, M. L., Lanzon, J., & DeFlaun, M. F. (2011). Precipitation of arsenic under sulfate reducing conditions and subsequent leaching under aerobic conditions. *Applied Geochemistry*, *26*, 269–285.

Patel, D. V. (1989). *Assessment of groundwater effects at Gulf Power Companys Lynn Haven substation site*. Technical Report Southern Company Services.

Pi, K., Wang, Y., Xie, X., Ma, T., Su, C., & Liu, Y. (2016). Role of sulfur redox cycling on arsenic mobilization in aquifers of datong basin, northern china. *Applied Geochemistry*, . [Available online 30 May 2016].

Rice, K. C., Conko, K. M., & Hornberger, G. M. (2002). Anthropogenic sources of arsenic and copper to sediments in a suburban lake, northern virginia. *Environmental science & technology*, *36*, 4962–4967.

Rickard, D., & Luther, G. W. (1997). Kinetics of pyrite formation by the H_2S oxidation of iron (II) monosulfide in aqueous solutions between 25 and 125 c: The mechanism. *Geochimica et Cosmochimica Acta*, *61*, 135–147.

Rieder, M., Crelling, J. C., Šustai, O., Drábek, M., Weiss, Z., & Klementová, M. (2007). Arsenic in iron disulfides in a brown coal from the north bohemian basin, czech republic. *International Journal of Coal Geology*, *71*, 115–121.

Rittle, K. A., Drever, J. I., & Colberg, P. J. S. (1995). Precipitation of arsenic during bacterial sulfate reduction. *Geomicrobiology Journal*, *13*, 1–11.

Saunders, J. A. (1998). Situ bioremediation of contaminated groundwater. US Patent 5,833,855.

Saunders, J. A., Lee, M.-K., Shamsudduha, M., Dhakal, P., Uddin, A., Chowdury, M., & Ahmed, K. (2008). Geochemistry and mineralogy of arsenic in (natural) anaerobic groundwaters. *Applied Geochemistry*, *23*, 3205–3214.

Saunders, J. A., Lee, M.-K., Wolf, L. W., Morton, C. M., Feng, Y., Thomson, I., & Park, S. (2005a). Geochemical, microbiological, and geophysical assessments of anaerobic immobilization of heavy metals. *Bioremediation Journal*, *9*, 33–48.

Saunders, J. A., Mohammad, S., Korte, N. E., Lee, M.-K., Fayek, M., Castle, D., & Barnett, M. O. (2005b). Groundwater geochemistry, microbiology, and mineralogy in two arsenic-bearing holocene alluvial aquifers from the united states. In *ACS symposium series* (pp. 191–205). Oxford University Press volume 915.

Saunders, J. A., Pritchett, M. A., & Cook, R. B. (1997). Geochemistry of biogenic pyrite and ferromanganese coatings from a small watershed: a bacterial connection? *Geomicrobiology Journal*, *14*, 203–217.

Schmidt, W., & Clark, M. W. (1980). *Geology of Bay County, Florida*. 57. Bureau of Geology, Division of Resource Management, Florida Department of Natural Resources.

Scott, T. B., Tort, O. R., & Allen, G. (2007). Aqueous uptake of uranium onto pyrite surfaces; reactivity of fresh versus weathered material. *Geochimica et Cosmochimica Acta*, *71*, 5044–5053.

Scott, T. M. (2001). *Text to accompany the geologic map of Florida*. Florida Geological Survey.

Southam, G., & Saunders, J. A. (2005). The geomicrobiology of ore deposits. *Economic Geology*, *100*, 1067–1084.

Starnes, P. (2015). *Hydrogeology and Geochemistry of Arsenic Contaminated Shallow Alluvial Aquifers in Florida and Alabama*. Master's thesis Auburn University.

Wolthers, M. (2003). *Geochemistry and environmental mineralogy of the iron-sulphur-arsenic system*. Ph.D. thesis Universiteit Utrecht.

Wolthers, M., Butler, I., & Rickard, D. (2007). Influence of arsenic on iron sulfide transformations. *Chemical Geology*, *236*, 217–227.

Zheng, C. (1990). {MT3D}, , a modular three-dimensional transport model for simulation of advection, dispersion, and chemical reactions of contaminants in groundwater systems: Report to the united states environmental protection agency.